Doctoral Thesis

Stability Augmentation of Grid Connected Wind Farm by Variable Speed Permanent Magnet Wind Generator

March 2013

MARWAN ROSYADI

Stability Augmentation of Grid Connected Wind Farm by Variable Speed Permanent Magnet Wind Generator

Approved by Supervisory Committee

Dr. Junji Tamura
Professor
Department of Electrical and Electronic Engineering
Committee Chair and Thesis Supervisor

Dr. Shinya Obara
Professor
Department of Electrical and Electronic Engineering
Member of the Supervisory Committee

Dr. Rion Takahashi
Associate Professor
Department of Electrical and Electronic Engineering
Member of the Supervisory Committee

Dr. Kousaku Yoshida
Professor
Department of Electrical and Electronic Engineering
Member of the Supervisory Committee

Dr. Hiroshi Tanimoto
Professor
Department of Electrical and Electronic Engineering
Member of the Supervisory Committee

Kitami Institute of Technology, Japan

Abstract

This thesis deals with the stability augmentation of grid connected wind farm by Variable Speed Permanent Magnet Wind Generators. Since last decade, the penetrations of large number of wind farms into electrical grid system have been increasing significantly. In many countries, increasing of the penetration level of the wind generators into grid system has led power system operators to revise the grid code connection requirements for their power system. The grid code prosecutes that the wind generator should give a contribution to the power control in case of abnormal operating conditions such as network disturbance. The wind generators should be remained stay online during a network disturbance. The Low Voltage Ride-Through (LVRT) grid code requirement should be taken into account when a short circuit occurs in grid system. Out of synchronism of a large number of wind generators becomes serious impact on power system stability. Therefore, the interaction between wind farm and main power system such as transient and steady state characteristics has become important to be analyzed in order to augment dynamic stability of wind farms.

The Fixed Speed Wind Turbines with Squire Cage Induction Generators (FSWT-SCIGs) are widely used in wind farm due to their advantages of mechanical simplicity, robust construction, and lower cost. However, the FSWT-SCIG directly connected to the grid does not have any LVRT capability when a short circuit occurs in the system. Moreover, under steady state condition its reactive power consumption cannot be controlled and hence terminal voltage of the wind generator lead to large fluctuation. In this thesis, a new control strategy of variable speed wind turbine with permanent magnet synchronous generator (VSWT-PMSG) for stability augmentation of wind farm including fixed speed wind turbine with SCIG is proposed. A suitable control scheme for back-to-back converters of PMSG is developed to augment dynamic behavior of the wind farms. In order to avoid the converter damage, the protection scheme using DC chopper is embedded on DC link circuit. The simulation studies have been performed and it is shown that the proposed control system can stabilize the wind farms effectively.

Three phase voltage source converter (VSC) is commonly used in VSWT-PMSG system when it is connected to the grid system. However, the converter operating at high switching frequencies can generate high order harmonics and power losses. To reduce harmonic injection to the grid system, LCL filter is an attractive solution because of its many potential advantages such as higher harmonic attenuation and smaller inductances. However, resonance frequency of the filter can cause stability problem. Therefore, design of the current controller of voltage source converter should be carefully considered. In this thesis new control scheme of VSWT-PMSG connected to grid system through LCL filter is proposed to enhance the

stability of wind farm including fixed speed wind turbine based squirrel cage induction generator. The current controlled voltage source converter of PMSG system is developed based on the d-q rotating reference frame, in which the dynamic stability of the control system is analyzed based on frequency response of the Bode diagram. The control strategies of overall wind farm have been investigated in transient and steady state analyses to show the capability and effectiveness of the proposed method. The results show that the terminal voltage of wind farm can be recovered effectively during and after the symmetrical and the unsymmetrical faults, and thus the transient stability of fixed speed wind generator can be enhanced.

Another salient feature of this thesis is an application of Fuzzy Logic Controller (FLC) to the current controlled VSC of PMSG in order to enhance dynamic stability of wind farms. The current controller is the most essential in design application of VSC, because it can dominate the performance of the distributed generation connected to a grid system. Change of parameters in the grid system can lead significant impact on the control system performance of the converter. The deviation of the grid system impedance will change gain margin and phase margin of the control system. The fuzzy logic controller is combined with conventional PI controller (Fuzzy-PI), and hence gain parameters of the PI controller can be adjusted based on tracking error. In addition, a simple method based on the Bode diagram is proposed in order to design the membership function of the FLC. It is concluded the voltage source converter can be controlled effectively by using the proposed Fuzzy-PI controller.

In industrial applications, PI controllers are most widely used because of their simple structure and good performances in a wide range of operating conditions. In fixed gain controllers, these parameters are determined by methods such as the Zeigler and Nichols, optimum modulus criterion, pole placement, etc. However these methods sometimes bring about oscillatory responses. In addition, for the strong nonlinear system the global optimum solution is difficult to be achieved by using these methods. In this thesis, a novel design method of current controlled voltage source converter for VSWT-PMSG is proposed. The method is based on optimum tuning process of PI gain parameters of voltage source converter control system with the artificial immune system (AIS) algorithm considered. Simulation results show that the proposed method is very effective in enhancing the dynamic stability of the wind generator system.

Considering all aspect of VSWT-PMSG with proposed control system, it can be concluded that the transient and steady state stabilities of a wind farm combined also with FSWT-SCIG can be augmented effectively for severe network disturbance as well as randomly fluctuating wind speed

Contents

Chapter 1

Introduction

1.1. Renewable Energy

Electrical power is the most popular form of energy, because it can be converted to other energy easily at high efficiency and reasonable cost. Electrical energy can be transmitted in a usable form from one place to another. A power plant is an industrial facility for the generation of electrical power [1]-[3]. The center of all power plant is a generator, a rotating machine that converts mechanical power into electrical power through relative motion between a magnetic field and a conductor. The energy source harnessed to turn the generator varies widely. In most of conventional power plants in the world fossil fuels are used, such as coal, oil, and natural gas, to generate electricity, and nuclear fission is also used. However, generating electrical power from fossil fuel and nuclear energy has environmental impact such as, greenhouse effect caused by increase of CO2 concentration, pollution, and the nuclear waste problem.

Due to the depletion of fossil fuel and the need to decrease the pollution production, utilization of renewable energy resources for electrical energy generation has been interested and received much attention all over the world. Renewable energy is energy which comes from natural resources such as wind, sunlight, water fall, geothermal heat, tides, and sea waves. Installation of global renewable energy for new electric capacity production is estimated about 208 GW in 2011. Total renewable energy capacity worldwide exceeded 1360 GW in 2011, increased by about 8% from 2010. Non-hydro renewable exceeded 390 GW, a 24% capacity increase over 2010. Globally, wind and solar PV accounted for almost 40% and 30% of new renewable capacity, respectively, followed by hydropower nearly 25%. By the end of 2011, operating renewable capacity reached more than 25% of total global power generating capacity and supplied an estimated 20.3% of global electricity, most of which is provided by hydropower [4].

1.2. Overview of Wind Power Capacity

Since 2010, wind energy becomes ongoing trend of renewable energy resource in market and industry highlights [4]. Fig. 1.1 shows the global total installed capacity of wind power in 2011-2012 reported by World Wind Energy Association (WWEA). By the end of June 2012 the global wind power capacity reached 254000 MW, in which 16546 MW were added in the first six months of 2012. The global wind capacity grew by 7% within six months and by 16.4 % on

an annual basis compared with middle of 2011. In comparison, the annual growth rate in 2011 was 20.3%. In the end of 2012 the total capacity is predicted to reach 273000 MW [5].

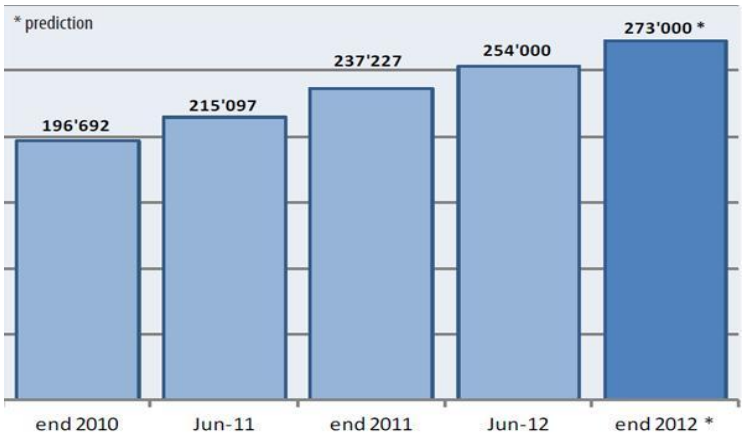

Fig. 1.1. Total installed capacity of wind power in 2011-2012 (MW) [5]

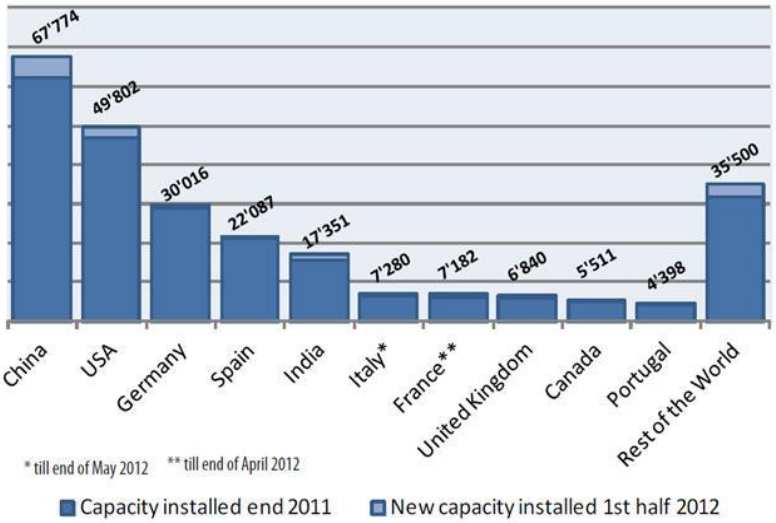

Fig. 1.2. Total installed capacity of wind power in 2011-2012 in each country (MW) [5]

According to WWEA, the five leading countries, China, USA, Germany, Spain and India, represent together a total share of 74% of the global wind capacity as shown in Fig. 1.2. Again in 2012, China represents by far the largest wind market, adding 5.4 GW in 6 months. By June 2012, China had an overall installed capacity of around 67,7GW. In second place, the US market added 2883 MW between January and June 2012, about 28 % more than in the same period in 2011. The top markets in Europe continue to be Germany with a new capacity of 941 MW and a total of 30016 MW, Spain (414 MW, 22087 MW in total), Italy (490 MW, 7280 MW in total), France (650MW, 7182MW in total), the United Kingdom (822 MW, 6480 MW in

total) and Portugal (19 MW, 4398 MW in total). In number five, India had a stable market size with 1471 MW, a similar amount like in the first of 2011 [5].

1.3. Background of Thesis

The integration of large scale wind farms into electrical grid system have been significantly increased since last decade. Global Wind Energy Council (GWEC) predicted that global wind power generation capacity will reach to 459 GW and new capacity of 62.5 GW will be added to the global total at the end of 2015 [5]. It is well known that power production of wind generator fluctuates depending on wind speed variation which affects power system stability and power quality [6]-[9]. Increasing of the penetration level of the wind generator into grid system has led power system operators to revise the grid code connection requirements for their power system in many countries [10]. The grid code prosecutes that the wind generator should give a contribution to control the power in case of abnormal operating conditions such as network disturbance. The wind generators should be remained stay online during a network disturbance. The low voltage ride through grid code requirement should be taken into account when a short circuit occurs in grid system. Out of synchronism of a large number of wind generators becomes serious impact on power system stability. Therefore, the interaction between wind farm and power system such as transient and steady state characteristics of wind farm has become important to be analyzed in the few last years.

The Fixed Speed Wind Turbines with Squirrel Cage Induction Generators (FSWT-SCIG) are most widely used in wind farms. This type of wind turbine is very popular and it has the advantages of mechanical simplicity, robust construction, low specific mass and smaller outer diameter, and lower cost [11]. However, some papers reported that the FSWT-SCIG directly connected to the grid does not have any low voltage ride-trough (LVRT) capability when a short circuit occurs in the system [12]-[14]. The squirrel cage induction generators require large reactive power to recover the air gap flux when a short circuit fault occurs in the grid system. If the sufficient reactive power is not available enough, the electromagnetic torque of the SCIG decreases significantly, and then rotor speed of the generator increases rapidly and becomes unstable [15]. As a result, the induction generator becomes unstable and it requires to be disconnected from the grid system. Moreover, under steady state condition the reactive power consumption cannot be controlled and hence terminal voltage of the wind generator leads to large fluctuation which is a serious disadvantage of the SCIG wind turbine [16].

The FSWT-SCIG always requires reactive power, and its value cannot be controlled. This makes it impossible to support grid voltage control. Reactive power compensation is a major issue, especially for a fixed speed wind generators, in both steady state and transient conditions. Usually, a capacitor bank is installed at each induction generator terminal to

provide reactive power. But it cannot maintain the wind generator terminal voltage constant under randomly fluctuating wind speed. Moreover, the induction generator needs large reactive power during a short circuit fault in the grid system as explained above. Therefore, control strategy for stabilization of the FSWT-SCIG still needs to be studied.

Some methods [17]-[19] have been considered in order to improve FRT of FSWT-SCIG. Utilization of Flexible AC Transmission System (FACT) devices such as Static Var Compensator (SVC), Static Synchronous Compensator (STATCOM), Dynamic Voltage Restore (DVR), Solid State Transfer Switch (SSTS), and Unified Power Flow Controller (UPFC) can be a better choice due to their abilities of flexible power flow control and good damping capability for power system dynamic oscillations. Superconducting Magnetic Energy Storage (SMES) and Battery Energy Storage System (BESS) integrated with a STATCOM are a very good system for wind power smoothing due to its response speed and high efficiency [20]-[22]. However, the system cost becomes expensive when the FACTS devices are installed in wind farm

Over recent years, the variable speed wind turbine (VSWT) generator system has become the dominant type among installed wind turbine systems. VSWT system is designed to achieve maximum aerodynamic efficiency over the wide range of wind speed, increase energy capture, improve power quality and reduce mechanical stress on the wind turbine [16]. In addition, VSWT system equipped with full or partial rating power electronic converters has strong fault ride through capability during a network disturbance [23]-[27]. Moreover, the VSWT system with fully scale converter not only recovers a network voltage drop preventing instability of FSWT -SCIG when fault occurs, but also generates electric power in steady state. Therefore, it is considered to be much effective for VSWT to be installed with SCIG in wind farm. VSWT with Doubly Fed Induction Generator (DFIG) have been proposed to enhance stability of wind farm including FSWT- IG [27-29]. However, in steady state the DFIG needs to absorb large reactive power in order to maintain terminal voltage of the wind farm when the IG is not sending so much active power to the grid. As a consequence the active power of the DFIG needs to be reduced although the wind speed is at the maximum condition. Moreover, as they have brushes which need regular inspection and replacement, they have a potential cause of machine failure and losses [11]. In addition below the synchronous speed, the rotor actually absorbs active power, which contributes to its low efficiency at slow speed.

Variable Speed Wind Turbine with Permanent Magnet Synchronous Generator (VSWT-PMSG) has become a promising and attractive type of wind turbine concept [16]. Megawatt class of VSWT-PMSGs have been installed in large wind power stations and directly connected to electrical power transmission system. The advantages of VSWT-PMSG configuration are: 1) No Gearbox and no brushes, and thus higher reliability; 2) The full power converter totally decouples the generator from the grid, and hence grid disturbances have no

direct effect on the generator; 3) No additional power supply for magnetic field excitation is needed; 4) The converter permits very flexible control of active and reactive power in cases of normal and disturbed grid conditions; 5) The amplitude and frequency of the generator voltage can be fully controlled by the converter [30], [31]. The VSWT-PMSG system is equipped with back to back power electronic converters, and it has strong low voltage ride through capability during and after fault condition on grid system [32]-[36]. Compared with DFIG, PMSG is more efficient, and, it can support large reactive power [37]. However, this type of wind generator has more complex construction and more expensive compared with other types. Therefore, combined installation of VSWT-PMSG and FSWT- SCIG in a wind farm can be efficient due to reduced system investment cost. VSWT-PMSG with power converters can be used to supply reactive power to recover network voltage in order to improve the LVRT of FSWT-SCIG when a fault occurs as well as to generate electric power in steady state operation.

As previously mentioned, VSWT-PMSG has more complex construction compared with other types. In addition, this type of wind generator has more complicated controller system. The VSWT-PMSG is, in general, connected to the utility power system through the voltage source power converters. However, the converter is operated at high switching frequencies between 2-15 kHz resulting high order harmonics which can disturb devices on the grid and generate power losses [38], [39]. In order to reduce harmonic currents injected to the grid, LCL filter is an attractive solution because of its many potential advantages such as higher harmonic attenuation and smaller inductances compared with L filter [40]. However, resonance at high frequency caused by the filter can lead stability problem. Determination of controller parameters should be considered in design application. To avoid the resonance problem, a passive damping resistance should be adopted in the LCL filter although this method can reduce the filter effectiveness and increase losses [39]. Selection of a damping resistance value should also be taken into account in the controller design of VSC as well as the filter effectiveness and its losses. Therefore, the analysis method and design controller system for the generator still needs to be improved.

Traditionally, the conventional PI controller is very common in the control of the power converter of PMSG because of their simple structure and good performances in a wide range of operating conditions. PI controllers cannot always effectively control systems with changing parameters or strong nonlinearities, and they may need frequent online retuning of their parameters [41]. Change of parameters in the grid system leads significant impact on the control system performance of the converter. The deviation of the grid system impedance will change gain margin and phase margin of the control system. Fuzzy logic controller has been attracted the attention of researchers because it can deal with nonlinear system without a precise mathematical modeling of the system [42]-[44]. Compared with conventional PI controller, fuzzy logic controller has the potential to provide an improved method even in the wide

parameter variations [45]. The fuzzy logic controller can take the place of conventional PI Controller. Integration of fuzzy logic controller with conventional PI controller can be an effective way to solve the problem of system parameter change. The fuzzy logic control can be used to adjust the gain parameters of the PI controller for any operating conditions. Hence, a good control performance can be achieved. However, the membership function of the fuzzy set should be carefully determined in the controller design. It is difficult to achieve an optimal controller performance by using trial and error method.

The current controller is the most essential in design application for Voltage Source Converter (VSC) of PMSG, because it can dominate the performance of the distributed generation connected to a grid system. The VSC is required to ensure the power produced by the distributed generation to be delivered to the network effectively. The tuning of gain parameters of PI controller should be carefully considered in design application of the VSC. In fixed gain PI controllers, these parameters are determined by methods such as the Zeigler and Nichols, optimum modulus criterion, pole placement, etc. However a common disadvantage of the methods are that the resulting closed loop system is often more oscillatory than that desired [46]. In order to provide closed loop responses with a damping ratio of 25%, Cohen and Coon technique is proposed [47]. However this technique sometimes brings about oscillatory responses [48]. In addition, for the strong nonlinear system the global optimum solution is difficult to be achieved by using these methods. Over the ten years, interests in studying biologically inspired systems such as genetic algorithm, artificial neural network, and artificial immune systems, have been increased. The immune system of human body is a complex of cells, molecules and organs and has the ability to perform multiple tasks like pattern recognition, learning, distributed detection, optimization, etc. [49]. Artificial immune system (AIS) is computational techniques based on immunological principles. The computation with AIS technique has some merits: the feasibility and diversity of spaces can be better ensured, the method operates on a big population of antibodies simultaneously, hence stagnation in computation process can be eliminated, and the global optimum can be achieved easily [50].

1.4. Purpose and Contribution of Thesis

The main purpose of this thesis is stability augmentation of grid connected wind farm by using VSWT-PMSG. Design and analysis of suitable control strategy of PMSG are developed in order to enhance both transient and steady state stabilities of the wind farm including FSWT-SCIG. The concentration of the research is focused on design and analysis of the back to back power converter controller system of PMSG. Several approach methods are presented in this thesis in order to improve performance of the controller system of PMSG, and hence the stability augmentation of overall wind farm can be achieved.

The results of this work are expected to provide valuable contributions in the following aspects:

1) The VSWT-PMSG system with power electronic converters has strong low voltage ride through capability. The power converter permits to control active and reactive power delivered to the grid system. Therefore, it is considered to be much effective and efficient for VSWT-PMSG to be installed with FSWT-SCIG in wind farm without additional FACT devices. Hence investment cost of wind farm can be reduced. In this thesis, a suitable control scheme for back-to-back converter of VSWT-PMSG is proposed to improve the voltage stability as well as reactive power compensation of the FSWT-SCIG in cases of disturbed and normal conditions. The simulation analysis by using PSCAD/EMTDC shows that the VSWT-PMSG can stabilize the overall wind farm effectively.
2) High switching frequency of power converter of the VSWT-PMSG can lead harmonics injected into the grid system. LCL filter can the best solution due to its advantages of higher harmonic attenuation and smaller inductances. However, the stability problem occurs on the controller system because of resonance. Therefore, the gain parameters of the controller should be carefully considered on design application. In this thesis simple mathematical model of inverter connected to grid system through LCL filter is developed. The stability margin of the controller system can be investigated using mathematic expression. By using Bode diagram, gain parameters of the VSWT-PMSG can be obtained.
3) The conventional PI controllers cannot always effectively control systems with changing parameters or strong nonlinearities. The deviation of the grid system impedance will change gain margin and phase margin of the control system. Fuzzy Logic controller is proposed for current controlled VSC of PMSG in order to improve stability of wind farm. Variation techniques of Fuzzy Logic Controller design are proposed in different model systems. Comparison and evaluation between the proposed fuzzy logic controller and conventional PI controller are made. The results of this investigation are also expected to provide valuable knowledge in design and analysis of current controller of VSC system using fuzzy logic controller. Finally the results show that the controller with fuzzy logic controller embedded can effectively enhance stability of wind farm.
4) The current controller is the most essential in design application for Voltage Source Converter (VSC) of PMSG. PI controller is common in VSC control system. In fixed gain controllers, their parameters are determined by methods such as the Zeigler and Nichols, optimum modulus criterion, pole placement, etc. However a common disadvantage of the methods are that the resulting closed loop system is often more

oscillatory than that desired. In this thesis, artificial immune system (AIS) is proposed to tune PI controller parameters of current controlled voltage source converter of the VSWT-PMSG. The uniqueness, advantages and drawbacks of AIS can be addressed as alternative method when global optimum solution cannot be achieved by the conventional method. Comparison between AIS and other conventional methods is investigated to show the effectiveness of the method.

1.5. Outline of Thesis

Chapter 2 describes the detail of wind turbine generator modeling considered in this thesis. The general overview to basic principles of electrical power extraction from wind energy is presented. The drive train and pitch angel control models of wind turbine generator system are discussed. Finally, the topological overview and modeling are presented in detail for both FSWT-SCIG and VSWT-PMSG.

In Chapter 3, consideration on combined VSWT-PMSG and FSWT-SCIG from a view point of dynamic stability augmentation of wind farm is presented. A control strategy of power converter of VSWT-PMSG is developed to augment both transient and steady state stabilities of the wind farms. During fault condition the DC link voltage increase significantly due to unbalance in power produced by the generator and delivered to grid system. In order to avoid the converter damage, the protection scheme using DC chopper is embedded on DC link circuit. In order to evaluate the effectiveness and capability of the proposed control strategy, two wind farms composed of aggregate model of VSWT-PMSG and FSWT-SCIG, which are connected to an infinite bus and a multi-machine power system, is analysed.

In chapter 4, a new control scheme for variable speed permanent magnet wind generator connected to grid through LCL filter is proposed in order to enhance stability of wind farms including fixed speed induction generators. Design and control approaches of back to back converters are developed for both active and reactive powers delivered to a power grid system to be controlled effectively. The stability performances of the controller system such as dynamic response and good margin are also investigated based on the Bode diagram. By using this method the gain parameters of PI controller can be easily obtained. To evaluate the controller system capabilities, simulation analyses for both transient and steady state conditions are performed on a model system composed of two wind farms connected to an infinite bus.

Chapter 5 presents new fuzzy logic based controller of variable speed permanent magnet wind generator connected to a grid system through LC-filter. A new current control method of grid side AC/DC/AC converter is developed with integrating the fuzzy controller, in which both active and reactive power delivered to a power grid system are controlled effectively. The fuzzy logic controller is designed to adjust the gain parameters of the PI controllers under any

operating conditions for the dynamic stability to be enhanced. A simple method based on frequency response of Bode diagram is proposed in the design of the fuzzy logic controller. Stabilizing effect of the proposed fuzzy logic controlled PMSG system on the fixed speed wind generators is also investigated. The significant effect of proposed control system has been demonstrated and it is concluded that the proposed Fuzzy controller is very effective in improving the transient stability of overall wind farm system during temporary and permanent fault conditions.

In Chapter 6 a novel design method of current controlled voltage source converter for variable speed permanent magnet wind generator is proposed. The method is based on optimum tuning process of PI gain parameters of voltage source converter control system with the artificial immune system (AIS) algorithm considered. The analytical simulation studies have been performed using mfile/Matlab. In order to verify the effectiveness of the proposed method, the simulation studies using PSCAD/EMTDC have also been performed. Simulation results show that the proposed method is very effective in enhancing the dynamic stability of the wind generator system.

Finally, overall conclusions of all the chapters regarding this work are presented in Chapter 7.

Chapter 2

Wind Turbine Model

This chapter describes the overview of wind turbine generation system. First, a brief introduction to basic principles of energy extraction from wind is presented. Then, drive train and pitch angel control models of wind turbine generator system are presented. The topological overview and modeling are presented for both fixed speed and variable speed wind turbine generator systems. In additional, the two levels and three levels of back to back converters for PMSG are discussed.

2.1. Wind Turbine Generator System

The modern wind turbine generator systems are mainly constructed as system with a horizontal axis rotation, a wind turbine, generator with gear box and transformer located in nacelle, and tower (see Fig 2.1). The turbine captures power from wind and drives a generator. The tower supports the nacelle and usually contains the electrical conduits and yaw motor.

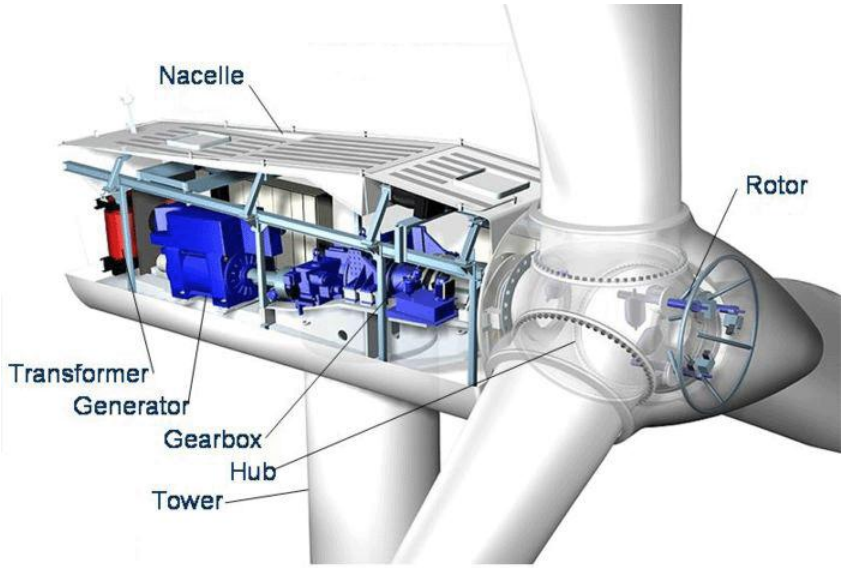

Fig. 2.1. Wind turbine generator system [51]

The each part of wind generator system is shown in Fig 2.2. The modern wind turbine (sometimes called the rotor), mostly have either two or three blades. Wind blowing over the blades causes the blades rotate. Wind speed is measured by using anemometer, and its data is transmitted to the controller. A disc brake can be applied mechanically, electrically, or

hydraulically to stop the rotor in emergencies. Wind vane measures wind direction and communicates with the yaw drive to orient the turbine properly with respect to the wind. The yaw drive is used to keep the rotor facing into the wind as the wind direction changes.

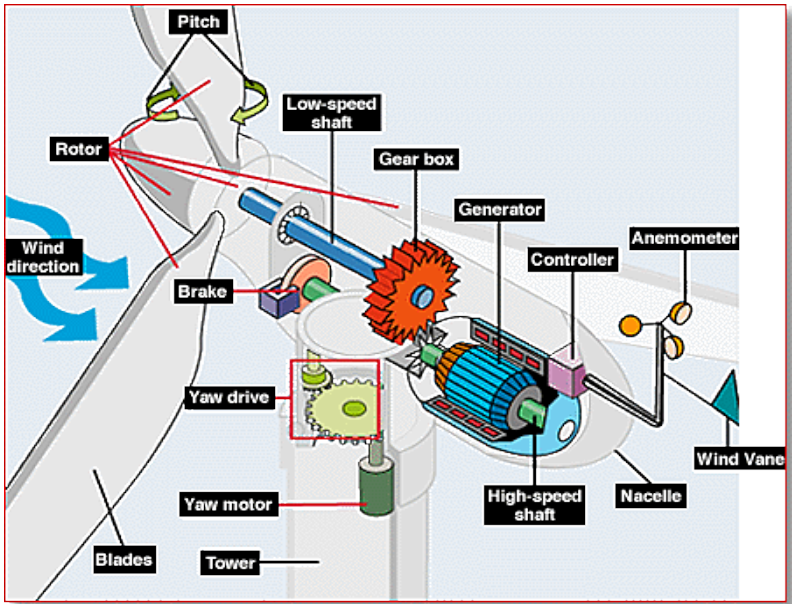

Fig. 2.2. Each part of wind generator system [52]

The modern wind turbine generator system can operate as fixed speed or variable speed. The fixed speed wind turbines are equipped with an induction generator (squirrel cage rotor or wound rotor). This type of wind turbine is designed to achieve maximum efficiency at one particular wind speed. Some fixed speed wind turbine has two winding set which are used at low and high wind speed respectively in order to increase power production. In variable speed wind turbines, it is possible to adapt continuously the rotational speed of the wind turbine to the wind speed. By this way, the maximum aerodynamic efficiency can be achieved over a wide range of wind speed [53]. The variable speed wind turbine is typically equipped with an induction or synchronous generator. The Doubly Fed Induction Generator (DFIG) and Permanent Magnet Synchronous Generator (PMSG) are mostly used as variable speed wind generator.

2.2. Extracting Power from the wind Energy

2.2.1. Wind Energy

Wind is one form of solar energy. Winds are caused by the uneven heating of the atmosphere by the sun, the irregularities of the earth's surface, and rotation of the earth. Wind flow patterns are modified by the earth's terrain, bodies of water, and vegetative cover [53].

Wind energy can be converted into useful form of energy, for example, modern wind turbines to generate electricity, windpumps for water pumping or drainage, windmills for mechanical power, or sails to propel ships. Wind energy, as an alternative to fossil fuels, is plentiful, renewable, widely distributed, clean, produces no greenhouse gas emissions during operation and uses little land [54]. Effects on the environment are generally less problematic than those from other power sources. As of 2011, more than 83 countries around the world are using wind power on a commercial basis.[4]

A basic understanding of the theory for extracting energy from the wind is helpful for understanding the fundamental of wind power technology. The kinetic energy of a volume of air *V*, moving at speed U_w is [55]:

$$E_k = 0.5\rho V U_w^2 \tag{2-1}$$

where:

E_k = kinetic energy (Kg m^2/sec^2 or Joules)
ρ = air density (kg/m^3)
V = volume of air (m^3)
U_w = wind speed (m/sec)

Power is expressed in kinetic energy per unit time, $d(E_k)/dt$. To obtain the expression of wind power, equation (2-1) can be rewritten as:

$$K_e = 0.5\rho(A.dx)V_w^2 \tag{2-2}$$

The volume of air *V* is expressed by an area *A* perpendicular to the wind flow multiplied by horizontal displacement in the direction of wind flow *dx*. The power from wind *P* or change in kinetic energy per unit time is expressed by:

$$P = \frac{d(K_e)}{dt} = \frac{d}{dt}(0.5\rho(A.dx)V_w^2) = 0.5\rho(A.\frac{dx}{dt})V_w^2 \tag{2-3}$$

Since dx/dt is in fact the wind speed V_w, the power *P* can be expressed by:

$$P = 0.5\rho A.V_w^3 \tag{2-4}$$

2.2.2. Power Output from Ideal Wind Turbine [55]

Figure 2.3 shows a wind turbine with rotor radius *R*, exposed to a uniform, non turbulent flow. The undistributed velocity has magnitude U_{wo} and a direction perpendicular to the rotor. Behind the rotor, a circular wake with a uniform speed deficit aU_{wo} expands. On the other words, "*a*" represents the fractional loss of wind speed through the rotor. It is assumed that the wake at the point of the creation has radius equal to rotor radius *R*, increasing to *r*

some distance downstream. Outside of this area impacted by the wind turbine, the wind speed is assumed to have the free stream value U_{wo}. A cylindrical control volume is devised so that it starts in the undisturbed upstream flow (to the left) and has a radius r, coinciding with the wake radius where it ends (to the right). Thus the flow speed is $U_{wa}=U_{wo}-aU_{wo}=U_{wo}(1-a)$ at the right end of the cylinder and the uniform flow speed outside the control volume is U_{wo}.

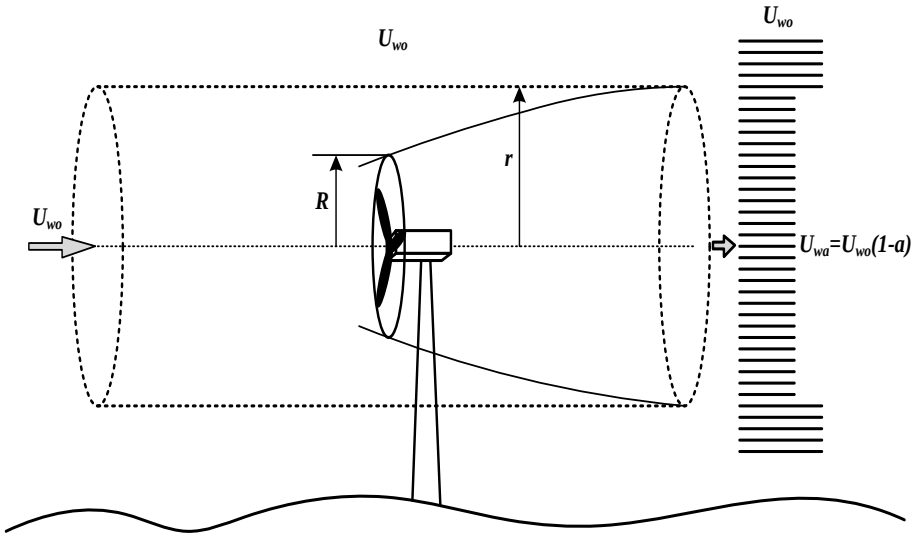

Figure 2.3. Air steam around the wind turbine [55]

The volume of air V in the cylinder is equal to the cross-sectional area πR^2 multiplied by the horizontal displacement, dx. By setting the horizontal depth of the air volume equal to distance travelled by U_{wa} per unit of time dt, the horizontal displacement dx equals U_{wa}. Thus, the volume air V is equal to $\pi R^2 U_{wa}$, and the kinetic energy of the air volume at any given time is equal to $0.5\pi R^2 U_{wa} U_w^2$. Power equals the change in kinetic energy over time. At left end of the cylinder in Fig. 2.3 the wind speed is U_{wo}, and the kinetic energy is $0.5\pi R^2 U_{wa} U_{wo}^2$, while at the right end of the cylinder the wind speed is U_{wa}, and the kinetic energy is $0.5\pi R^2 U_{wa} U_{wa}^2$. Therefore, the power extracted by the wind turbine, P_{wt}, represented by change in kinetic energy through the cylinder is given by:

$$P_{wt} = 0.5\rho\pi R^2 U_{wa}(U_{wo}^2 - U_{wa}^2) \tag{2-5}$$

The power is often expressed in terms of the free wind speed U_{wo}, the swept rotor area defined as the area of the circular disc by blade tips (πR^2), and the power coefficient, C_p, representing the fraction of the wind kinetic energy extracted by the wind turbine. In the other expression, the power is given by:

$$P_{wt} = 0.5\rho\pi R^2 C_p U_{w0}^3 \tag{2-6}$$

The power coefficient of wind turbine can reach to the maximum of 16/27 = 0.593 and it is called the *Betz* coefficient [56]. It is known that an actual turbine cannot extract more than 59.3 percent of the wind power in an undisturbed tube of air of the same area. In practice, the fraction of power extracted will always be less because of mechanical imperfections. A good fraction is 35 – 40 % under optimum conditions, although fractions as high as 50 % have been claimed. A turbine, which can extract 40 % of the power in the wind, is extracting about two-third of the amount that would be extracted by an ideal turbine. This is rather good, considering the aerodynamic problems of constantly changing wind speed and direction as well as the frictional loss due to blade surface roughness.

2.2.3. Power Output from Practical Wind Turbine

The fraction of power extracted from the power in the wind by a practical wind turbine is usually given by the symbol C_p, standing for the coefficient of performance or power coefficient. Using this notation and dropping the subscripts of Eq. 2.6, the actual mechanical power output can be written as [57]:

$$P_{wt} = 0.5\rho\pi R^2 U_w^3 C_p(\lambda,\beta) \tag{2-7}$$

where

P_{wt} = captured wind power (watts)
ρ = air density (Kg/m3)
R = radius of rotor blade (m)
U_w = wind speed (m/s)
C_p = the power coefficient.

The value of C_p is depended on tip speed ratio (λ) and blade pitch angle (β) based on the turbine characteristics as follows [57].

$$C_p(\lambda,\beta) = c_1\left(\frac{c_2}{\lambda_i} - c_3\beta - c_4\right)e^{\frac{-c_5}{\lambda_i}} + c_6\lambda \tag{2-8}$$

with

$$\lambda = \frac{\omega_r R}{U_w} \tag{2-9}$$

$$\frac{1}{\lambda_i} = \frac{1}{\lambda - 0.08\beta} - \frac{0.035}{\beta^3 + 1} \tag{2-10}$$

where c_1 to c_6 denote characteristic coefficients of wind turbine (c_1=0.5176, c_2=116, c_3=0.4, c_4=5, c_5=21 and c_6=0.0068) and ω_r is rotational speed of turbine in rad/sec [58].

The *Cp*-λ characteristic for different values of β is shown in Fig. 2.4. It is seen that the optimum value of C_p (C_{popt}=0.48) is achieved at λ = 8.1 with $\beta = 0^0$. This value of λ is set as the optimal value (λ_{opt}).

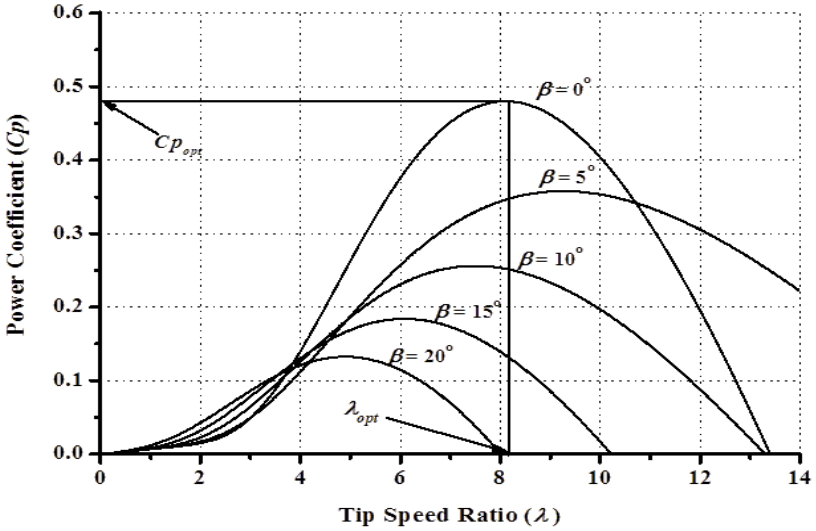

Figure 2.4. *Cp* - λ characteristic for different pitch angle

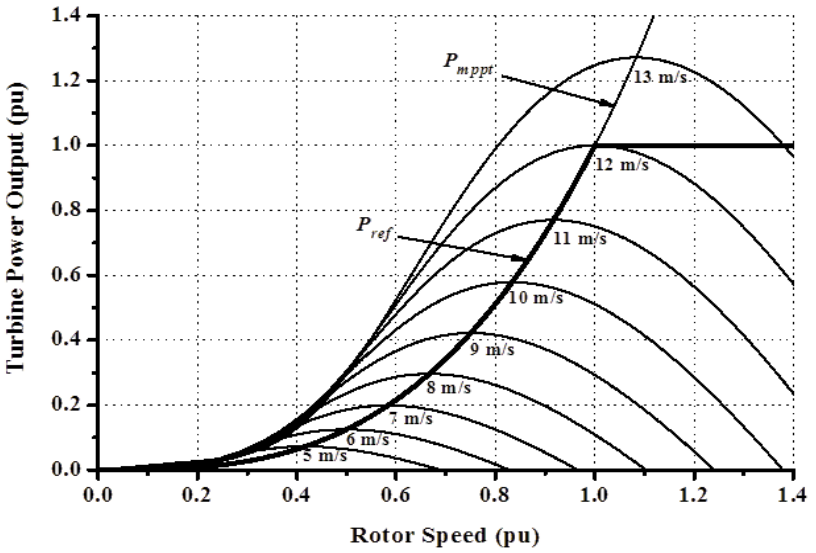

Fig. 2.5. Turbine power characteristic ($\beta = 0^0$)

Fig. 2.5 depicts the turbine output power as a function of the rotor speed for different wind speeds with the blade pitch angle β=0^0. This figure is obtained with the default parameters (base wind speed = 12 m/sec, maximum power at base wind speed = 1 pu, and base rotational speed = 1 pu). In variable speed wind turbines, the rational speed (ω_r) of wind turbine is controlled to follow the Maximum Power Point Trajectory (MPPT). Since the precise measurement of wind speed is difficult, it is better to calculate the maximum power without measuring the wind speed as follows [59]:

$$P_{mppt} = 0.5\rho\pi R^2 \left(\frac{\omega_r R}{\lambda_{opt}}\right)^3 C_{p\_opt} \tag{2-11}$$

where λ_{opt} and C_{p_opt} are optimum values of tip speed ratio and power coefficient, respectively. From eq. (2-11), it is clear that the maximum power generated is proportional to the cube of the rotational speed. The maximum power (P_{mppt}) is calculated based on the MPPT, which becomes the reference power (P_{ref}).

2.3. Drive Train Modeling

The drive train of a wind turbine generator system consists of the following elements: a blade-pitching mechanism with a spinner, a hub with blades, a rotor shaft and a gearbox with breaker and generator [60]. Depending on the complexity of the study, the complexity of the drive train modeling differs. For example, when the problems such as torsional fatigue are studied, dynamics of all parts have to be considered. For these reasons, two-lumped mass or more sophisticated models are required. However, when the study focuses on the interaction between wind farms and grid system, the drive train can be treated as one-lumped mass model with acceptable precision for the sake of time efficiency [61], [62]. In the present study, it is defined by the following equation:

$$\frac{d\omega_r}{dt} = \frac{T_e - T_m}{J_{eq}} - \frac{B_m}{J_{eq}}\omega_r \tag{2-12}$$

where ω_r is the mechanical angular speed [rad/s] of the generator, B_m is the damping coefficient [Nm/s], T_e is the electromechanical torque [Nm], T_m is the mechanical torque of the wind turbine, and J_{eq} is the equivalent rotational inertia of the generator (kg.m^2), which is derived from [61]

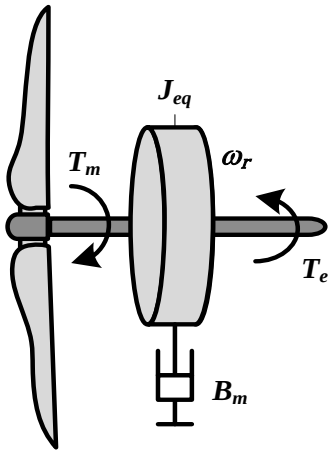

Fig. 2.6. One mass model of wind turbine

$$\frac{d\omega_r}{dt} = J_g + \frac{J_{wt}}{n_g^2} \tag{2-13}$$

where J_g and J_{wt} are the generator and the rotor rotational inertias (kg.m^2) respectively, *ng* is the gear ratio, which can be set 1 if no gearbox is used (in case of direct drive system). The scheme of the one-mass wind turbine model is given in Fig. 2.6.

2.4. Pitch Angle Controller

Wind power extraction by wind turbine depends on the wind speed, and thus, the output power of a wind generator always fluctuates due to the wind speed variations. In order to maintain the output power of generator under the rated level, two pitch controllers are considered in this paper. Figs. 2.7 and 2.8 show the models of the pitch controllers for fixed speed and variable speed wind turbines, respectively. The control loop of the pitch actuator is represented by a first-order transfer function with an actuator time constant (T_s=5) and the pitch rate limiter of 10 deg/s [59]. A classical PI controller is used to manage tracking error. In fixed speed wind turbine, the pitch controller is used to regulate power output of SCIG under the rated power (P_{IG} =1 pu), and in variable speed wind turbine, the pitch controller is used to regulate rotational speed of PMSG under its rated value (ω_r=1pu).

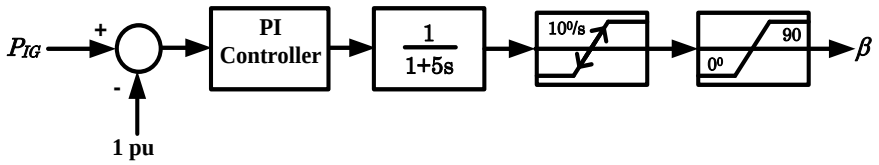

Fig. 2.7. Pitch controller used in fixed speed wind turbine

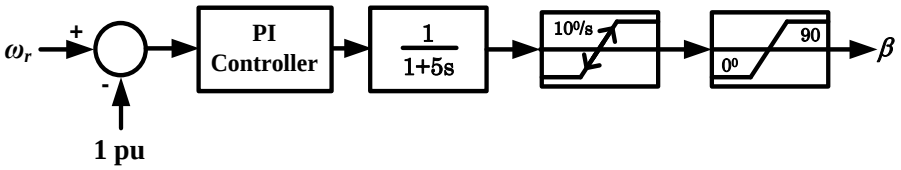

Fig. 2.8. Pitch controller used in variable speed wind turbine

2.5. Fixed Speed Wind Generator

2.5.1. Induction Generator Principle [63]

An induction generator or asynchronous generator is a type of AC electrical generator that uses the principles of induction motors to produce power. Induction generators operate by

mechanically turning their rotor in generator mode, giving negative slip. In most cases, a regular AC asynchronous motor is used as a generator, without any internal modifications.

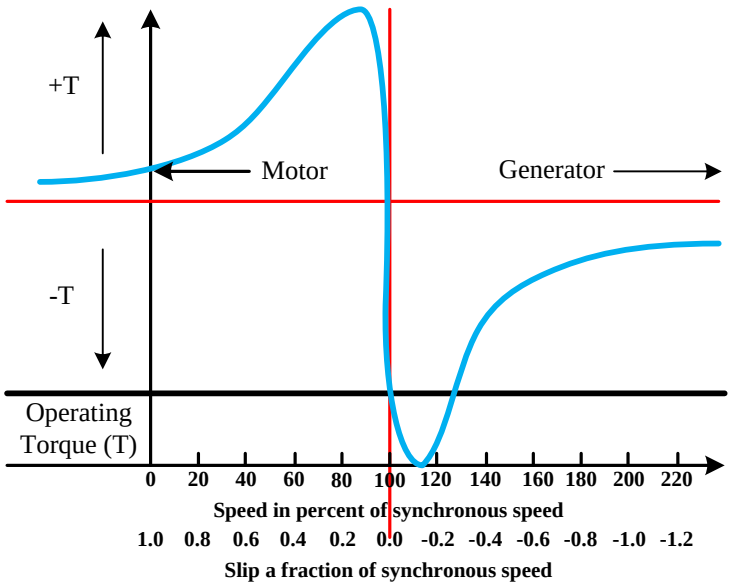

Fig. 2.9. Torque slip diagram of an induction machine

Induction generators produce electrical power when their shaft is rotated faster than the synchronous frequency. For a typical four-pole motor (two pairs of poles on stator) operating on a 60 Hz electrical grid, synchronous speed is 1800 rotations per minute. Similar four-pole motor operating on a 50 Hz grid will have synchronous speed equal to 1500 rpm. In normal motor operation, stator flux rotation is faster than the rotor rotation. This is causing stator flux to induce rotor currents, which create rotor flux with magnetic polarity opposite to stator. In this way, rotor is dragged along behind stator flux, by value equal to slip. In generator operation, certain prime mover is driving the rotor above the synchronous speed. Stator flux still induces currents in the rotor, but since the opposing rotor flux is now cutting the stator coils, active current is produced in stator coils, and motor is now operating as a generator, and sending power back to the grid system. The rotating magnetic flux from the stator induces currents in the rotor, which also produces a magnetic field. If the rotor turns slower than the rate of the rotating flux, the machine acts like an induction motor. If the rotor is turned faster, it acts like a generator, producing power at the synchronous frequency. As illustrated in Fig. 2.9 an induction motor becomes a generator if it is driven by an external torque at greater than 100% of the synchronous speed. This corresponds to a few % of negative slip. This means that the rotor is rotating faster than the stator rotating magnetic field. Since the rotor is cutting the stator magnetic field in the opposite direction (leading), the rotor induces a voltage into the stator feeding electrical energy back into the power line.

Active power delivered to the line is proportional to slip above the synchronous speed. Full rated power of the generator is reached at very small slip. 60Hz generator with 4 poles will not generate power at synchronous speed of 1800 rpm. When the driving speed is increased to, for example, 1860 rpm, however, full output power is produced. If the prime mover is unable to produce enough power to fully drive the generator, speed will remain somewhere between 1800 and 1860 rpm range.

2.5.2. SCIG Wind Turbine Topology

A fixed speed wind turbine with SCIG is simplest electrical topology in a wind turbine concept. The schematic configuration of the fixed speed wind turbine is depicted in Fig. 2.10. It consists of SCIG directly connected to the grid, a soft-starter and a capacitor bank. The wind turbine transfers the kinetic energy of wind flow into mechanical energy. The SCIG transforms the mechanical power into electrical power and delivers the power directly to the grid system. Generally, the rotational speed of the generator is relatively high compared with that of wind turbine. Therefore, the generator speed needs to be stepped down by using a multiple-stage gearbox with an appropriate gear ratio.

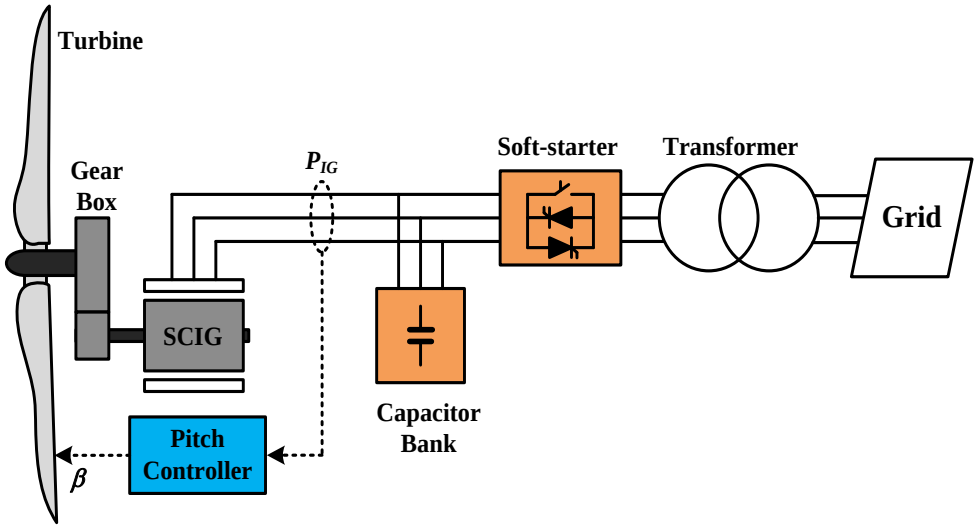

Fig. 2.10. Fixed speed wind turbine with SCIG configuration

The SCIG absorbs significant amount of reactive power from the grid. The reactive power consumption increases along with active power output. In order to compensate reactive power consumption a capacitor bank should be installed close to the generator terminal.

Since mechanical power is converted directly to electrical power by the generator, complex controller is not needed in the electrical part of a fixed speed wind turbine. However, a pitch controller is needed to regulate the pitch angle of the turbine blades (β) to keep power

output of SCIG (P_{IG}) under the rated value. The advantages of a fixed-speed wind turbine are that it has a simple design with high reliability and has low investment and maintenance costs. However, low aerodynamic efficiency, high mechanical stress during gusty wind speeds, and difficulties in adapting to new grid compliances, such as fault ride-through and reactive power support, are the shortcomings of this concept.

2.5.3. SCIG Model

The electrical part of the machine is represented by a fourth-order state-space model. All electrical variables and parameters are referred to the stator. All stator and rotor quantities are in the arbitrary dq-axis reference frame. Fig. 2.11 show the equivalent circuit of induction machine in the dq-axis reference frame. R'_s and R'_r are the resistance of the stator and rotor windings, respectively. V'_{ds}, V'_{qs}, I'_{ds}, I'_{qs}, ψ'_{ds}, and ψ'_{qs} are the d and q axis components of voltage, current and flux of the stator. V'_{dr}, V'_{qr}, I'_{dr}, I'_{qr}, ψ'_{dr}, and ψ'_{qr} are the d and q axis components of voltage, current and flux of the rotor.

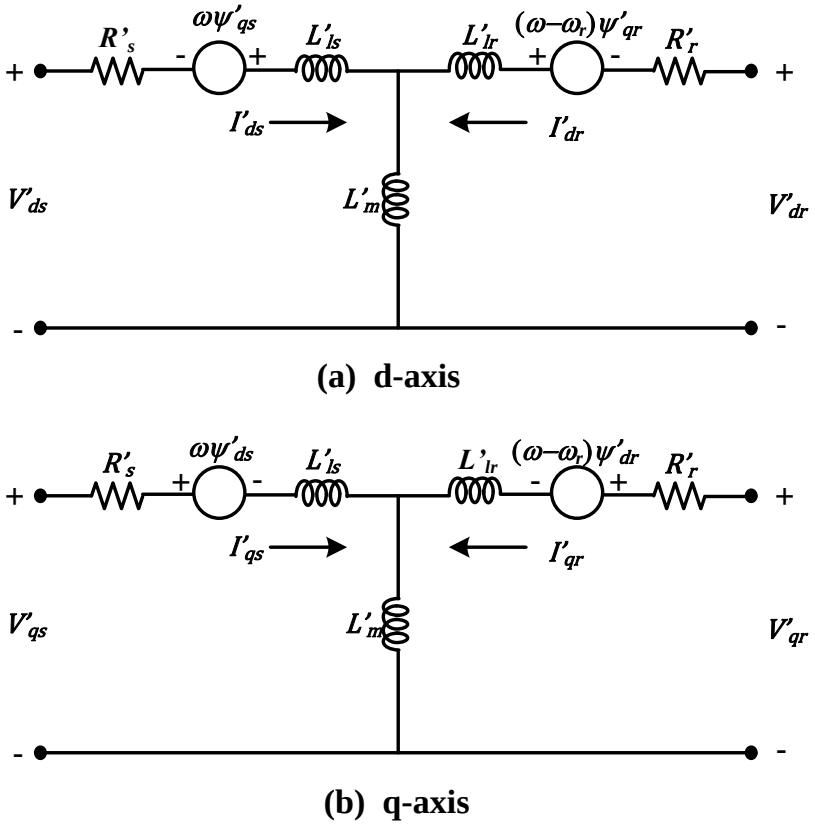

Fig. 2.11. Equivalent circuit of induction machine in the dq-axis reference frame

The differential equations of induction generator model are expressed as [58]:

$$V'_{ds} = R'_s I'_{ds} + \frac{d\psi'_{ds}}{dt} - \omega\psi'_{qs} \tag{2-14}$$

$$V'_{qs} = R'_s I'_{qs} + \frac{d\psi'_{qs}}{dt} + \omega\psi'_{ds} \tag{2-15}$$

$$V'_{dr} = R'_r I'_{dr} + \frac{d\psi'_{dr}}{dt} - (\omega - \omega_r)\psi'_{qr} \tag{2-16}$$

$$V'_{qr} = R'_r I_{qr} + \frac{d\psi'_{qr}}{dt} + (\omega - \omega_r)\psi'_{dr} \tag{2-17}$$

The stator and rotor flux linkages can be expressed as :

$$\psi'_{ds} = L'_s I'_{ds} + L'_m I'_{dr} \tag{2-18}$$

$$\psi'_{qs} = L'_s I'_{qs} + L'_m I'_{qr} \tag{2-19}$$

$$\psi'_{dr} = L'_r I'_{dr} + L'_m I'_{ds} \tag{2-20}$$

$$\psi'_{qr} = L'_r I'_{qr} + L'_m I'_{qs} \tag{2-21}$$

where $L'_s = L'_{ls} + L'_m$ and $L'_r = L'_{lr} + L'_m$. The electromagnetic torque of the induction machine can be expressed as:

$$T_{e=} 1.5p\left(\psi'_{ds} I'_{qs} - \psi'_{qs} I'_{ds}\right) \tag{2-22}$$

where p is the number of pole pairs.

The equations for active power generated, P_{IG}, and reactive power consumed, Q_{IG}, are:

$$P_{IG=} V'_{ds} I'_{ds} + V'_{qs} I'_{qs} \tag{2-23}$$

$$Q_{IG=} V'_{qs} I'_{ds} - V'_{ds} I'_{qs} \tag{2-24}$$

2.6. Variable Speed Wind Turbine with PMSG

Variable-speed wind turbines are designed to operate at a wide range of rotor speeds. Their rotor speed varies with the wind speed or other system variables, based on the design employed. Additional speed and power controls allow variable-speed turbines to extract more energy from a wind regime than would be possible with fixed-speed turbines [16]. The advantage of converter-based systems is that they allow independent real and reactive power control.

2.6.1. PMSG Wind Turbine Topology

Typical configuration of a PMSG wind turbine is shown in Fig. 2.12. A direct-drive PMSG wind turbine uses a synchronous generator whose rotor is excited by permanent magnets and whose stator windings are connected to the grid through a full-rating power converter. The large number of poles mounted on the rotor allows the generator to operate at low speeds. This means that the gearbox can be omitted, and the generator is directly coupled to the wind turbine rotor.

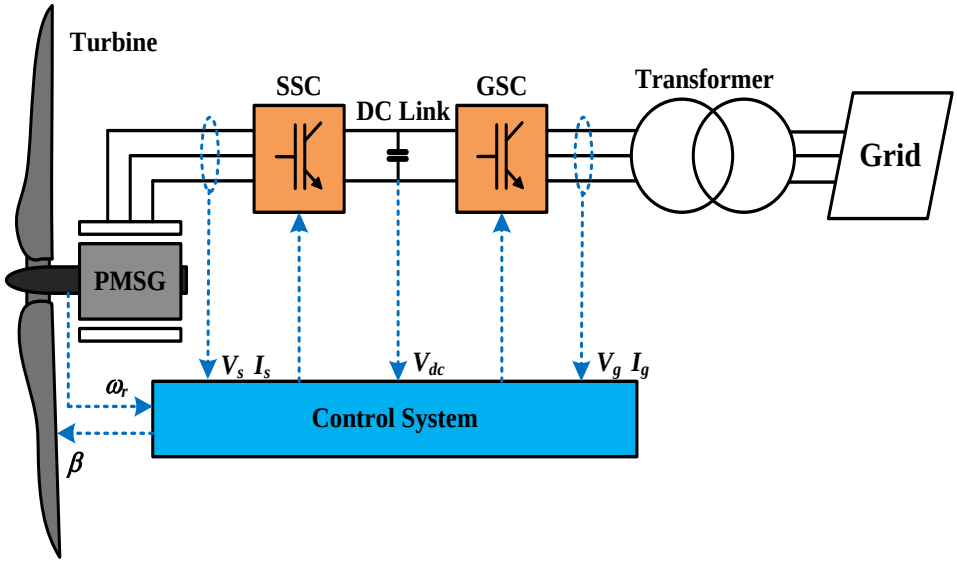

Fig. 2.12. Variable speed wind turbine with PMSG configuration

The back to back power converter consists of stator side converter (SSC) and the grid side converter (GSC) linked by a DC link circuit. The three-phase AC output of the generator is converted to DC output, and then it is fed to an IGBT-based inverter. The GSC output is supplied to a step-up transformer, which delivers the energy to the grid system. The rating of the power converter depends on the rated power of the generator. The full scale power converters control the generated power and the power flow to the grid. In addition, it decouples the electrical grid frequency and the mechanical rotor frequency, and thus the variable speed generation can be possible.

2.6.2. PMSG based Wind Turbine Model

The electrical model of PMSG wind turbine can be represented by the equivalent circuit shown in Fig. 2.13 [34]. The equivalent circuit model is divided in three parts; generator side, DC-link circuit, and grid side.

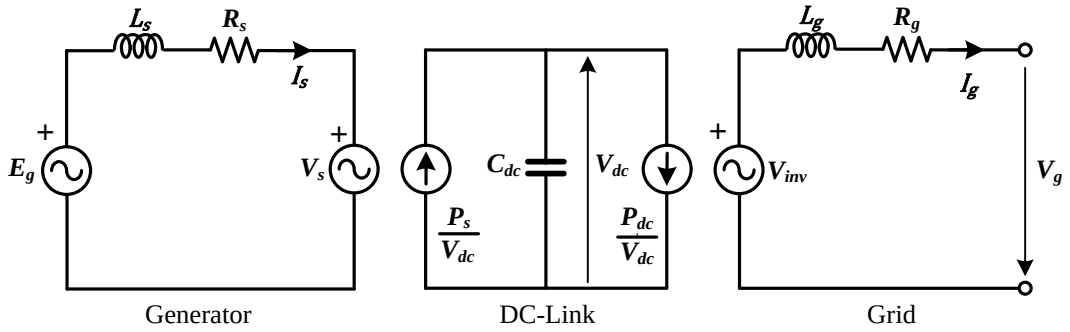

Fig. 2.13. Equivalent circuit of PMSG based wind turbine [34]

2.6.2.1. PMSG model

As the generator is directly coupled to the wind turbine rotor, the generator electrical angular frequency (ω_e) is derived from the mechanical rotor speed ω_r and the number of generator poles n_p.

$$f_e = \frac{n_p}{2} f_r = \frac{n_p}{2} \frac{\omega_r}{2\pi} \tag{2-25}$$

$$\omega_e = 2\pi f_e = \frac{n_p}{2} \omega_r \tag{2-26}$$

Where f_e and f_r are electrical and rotor angular frequency (in Hz) of PMSG, respectively.

The generation system is composed of a PMSG and a full-rating power converter. In power system analyses, the magnetic flux distribution around the air gap of a synchronous generator is assumed to be sinusoidal. Therefore, the flux distribution linked with the stator coil is sinusoidal, and then the electromotive forces are also sinusoidal [64]. In fact, the induced voltage E_g generated by the permanent magnets can be expressed as:

$$E_g = 2\pi f_e \psi_m = \omega_e \psi_m \tag{2-27}$$

where ψ_m is the flux linkage of stator coil.

A commonly used PMSG transient model is the Park model. Using the generator convention, the space vector theory yields the stator voltage equations in the form as follows [33]:

$$\begin{pmatrix} V_{ds} \\ V_{qs} \end{pmatrix} = -R_s \begin{pmatrix} I_{ds} \\ I_{qs} \end{pmatrix} - \frac{d}{dt} \begin{pmatrix} \psi_{ds} \\ \psi_{qs} \end{pmatrix} + \omega_e \begin{pmatrix} 0 & -1 \\ 1 & 0 \end{pmatrix} \begin{pmatrix} \psi_{ds} \\ \psi_{qs} \end{pmatrix} \tag{2-28}$$

where R_s is the resistance of the stator winding and V_{ds}, V_{qs}, I_{ds}, I_{qs}, ψ_{ds}, and ψ_{qs} are the d and q axis components of the stator voltage, current and flux. If the d-axis is aligned along the rotor-flux position, the stator flux linkages are

$$\begin{pmatrix}\psi_{ds}\\ \psi_{qs}\end{pmatrix}=\begin{pmatrix}L_s+L_{dm} & 0\\ 0 & L_s+L_{qm}\end{pmatrix}\begin{pmatrix}I_{ds}\\ I_{qs}\end{pmatrix}+\begin{pmatrix}\psi_m\\ 0\end{pmatrix} \quad (2\text{-}29)$$

where L_s is the leakage inductance of the stator winding, L_{dm} and L_{qm} are the d and q axis magnetizing inductances. Substituting eq.(2-29) into (2-28), the stator voltage equations become

$$\begin{pmatrix}V_{ds}\\ V_{qs}\end{pmatrix}=-R_s\begin{pmatrix}I_{ds}\\ I_{qs}\end{pmatrix}-\frac{d}{dt}\begin{pmatrix}L_{ds}I_{ds}\\ L_{qs}I_{qs}\end{pmatrix}+\omega_e\begin{pmatrix}-L_{qs}I_{qs}\\ L_{ds}I_{qs}+\psi_m\end{pmatrix} \quad (2\text{-}30)$$

where $L_{ds} = L_s + L_{dm}$ and $L_{qs} = L_s + L_{qm}$. Under the steady-state condition, eq.(2-30) reduces to

$$\begin{pmatrix}V_{ds}\\ V_{qs}\end{pmatrix}=\begin{pmatrix}-R_s & -\omega_e L_{qs}\\ \omega_e L_{ds} & -R_s\end{pmatrix}\begin{pmatrix}I_{ds}\\ I_{qs}\end{pmatrix}+\begin{pmatrix}0\\ \omega_e\psi_m\end{pmatrix} \quad (2\text{-}31)$$

The electromagnetic torque, stator active and reactive powers are expressed as follows:

$$T_{e=}\frac{1}{2}n_p\left(\psi_{ds}I_{qs}-\psi_{qs}I_{ds}\right)=\frac{1}{2}n_p\left(\psi_m I_{qs}+\left(L_{ds}-L_{qs}\right)I_{ds}I_{qs}\right) \quad (2\text{-}32)$$

$$P_s = V_{ds}I_{ds}+V_{qs}I_{qs} \quad (2\text{-}33)$$

$$Q_s = V_{qs}I_{ds}-V_{ds}I_{qs} \quad (2\text{-}34)$$

2.6.2.2. DC-link circuit model

The SSC, which acts as a rectifier, converts the low frequency output of the generator to DC power, which is supplied to the GSC through the DC link and finally fed to the grid. The DC link contains a capacitor that is charged and discharged by SSC and GSC currents, respectively. When the power losses in the DC link are ignored, the dynamic behaviour of DC voltage across capacitor (V_{dc}) can be expressed by the following equation:

$$\frac{dV_{dc}}{dt}=\frac{1}{CV_{dc}}\left(P_{s-}P_{dc}\right) \quad (2\text{-}35)$$

where C is the value of DC link capacitor, and P_{dc} is the power supplied to GSC expressed as

$$P_{dc} = V_{dc}I_{dg}+V_{qc}I_{qg} \quad (2\text{-}36)$$

where I_{dg} and I_{qg} are the component of the current delivered to the grid.

2.6.2.3. Grid side model

The GSC is also a current controlled voltage source converter controlled by IGBT switches. The voltage is controlled in such a way to transmit the active power from the DC link

to the grid and to achieve the desired power factor/voltage on the grid. The dynamic model of the grid voltage and current on the reference frame rotating synchronously with the grid voltage space vector is

$$\begin{pmatrix} V_{dg} \\ V_{qg} \end{pmatrix} = \begin{pmatrix} V_{dc} \\ V_{qc} \end{pmatrix} + R_g \begin{pmatrix} I_{dg} \\ I_{qg} \end{pmatrix} + \omega L_g \begin{pmatrix} 0 & 1 \\ -1 & 0 \end{pmatrix} \begin{pmatrix} I_{dg} \\ I_{qg} \end{pmatrix} + L_g \frac{d}{dt} \begin{pmatrix} I_{dg} \\ I_{qg} \end{pmatrix} \quad (2\text{-}37)$$

where R_g and L_g are the grid inductance and resistance, respectively. V_{dc} and V_{qc} are voltage components of GSC. V_{dg} and V_{qg} are grid voltage components, and ω is the grid frequency.

Under steady state condition, the derivative terms are reduced to zero. Hence, eq.(2-37) can be expressed by:

$$\begin{pmatrix} V_{dg} \\ V_{qg} \end{pmatrix} = \begin{pmatrix} V_{dc} \\ V_{qc} \end{pmatrix} + \begin{pmatrix} R_g & \omega L_g \\ -\omega L_g & R \end{pmatrix} \begin{pmatrix} I_{dg} \\ I_{qg} \end{pmatrix} \quad (2\text{-}38)$$

The active and reactive power delivered to the grid can be expressed as

$$P_g = V_{dg} I_{dg} + V_{qg} I_{qg} \quad (2\text{-}39)$$

$$Q_g = V_{qg} I_{dg} - V_{dg} I_{qg} \quad (2\text{-}40)$$

2.6.3. Back to Back Converter of PMSG

A back-to-back converter provides an indirect AC-DC-AC connection in variable speed wind turbine system, resulting independence between the rotational speed of the blades and the frequency of the grid connected. This connection gives some advantages: voltage and frequency control of the local grid, improvement of the power quality, and better integration of wind energy to the electrical grid under both steady-state and transient operations [65].

Two level and three-level converters are commonly used in wind energy applications. Figs 2.14 and 2.15 shows two level and three level of the back to back converters, respectively. The back to back converter depicted in each figure consists of two three phase PWM converters with a common DC link circuit.

2.6.3.1. Two level converters

In two level converters a power circuit of three-phase voltage-source back-to-back converters is composed of twelve power semiconductor switches as shown in Fig. 2.14, where the two converters are linked through a DC capacitor. The stator side converter has three phase input voltages (V_{sa}, V_{sb}, V_{sc}) and coverts them to DC voltage (V_{dc}), which is the input voltage of the grid side converter, whereas the three phase voltages (V_{ga}, V_{gb}, V_{gc}) are the output voltages of the grid side converter.

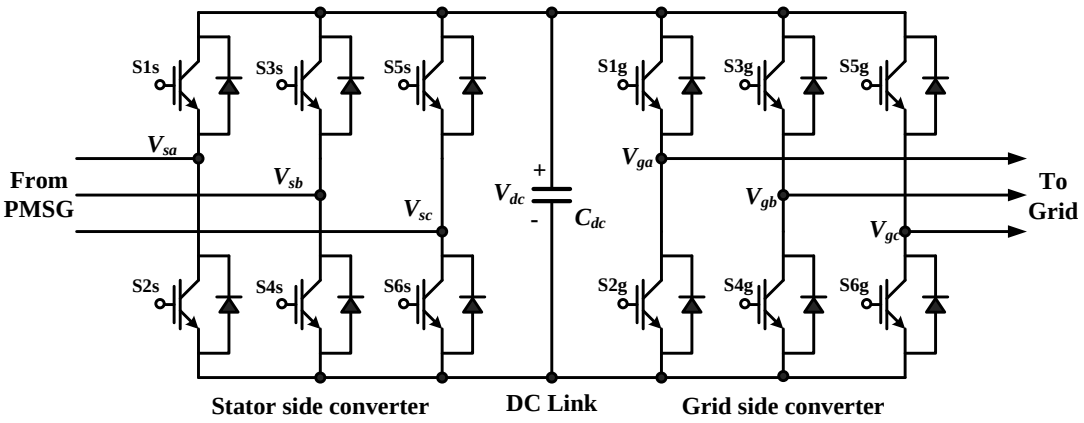

Fig. 2.14. Circuit configuration of two level back two back converters

The SPWM technique for modulation is considered. A triangular carrier waveform is compared with the reference sinusoidal waveform at the fundamental frequency of the output voltage. Then, the switching pulses (S1; S2) for phase A, (S3; S4) for phase B, and (S5; S6) for phase C, are generated [65], [66]. The switching states of the switches and the input voltage for three phase converters are listed in Table 3.1.

Table 3.1.

Switching state of two level converter

Input Voltage	Switching states					
	S_1	S_2	S_3	S_4	S_5	S_6
$+V_{dc}/2$	1	0	0	1	0	0
$+V_{dc}/2$	1	0	0	0	0	1
0	0	0	1	0	0	1
$-V_{dc}/2$	0	1	1	0	0	0
$-V_{dc}/2$	0	1	0	0	1	0
0	0	0	0	1	1	0

2.6.3.2. Three level converters

The circuit configuration of three-level back-to-back PWM converters consists of two neutral-point clamped converters linked through DC capacitors, as shown in Fig. 2.15. Each converter uses twelve switches and six additional diodes. To generate the switching pulses for the converters, two carrier waveforms are simultaneously compared with a sinusoidal waveform at the fundamental frequency. The switching states for the four switches of each phase and the input phase voltages for the AC/DC converters are described in Table 3.2 [65], [66].

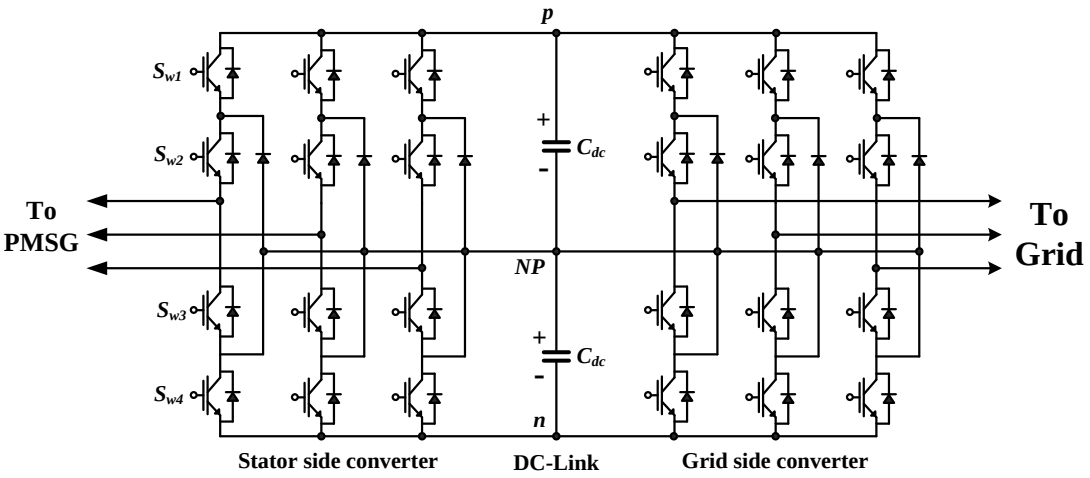

Fig. 2.15. Circuit configuration of three level back to back converters

Table 3.2.

Switching state of three level converter

Input Voltage	Switching states			
	Sw_1	Sw_2	S_{3w}	Sw_4
$+V_{dc}/2$	1	1	0	0
0	0	1	1	0
$-V_{dc}/2$	0	0	1	1

2.7. Chapter Summary

In this chapter, the basic theory of energy extraction from wind is described briefly. Then, wind turbine, drive train and pitch angel control models of wind turbine generator system are presented. The fixed speed and variable speed wind turbine topology overview and electrical modeling system are explained in detail. In additional, the two levels and three levels of back to back converters for PMSG has been discussed.

Chapter 3

A Control Strategy of PMSG based Variable Speed Wind Turbine for Wind Farm Stability Augmentation

In this chapter a control strategy of variable speed wind turbine with permanent magnet synchronous generator (VSWT-PMSG) for stability augmentation of wind farm including fixed speed wind turbines with SCIG is investigated. A suitable control scheme for back-to-back converters of PMSG is developed to augment dynamic behaviour (both transient and steady state stability) of the wind farm. During fault condition the DC link voltage increase significantly due to unbalance between powers produced by the generator and delivered to the grid system. In order to avoid the converter damage, the protection scheme using DC chopper is embedded on DC link circuit. In order to evaluate the effectiveness and capability of the proposed control strategy, two power system models are analysed in simulations study. In power system model 1, two wind farms composed of aggregate model of VSWT-PMSG and FSWT-SCIG are connected to an infinite bus. In power system model 2, two wind farms are connected to a multi machine power system. Simulation analyses of both transient and steady state characteristics are performed by using PSCAD/EMTDC.

3.1. Control Strategy of PMSG

The block diagram of control system for VSWT-PMSG proposed in this study is shown in Fig. 3.1. The VSWT-PMSG consists of the following components: a direct drive PMSG, back to back converters based on two levels of IGBT which are composed of stator side converter (SSC) and grid side converter (GSC), a DC-link circuit composed of a chopper with a resistance (R_{ch}) and a capacitor (C_{dc}), and two voltage source converter controllers (stator side controller and grid side controller).

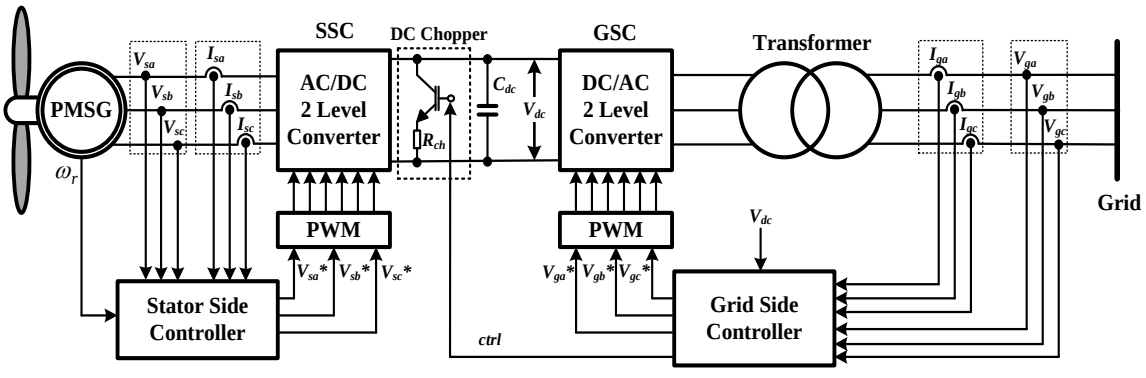

Fig. 3.1. Control system of PMSG

The SSC is connected to the stator of PMSG, and it converts the three phase AC voltage generated by PMSG to DC voltage. The three phase voltage and current are detected by the sensors on the stator terminal of PMSG. The rotor speed of PMSG is measured from the rotor of wind turbine. All outputs of the sensors are fed to the stator side controller as input signals in order to control the voltage references of the SSC for modulation.

In the GSC, the converter is connected to the grid system through a step up transformer. The grid current and the grid voltage are detected on the high voltage side of the transformer, respectively. The DC voltage (V_{dc}) is detected on the DC capacitor. The voltage reference of grid side voltage source converter for modulation is controlled by using the grid side controller. When a fault occurs in the grid, the V_{dc} increases significantly due to power unbalance between SSC and GSC. In order to protect the DC-link circuit, the controller activates the chopper by a trigger command (*ctrl*).

In both converters, the triangle signal is used as the carrier wave of Pulse Wave Modulation (PWM) operation. The Carrier frequency is selected to 3 KHz for both converters. The DC-link capacitor is 25000 μF. The rated DC-link voltage is 2.0 kV (1 pu).

3.1.1. SSC Controller System

The aim of the stator side controller is to control active and reactive power output of the PMSG. Detail of the stator side controller system is presented in the block diagram shown in Fig. 3.2. The current control loop is designed based on the d-q rotating reference frame. The rotor angle position (θ_r) used in the transformation between abc and dq variables is obtained from the rotor speed of generator. The active power (P_s) and reactive power (Q_s) of the

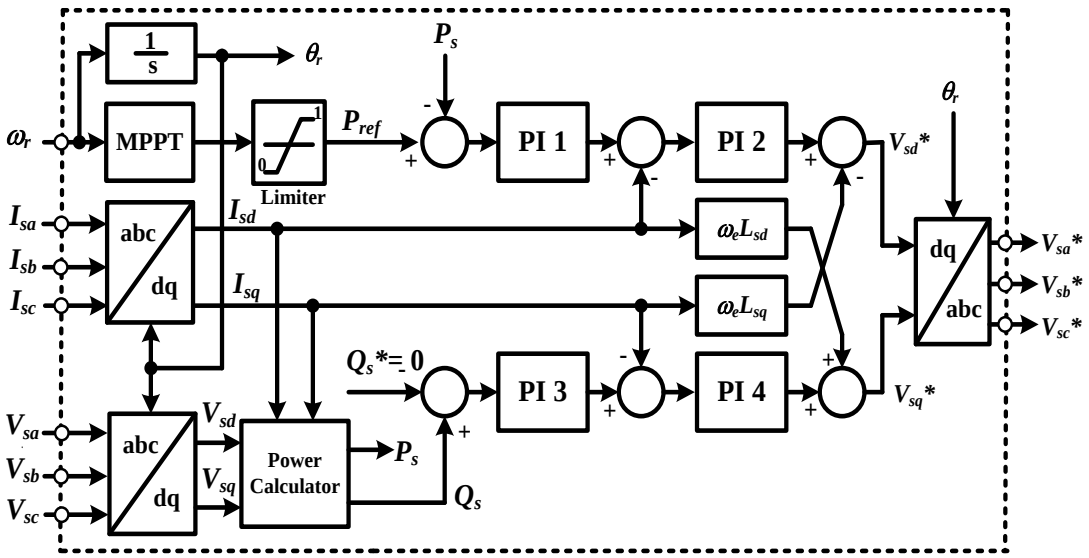

Fig. 3.2. Stator side controller system

generator are controlled by the d-axis current (I_{sd}) and the q-axis current (I_{sq}), respectively. The value of active power reference (P_{ref}) is determined by MPPT method. In order to maximize the active power output of PMSG, the reactive power reference (Q_s*) is set to zero to achieve unity power factor operation. The cross couplings, $I_{sd}\omega_e L_{sd}$ and $I_{sq}\omega_e L_{sq}$, should be compensated at the output of the current controllers in order to improve tracking capability of the control system. Finally, V_{sd}* and V_{sq}* are voltage reference of current controller which is used to generate the three phase reference voltage (V_{sa}*, V_{sb}*, V_{sc}*) to control stator currents of the PMSG

3.1.2. GSC Controller System

Grid side controller system is essential in design of overall control system for VSWT-PMSG connected to a grid system from a view point of stabilization of the FSWF-SCIG. In this paper, the aims of grid side controller system are: 1) to maintain DC link circuit voltage in order to transfer stably the active power of PMSG to grid system; 2) to maintain the grid voltage as well as to compensate the reactive power demand for SCIG.

Fig. 3.3 shows a block diagram of the grid side controller system. Again, in this control strategy, the control system based on the d-q rotating reference frame is implemented which has same rotational speed as the grid voltage. The three phase grid currents (I_{ga}, I_{gb}, I_{gc}) and the grid voltages (V_{ga}, V_{gb}, V_{gc}) are transferred into the d-q rotating reference frame by using Park transformation. The Phase Locked Loop (PLL) is used to extract the grid side phase angle (θ_g). The vector-type of PLL shown in Fig. 3.4 is used in this paper [67], [68].

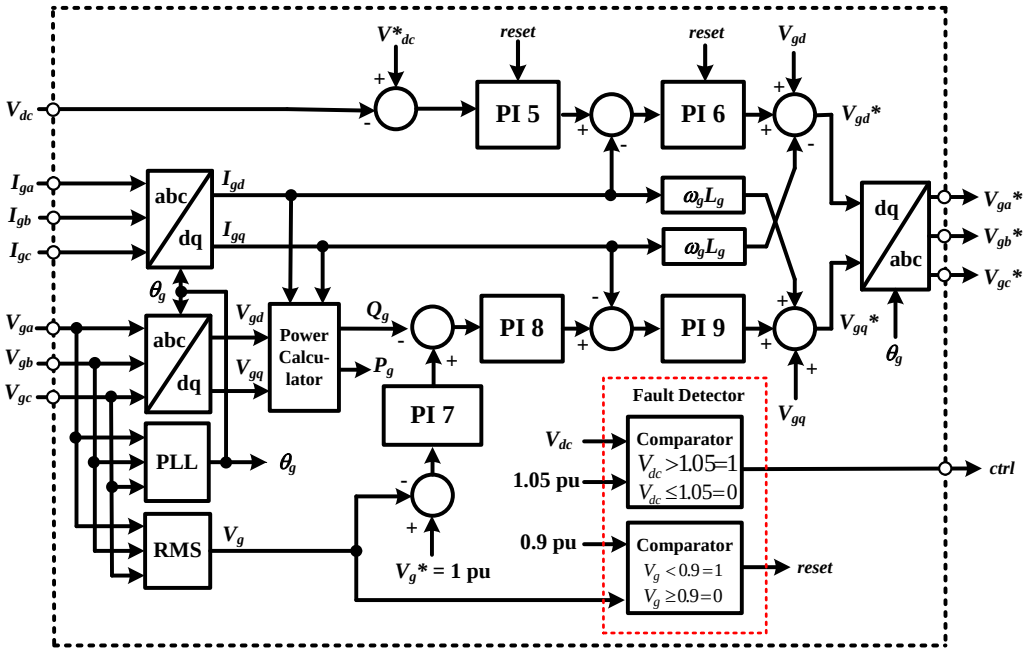

Fig. 3.3. Grid side controller system

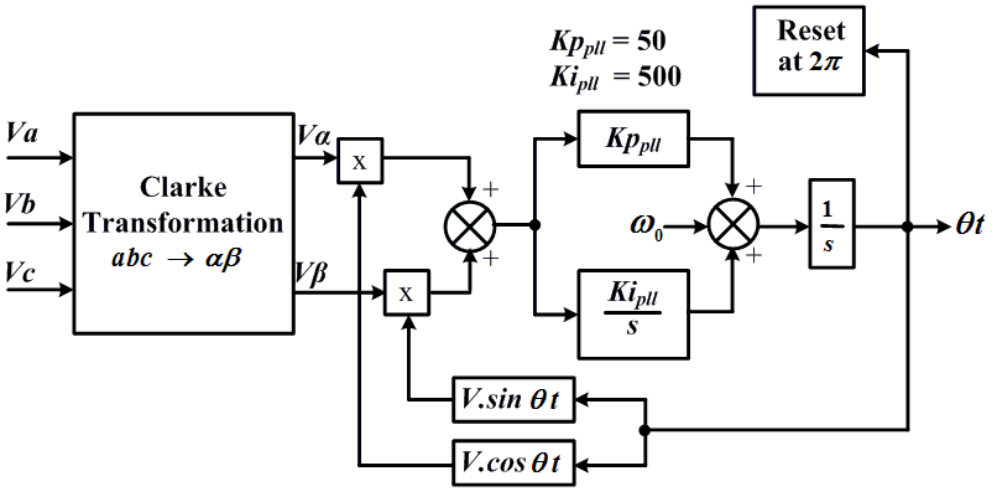

Fig. 3.4. Block diagram of Phase Locked Loop (PLL)

The controller is divided into two cascade loop control, one of which is for active power and the other is for the reactive power. When grid voltages on the stationary reference frame are transformed into the d-q rotating reference frame, V_{gd} is set to constant and V_{gq} is set to zero. Therefore, the active power (P_g) and reactive power (Q_g) delivered to the grid can be controlled separately by the d-axis current (I_{id}) and the q-axis current (I_{iq}), respectively. The voltage of DC-link capacitor (V_{dc}) is maintained constant in order to balance the active power generated by PMSG and the active power delivered to the grid. The d-axis current reference signal (I_{id_ref}) is determined from output of the DC-voltage controller, and the q-axis current reference signal (I_{iq_ref}) is obtained so that the grid terminal voltage (V_g) is kept constant at 1 pu. In order to improve tracking capability of the control system, the cross coupling should be canceled by adding $I_{gd}\omega L_g$ and $I_{gq}\omega L_g$ at the output of the current controllers. The output of current controller (V_{gd}* and V_{gq}*) is transformed into the stationery reference frame (V_{ga}*, V_{gb}*, V_{gc}*) which is used as reference signal for pulse wave modulation.

In normal mode operating condition, the voltage of DC-link capacitor (V_{dc}) is maintained constant in order to transfer the active power generated by PMSG to the grid. The d-axis current reference signal (I_{gd}*) is determined from output of the DC-voltage controller, and the q-axis current reference signal (I_{gq}*) is obtained from reactive power controller output. The reactive power reference (Q_g*) is set so that the terminal voltage at the high voltage side of the transformer remains constant. In grid fault mode condition, the active power transfer to the grid is set to zero by trigger reset command to PI 5 and PI 6. By using this way supplying reactive power to the grid can be maximized. At the same time the detector send the control signal command (*ctrl*) to trigger the DC link protection. The *reset* command is activated when the grid voltage decreases under 0.9 pu. The *ctrl* command is activated when the DC link voltage exceeds the predefined limit (2.1 kV, 1.05 pu).

Table 3.1.

The PI Controller Gains

PI Controller	K_p	K_i
PI 1	0.5	7
PI 2	0.01	0.5
PI 3	0.5	7
PI 4	0.01	0.5
PI 5	5.3	26
PI 6	0.05	2
PI 7	2	20
PI 8	2	20
PI 9	0.05	2

The coefficients of PI controllers (PI 1 to PI 9) were obtained based on the trial-and-error approach. A lot of values were investigated for different system conditions, and finally, the values shown in Table 3.1 are selected as best values.

3.1.3. DC-Link Protection Control

As explained before, during a network disturbance such as short circuit fault, the grid side converter output decreases and then the overvoltage can appear in the DC-link circuit of the back-to-back power converter of PMSG. In addition, the reactive power support from the grid side converter is proposed in this paper in order to enhance the stability of fixed speed wind generators, under which situation active power output from the grid side converter also needs to be decreased. Under these situations the DC-link voltage can increase due to the energy imbalance between the generator side converter and the grid side converter.

The breaking chopper circuit is proposed in this paper, which is embedded in the DC-link circuit in order to protect the DC-link capacitor during a fault condition as shown in Fig. 3.1. The chopper circuit is activated when the DC-link voltage exceeds the predefined limit (2.1 kV, 1.05pu) and then dissipates the active power in the protection resistance.

3.2. Stability Analysis of Wind Farm Connected to an Infinite Bus

3.2.1. Power System Model

The model system used in this study is shown in Fig. 3.5. Wind Farm 1 with PMSG rated at 15 MW is connected to 6.6 kV distribution system through a power converter, a 1.0/6.6 kV step up transformer and a short transmission line. The full-scale power converter is made up of two back-to-back IGBT bridges (the stator side converter, SSC, and the grid side converter,

GSC) linked by a DC bus. Wind Farm 2 with SCIG rated at 35 MW is connected to 6.6 kV distribution systems via a 0.69/6.6 kV transformer and a short transmission line. A capacitor bank is used for reactive power compensation at steady state. The value of capacitor C is chosen so that the power factor of the wind power station becomes unity during the rated condition. Total output of wind farms are supplied to the utility grid through a common step-up transformer (6.6/66 kV) and double circuit transmission line. In the figure, the transmission line parameters are numerically shown in the form of R+jX, where R and X represent the resistance and reactance, respectively. The system base is 100 MVA and parameters of the generators are shown in Table 3.2.

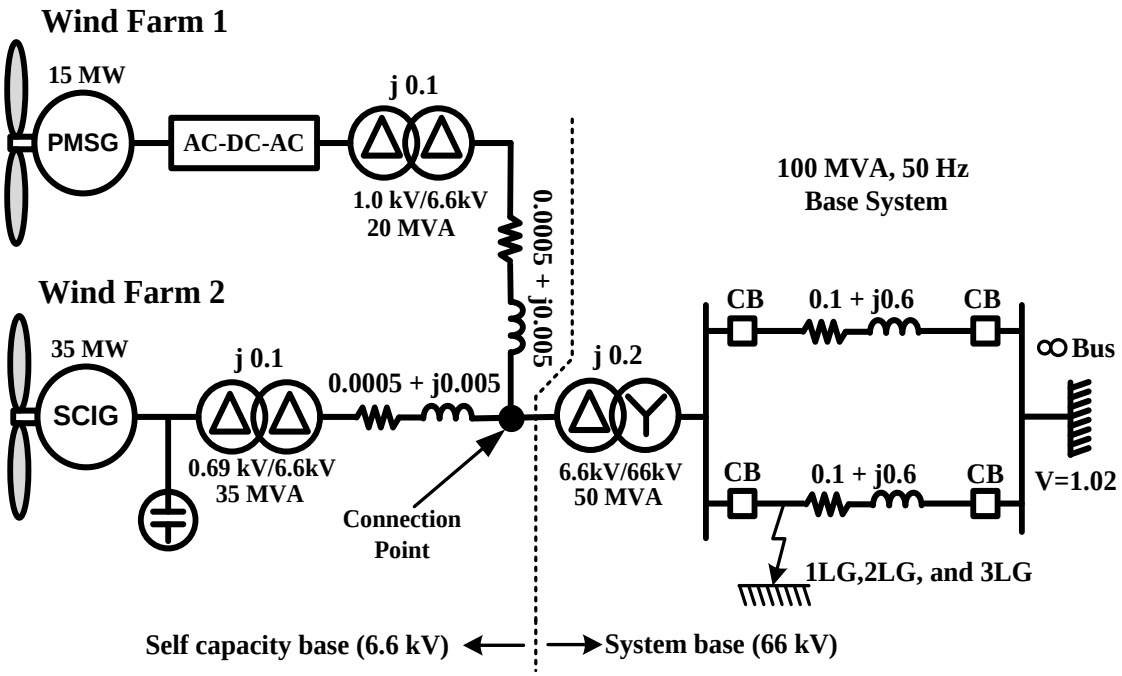

Fig. 3.5. Wind farms connected to infinite bus power system

Table 3.2

Generators parameters

IG	MW	35	**PMSG**	MW	15
	R1	0.01 (pu)		Rs	0.01 (pu)
	X1	0.1 (pu)		Ls	0.064 (pu)
	Xm	3.5 (pu)		Xd	0.9 (pu)
	R21	0.035 (pu)		Xq	0.7 (pu)
	R22	0.014 (pu)		Field Flux	1.4 (pu)
	X21	0.030 (pu)		H	3.0 s
	X22	0.089 (pu)			
	H	1.5 s			

3.2.2. Simulation study

In this study, a model system shown in Fig. 3.5, which is composed of two wind farms installed with fixed speed wind generators and variable speed wind generators respectively, is analyzed. The full-rating power converter of variable speed PMSG wind turbine system is controlled in such a way to maintain the grid voltage (voltage at the connection point) at desired reference level set by transmission system operator. Therefore, necessary reactive power for SCIG can also be supplied to restore the electromagnetic torque during a fault condition. Two cases are considered in the simulation study to show the effectiveness of the proposed control strategy. In Case 1, simulation study is performed using the model system of Fig. 3.5. In Case 2, simulation study is performed using another model system in which PMSG of Wind Farm 1 is replaced by SCIG (15 MW). Simulations were performed by using PSCAD/EMTDC.

3.2.2.1. Transient Stability Analysis

The asymmetrical single line to ground (1LG) fault, double line to ground (2LG) fault and the symmetrical three line to ground (3LG) fault at the transmission line are considered as network disturbance, as shown in Fig. 3.5. The fault occurs at 0.1 sec; the circuit breakers (CB) on the faulted line are opened at 0.2 sec, and at 1.0 sec the CBs are re-closed. In this transient analysis, the wind speeds for the wind generators are kept constant at the rated speed, assuming that the wind speed does not change dramatically within this small time duration.

Figs. 3.6 and 3.7 show responses of reactive powers, from which it is seen that the grid side converter of Wind Farm 1 can provide necessary reactive power during the severe asymmetrical 1LG and 2LG faults, and the symmetrical 3LG fault in Case 1. Therefore terminal voltages at the connection point can return back to the rated value quickly in Case 1 as shown in Fig. 3.8, and the rotor speeds can also become stable in Case 1 as shown in Figs. 3.9 and 3.10. The active power output of Wind Farm 1 and 2 are shown in Figs. 3.11 and 3.12, respectively. Though the DC-link circuit voltage of PMSG increases uncontrollably if the DC link protection is not used, it can be maintained almost constant by the proposed protection controller in Case 1 as shown in Fig. 3.13. On the other hand, the wind generators in both wind farms become unstable in Case 2 as shown in Figs. 3.6 – 3.12.

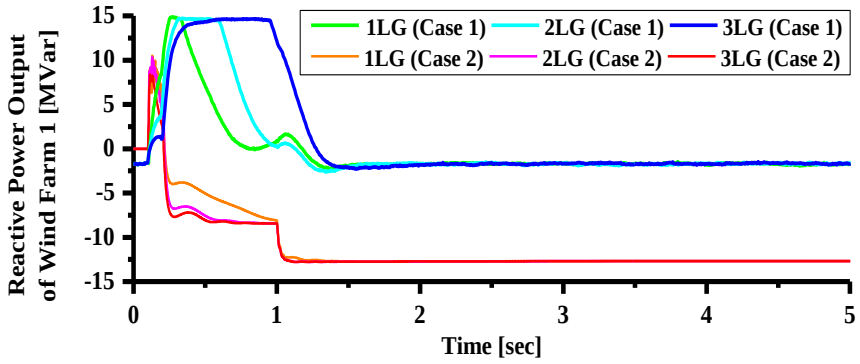

Fig. 3.6. Reactive power output of Wind Farm 1

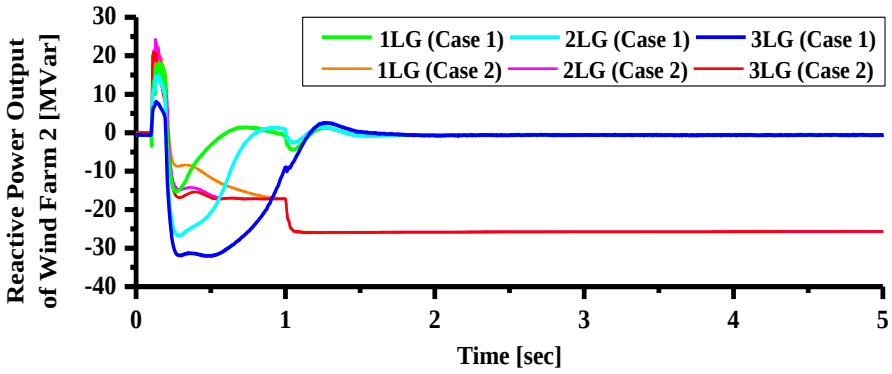

Fig. 3.7. Reactive power output of Wind Farm 2

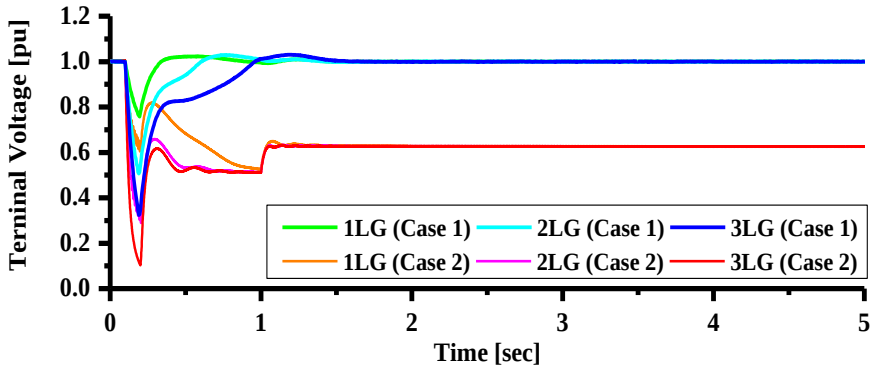

Fig. 3.8. Terminal voltage at connection point

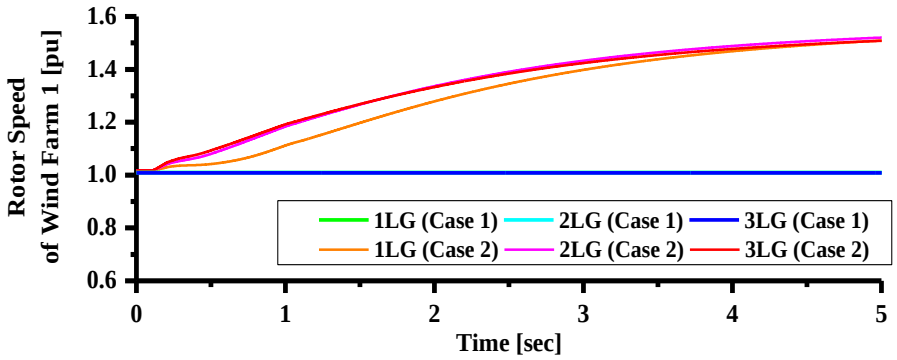

Fig. 3.9. Rotor speed of Wind Farm 1

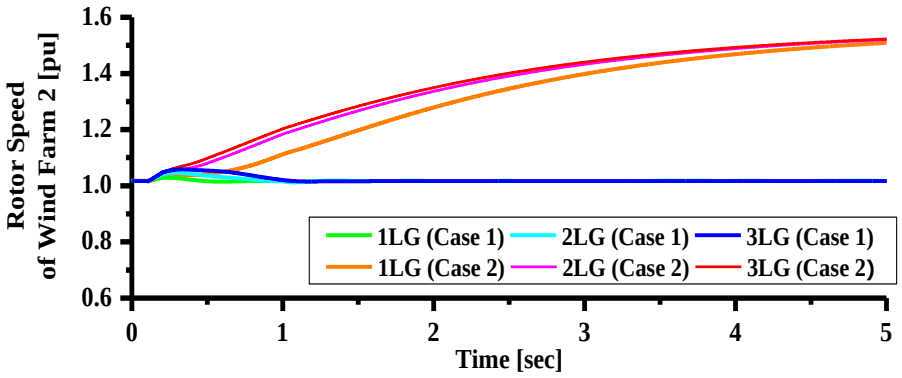

Fig. 3.10. Rotor speed of Wind Farm 2

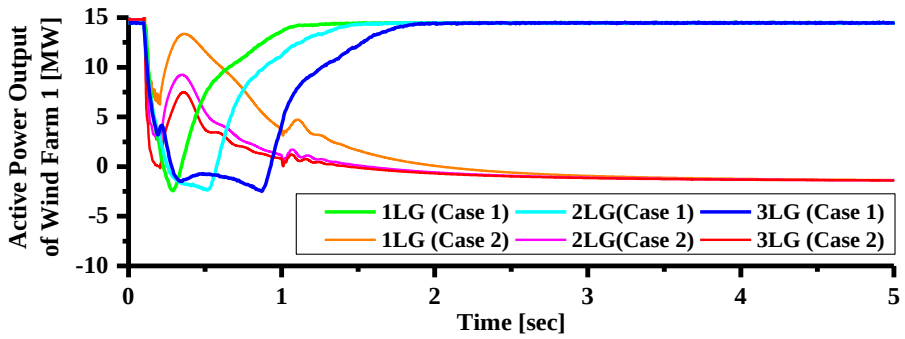

Fig. 3.11. Active power output of Wind Farm 1

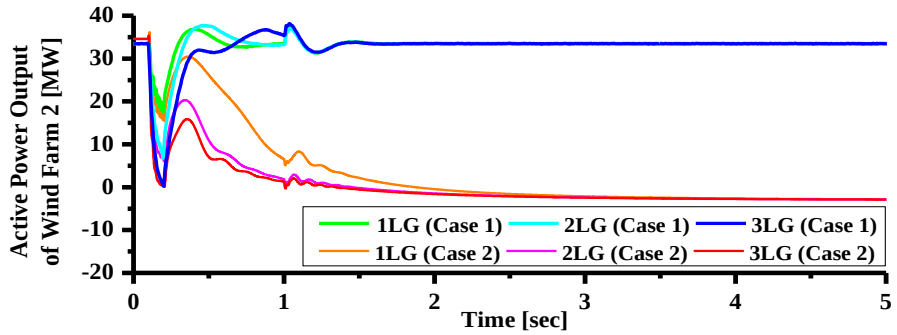

Fig. 3.12. Active power output of Wind Farm 2

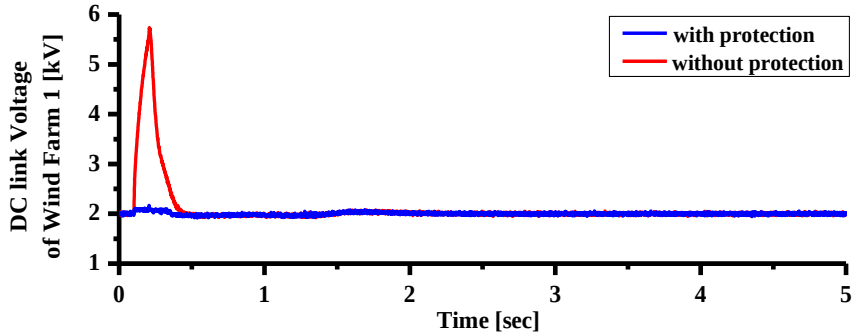

Fig. 3.13. DC-link circuit voltage (3LG in Case 1)

From these results, it is clear that PMSG with the proposed controller can enhance the transient stability of SCIG, the fixed speed wind generator, significantly by controlling its active and reactive powers delivered to the grid and thus the system performances can be improved effectively.

3.2.2.1. Steady State Analysis

To evaluate the steady state performance of the proposed system, responses for the real wind speed data measured in Hokkaido Island, Japan, shown in Fig. 3.14, were calculated. Fig 3.15 shows the reactive power output of wind farms in Case 1. It is seen that the reactive power from the grid side converter of Wind Farm 1 provides reactive power compensation for Wind Farm 2 for voltage regulation. Therefore the voltage and reactive power at the connection point are controlled almost constant in Case 1 as shown in Fig 3.16 and 3.17, respectively. As a result, the active power of wind farms can be delivered to the grid effectively as shown in Fig 3.18. Fig. 3.19 depicts the pitch angle response of both wind farms, from which it can be seen that the pitch controller works only when the wind speed exceeds the rated value in each wind farm.

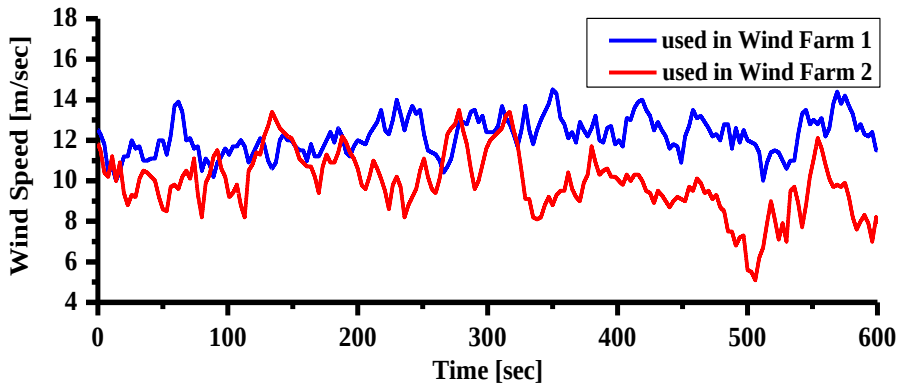

Fig. 3.14. Wind speed data

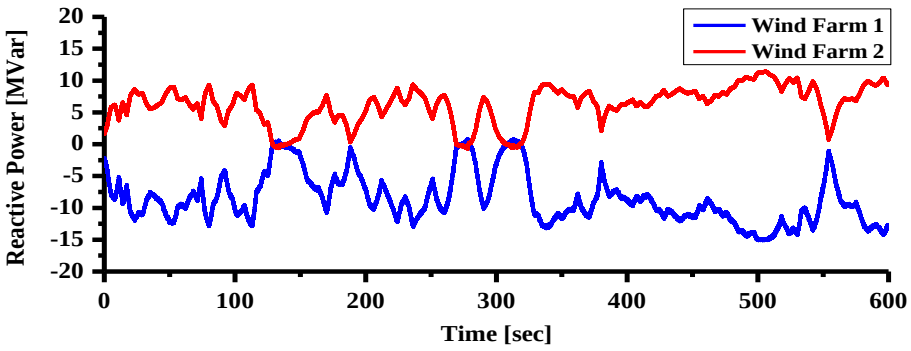

Fig. 3.15. Reactive power output of wind farms (Case 1)

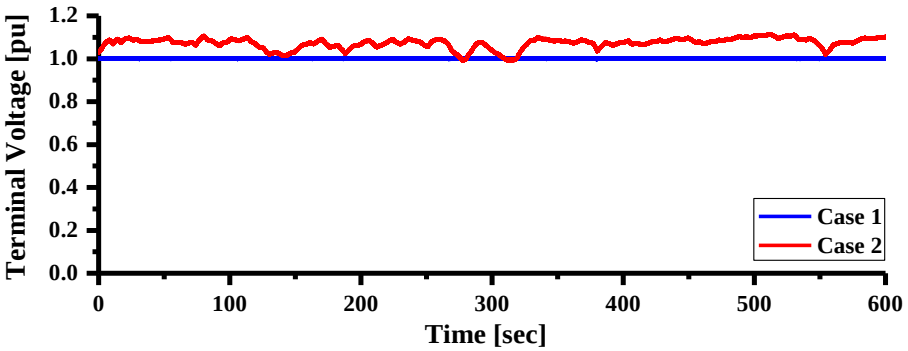

Fig. 3.16. Terminal voltage at connection point

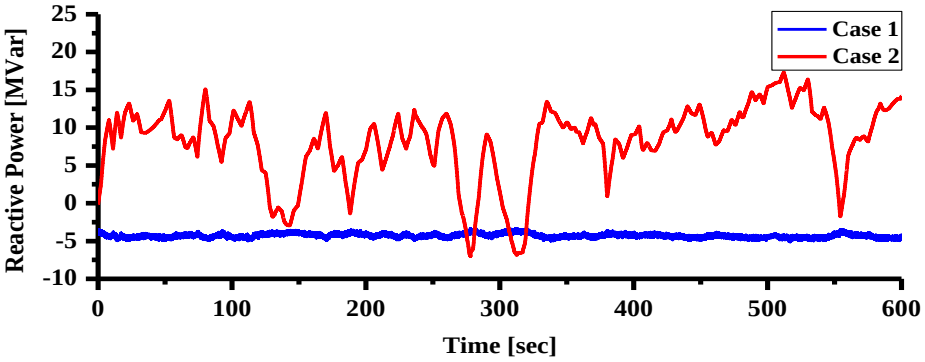

Fig. 3.17. Reactive power at connection point (Case 1)

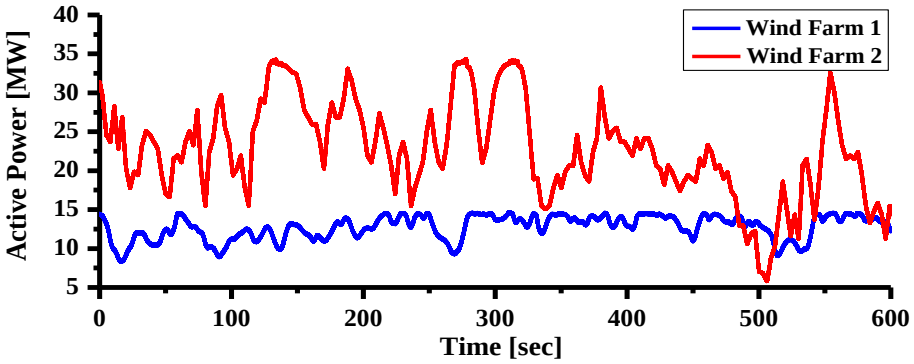

Fig. 3.18. Active power output of wind farms (Case 1)

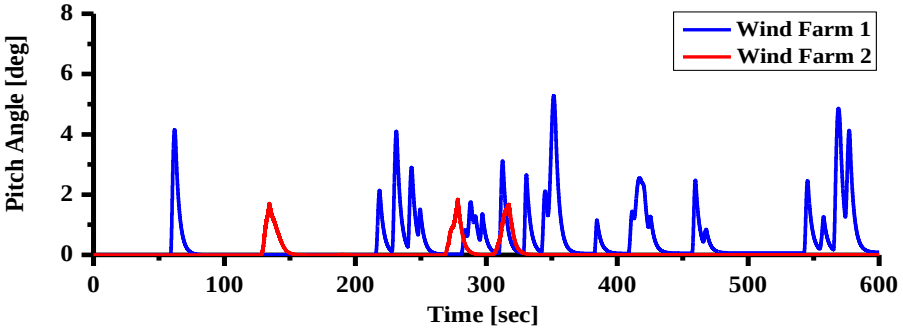

Fig. 3.19. Pitch angle of wind turbines (Case 1)

In this section a new control strategy of direct-drive permanent magnet wind generator for stabilization of wind farm composed of fixed speed wind generators is presented. The controllers for two levels back-to-back converter embedded with DC-link protection circuit are investigated. By using the proposed control method, the terminal voltage of wind farm can be recovered effectively during and after the asymmetrical (1LG and 2LG) faults as well as the symmetrical (3LG) fault, and thus the transient stability of fixed speed wind generator can be enhanced. It is also demonstrated that the DC link voltage can be maintained almost constant by the proposed protection controller during the fault conditions. Moreover, the steady state performance of the proposed system is analysed using real wind speed data. It is demonstrated that the voltage fluctuation of wind farm under randomly varying wind speed can be reduced and the active power of wind farms can be delivered to the grid effectively.

3.3. Low Voltage Fault Ride-Through Analysis of Wind Farm Connected to A Multi-machine Power System

In this paper, low voltage ride-through (LVRT) capability improvement of wind turbine generator system is investigated, in which a model system with two wind farms connected with multi-machine power system is considered. The wind farms considered consist of fixed speed wind turbine based induction generator and variable speed wind turbine with permanent magnet synchronous generator.

3.3.1. Power System Model

Fig. 3.20 shows a model system with 9-bus main system and two wind farms. Steam turbine and Hydro turbine driven synchronous generators are connected with the main system as generator SG1 and SG2, respectively. Automatic Voltage Regulator (AVR) and governor models in PSCAD/EMTDC package [67] are used in this paper. The IEEE type SCRX solid state exciter is considered for all synchronous generators as exciter model [69]-[70]. In SG1, the generic steam turbine model equipped with approximate mechanical-hydraulic controls of governor is used. In SG2, the hydro turbine with non-elastic water column without surge tank model and the hydro governor with PID controls including pilot and servo dynamics model are used [71]-[72].

Wind farms 1 and 2 are considered to be connected surrounding the hydro generator through long and short transmission lines respectively. Each wind farm power capacity is 50 MVA, in which G1 and G3 are 15 MVA VSWT-PMSG and G2 and G4 are 35 MVA FSWT-SCIG. The system base is 100 MVA. A capacitor bank, C, is used for reactive power compensation of each SCIG at steady state. The value of capacitor C is chosen so that the power

factor of the wind power station becomes unity during the rated condition. Parameters of generators are shown in Table 3.3.

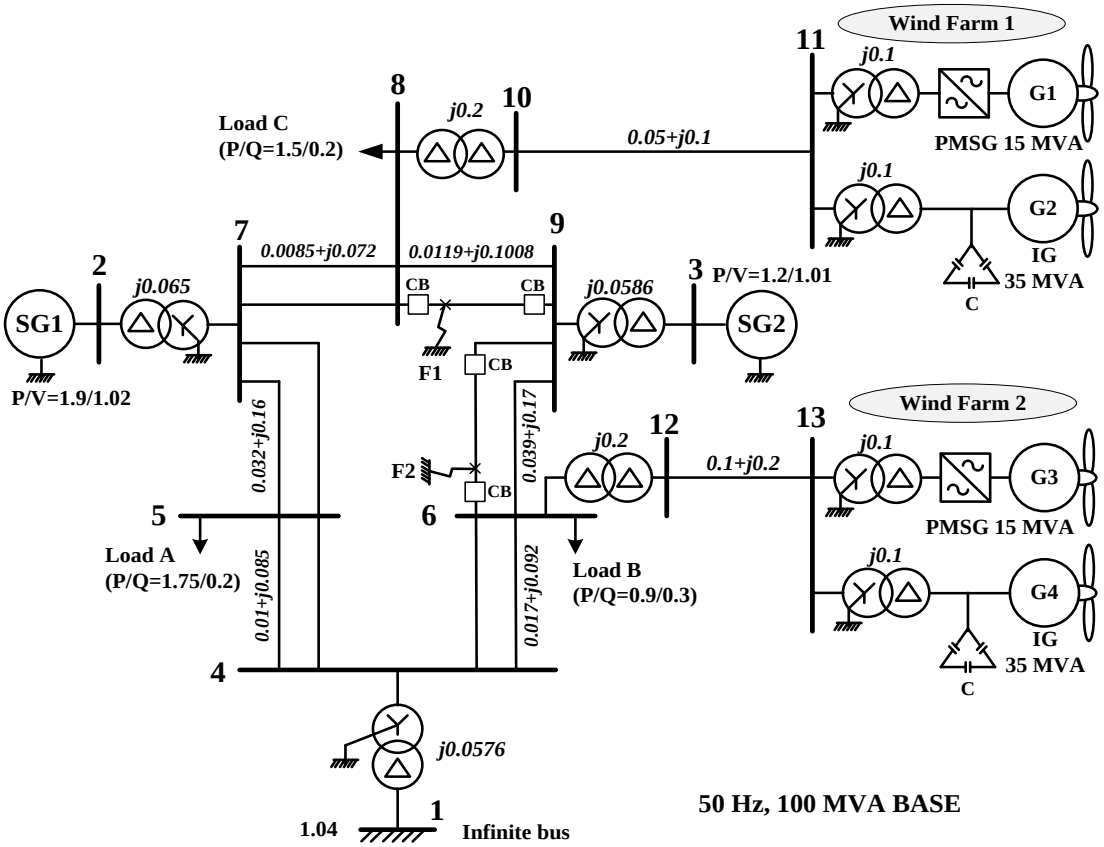

Fig. 3.20. Multi-machine power system model

Table 3.3.

Generator Parameters

	Synchronous Generators		SCIG		PMSG	
	SG1	SG2				
MVA	200	130	MVA	35	MVA	15
ra (pu)	0.003	0.004	R1 (pu)	0.01	Rs (pu)	0.01
Xa (pu)	0.102	0.078	X1 (pu)	0.1	Ls (pu)	0.064
Xd (pu)	1.651	1.22	Xm (pu)	3.5	Xd (pu)	0.9
Xq (pu)	1.59	1.16	R21 (pu)	0.035	Xq (pu)	0.7
X'd (pu)	0.232	0.174	R22 (pu)	0.014	Flux (pu)	1.4
X'q (pu)	0.38	0.25	X21 (pu)	0.03	H	3.0 s
X"d (pu)	0.171	0.134	X22 (pu)	0.089		
X"q (pu)	0.171	0.134	H	1.5 s		
T'do (sec)	5.9	8.97				
T'qo (sec)	0.535	1.5				
T"do (sec)	0.033	0.033				
T"qo (sec)	0.078	0.141				
H	9.0 s	6.0 s				

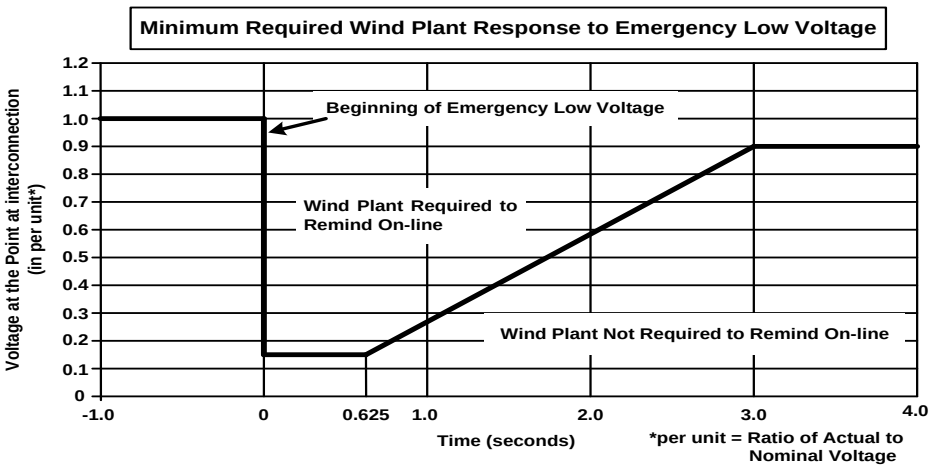

Fig. 3.21. Low voltage ride-through standard set by FERC, U.S.

Table 3.4.

Cases Study

Case	Wind Farm 1		Wind Farm 2		Fault Point
	G1	G2	G3	G4	
Case 1	PMSG	SCIG	PMSG	SCIG	F1
Case 2	PMSG	SCIG	PMSG	SCIG	F2
Case 3	SCIG	SCIG	SCIG	SCIG	F1
Case 4	SCIG	SCIG	SCIG	SCIG	F2

3.3.2. Simulation Study

The grid codes were originally decided with synchronous generator in mind. But due to the recent addition of huge amount of wind power to the grid, in many countries, the new grid codes have been developed to ensure secure power system operation. The wind farm grid codes are more or less similar to each other. In this study, simulation results are described in light of U.S. grid code, set by Federal Energy Regulatory Commission (FERC). If the voltage does not fall below the minimum voltage indicate by solid line in Fig. 3.21 and returns to 90% of the nominal voltage within 3 second after the beginning of the voltage drop, the plant must stay online [73].

In this study model system shown in Fig. 3.20 is analyzed, in which two wind farms are connected with multi-machine power system. The wind farms are installed with both VSWT-PMSG and FSWT-SCIG. The full-rating power converter of VSWT-PMSG wind turbine system is controlled in such a way to maintain the grid voltage (voltage at the connection point) at desired reference level set by transmission system operator. Therefore, necessary reactive power for FSWT-SCIG can also be supplied to restore the electromagnetic torque during a fault condition. Symmetrical three-line-to-ground faults (3LG) at fault point F1

and F2 are considered as network disturbances. Each fault occurs at 0.1 sec, the circuit breakers (CBs) on the faulted lines are opened at 0.2 sec, and at 1.0 sec the CBs are reclosed.

Four cases such as shown in Table 3.4 are considered in the simulation study to show the effectiveness of the proposed control strategy. In Case 1 and Case 2, simulation studies are performed using the model system of Fig. 3.20, in which the fault occurs at F1 or F2 respectively. In Case 3 and Case 4, simulation studies are performed using another model system in which PMSGs at G1 and G3 are replaced by SCIG (15 MW), in which the fault occurs at F1 or F2 respectively. Simulations were performed by using PSCAD/EMTDC.

In Wind Farm 1, responses of reactive power outputs of G1 and G2 are shown in Figs. 3.22 and 3.23, respectively. From these figures it is seen that the grid side converter of G1 can provide necessary reactive power for G2 during fault condition in Case 1 and Case 2. Therefore terminal voltage at Bus 11 can return back to the rated value quickly in Case 1 and Case 2 as shown in Fig. 3.24. The rotor speeds can also become stable quickly in Case 1 and Case 2 as shown in Figs. 3.25 and 3.26. The active power output of Wind Farm 1 and 2 are shown in Figs. 3.27 and 3.28, respectively. The wind generators in Wind farm 1 become unstable in Case 3 as shown in Figs. 3.22 – 3.28. In Case 4 the wind generators become stable, because the SG1 and SG2 can provide necessary reactive power for Wind Farm 1 during fault condition due to the short transmission lines between Wind Farm 1, SG1 and SG2, and fault point F2 is far from Wind Farm 1.

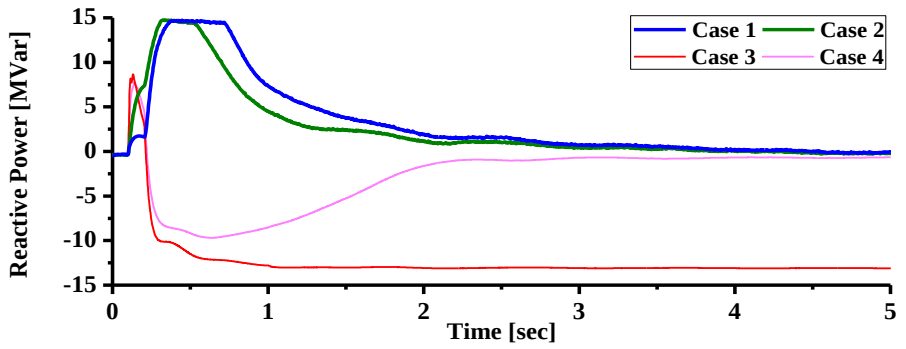

Fig. 3.22. Reactive power output of G1 in Wind Farm 1

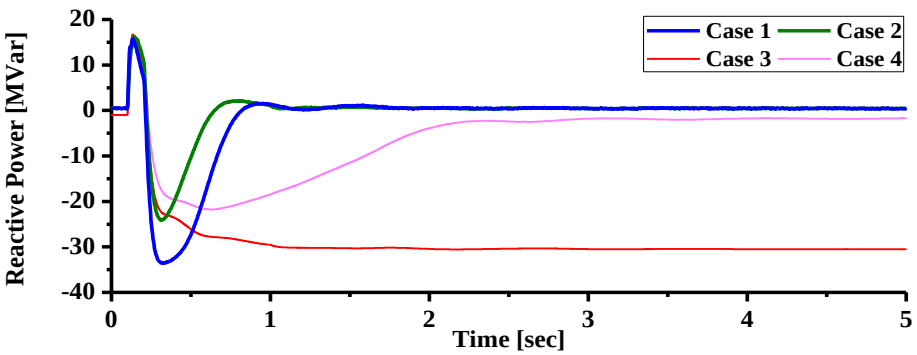

Fig. 3.23. Reactive power output of G2 in Wind Farm 1

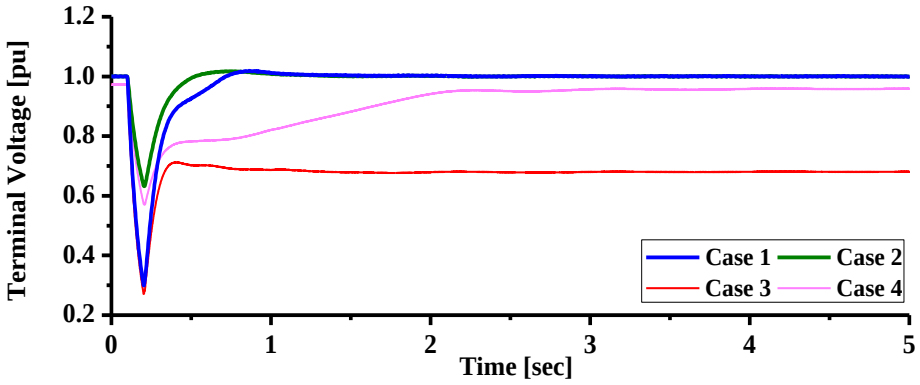

Fig. 3.24. Terminal voltage of Wind Farm 1 at Bus 11

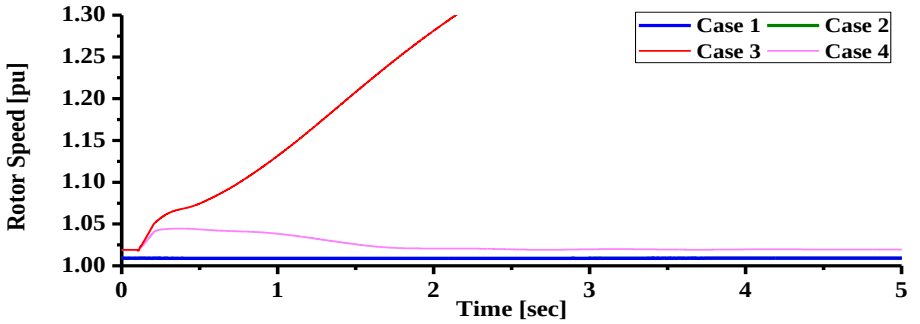

Fig. 3.25. Rotor speed of G1 in Wind Farm 1

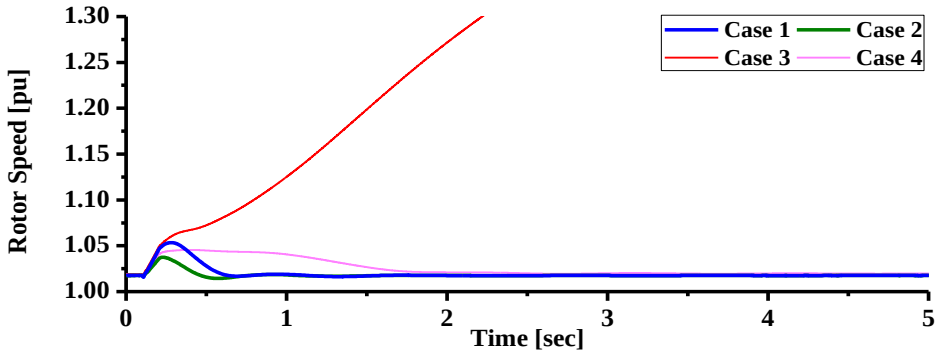

Fig. 3.26. Rotor speed of G2 in Wind Farm 1

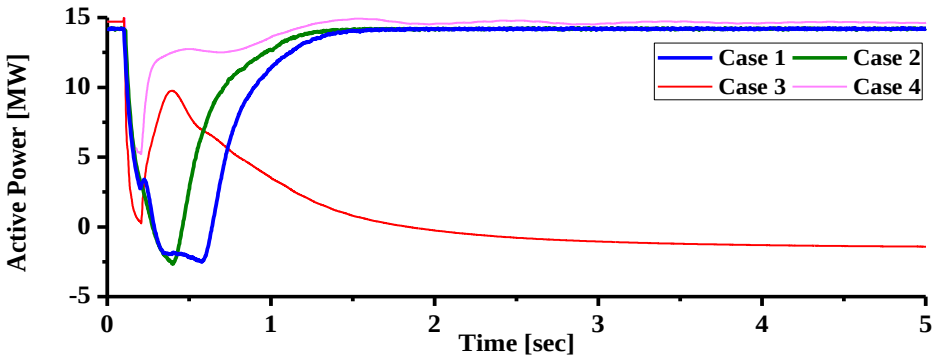

Fig. 3.27. Active power output of G1 in Wind Farm 1

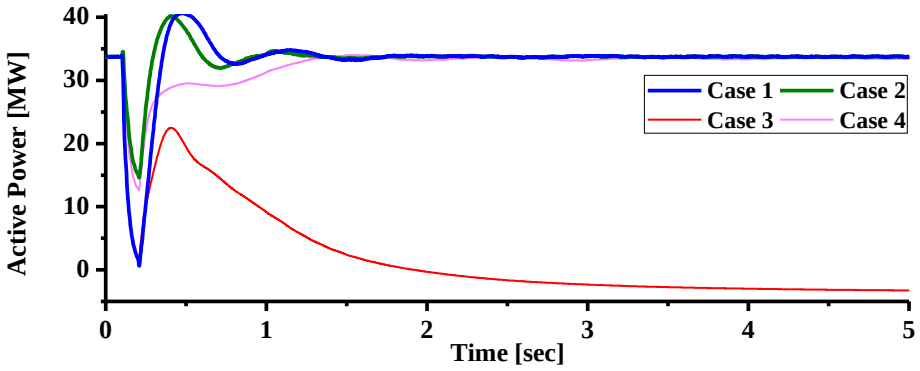

Fig. 3.28. Active power output of G2 in Wind Farm 1

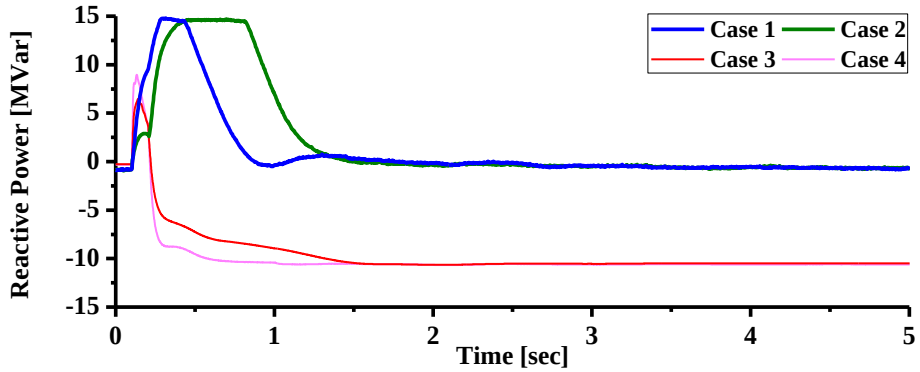

Fig. 3.29. Reactive power output of G3 in Wind Farm 2

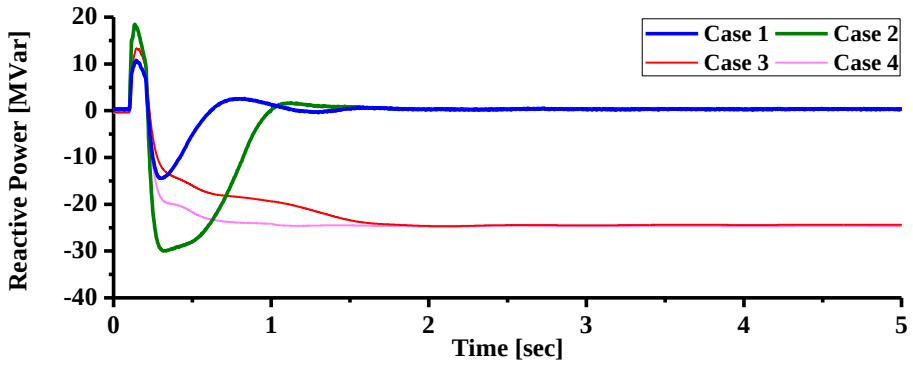

Fig. 3.30. Reactive power output of G4 in Wind Farm 2

Figs. 3.29 and 3.30 show responses of reactive power outputs of G3 and G4 in Wind Farm 2, from which it is seen that the grid side converter of G3 can provide necessary reactive power for G4 during fault in Case 1 and Case 2. Therefore terminal voltage of Wind Farm 2 at Bus 13 can return back to the rated value quickly in Case 1 and Case 2 as shown in Fig. 3.31. The rotor speeds can also become stable in Case 1 and Case 2 as shown in Figs. 3.32 and 3.33. The active power output of G3 and G4 are shown in Figs. 3.34 and 3.35, respectively. On the other hand, the wind generators in Wind farm 2 become unstable in Case 3 and Case 4 as shown in Figs. 3.29 – 3.35.

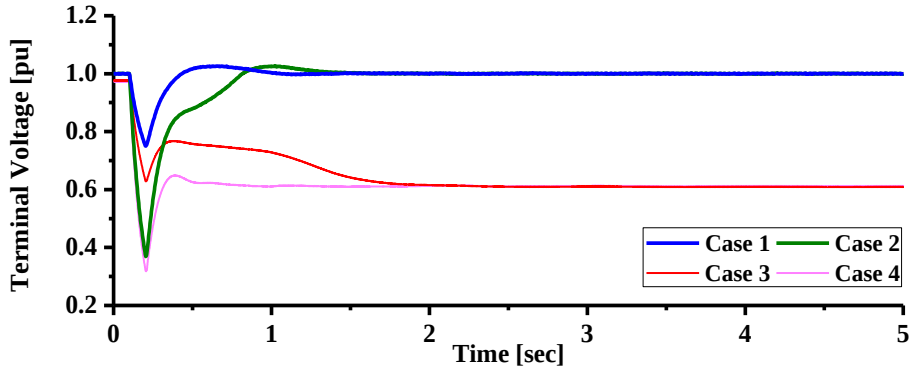

Fig. 3.31 Terminal voltage of Wind Farm 2 at Bus 13

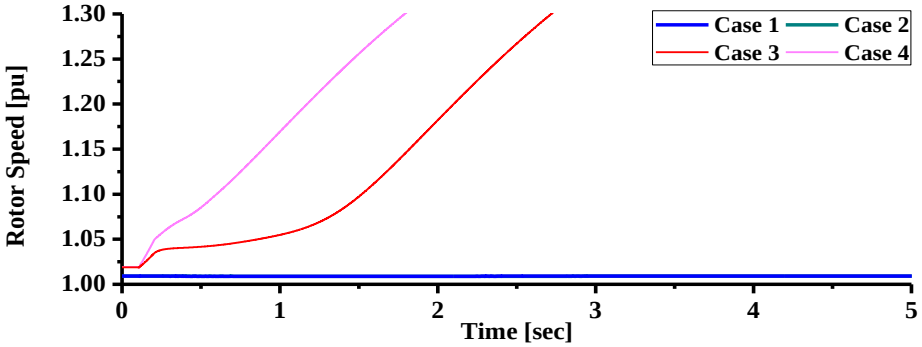

Fig. 3.32. Rotor speed of G3 in Wind Farm 2

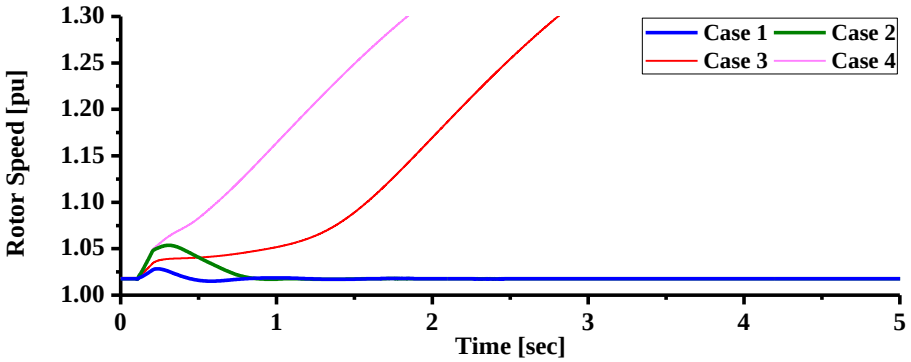

Fig. 3.33. Rotor speed of G4 in Wind Farm 2

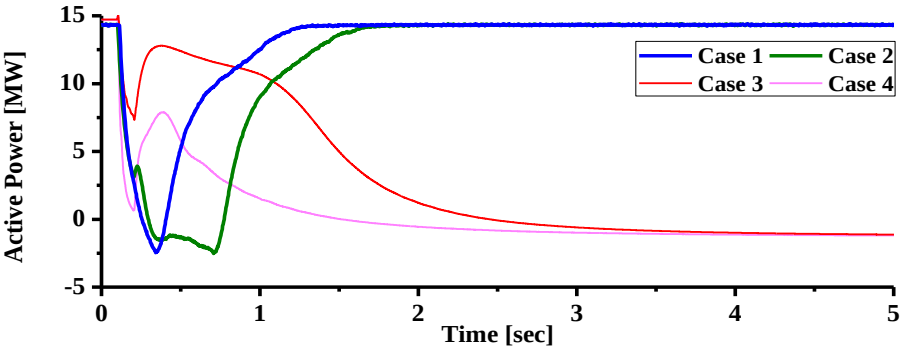

Fig. 3.34. Active power output of G3 in Wind Farm 2

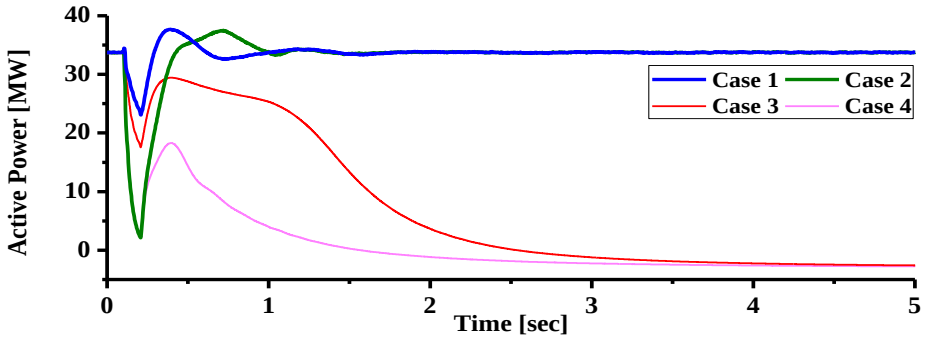

Fig. 3.35. Active power output of G4 in Wind Farm 2

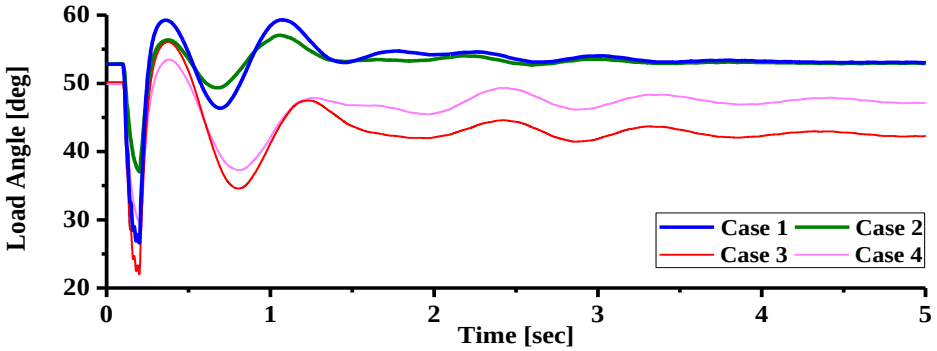

Fig. 3.36. Load angle of SG1

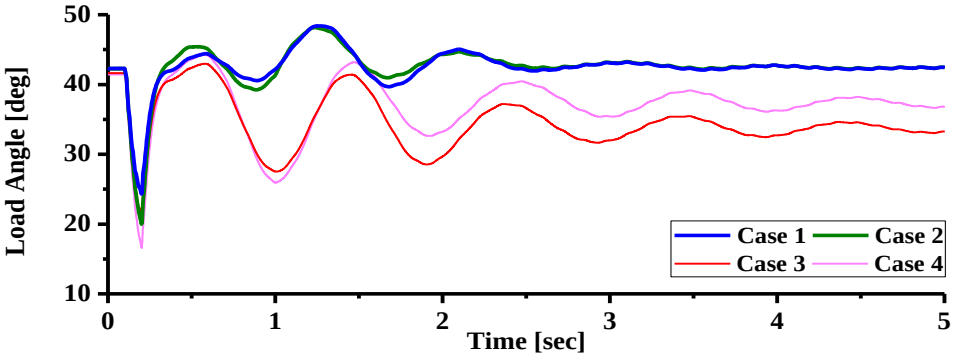

Fig. 3.37. Load angle of SG2

From the results shown in Figs 3.22 - 3.35, it is clear that PMSG with the proposed controller can enhance the LVRT capability of wind farms. The responses of terminal voltage of both wind farms at Bus 11 and 13 in Case 1 and Case 2 are shown in Figs. 3.24 and 3.31 and it is seen that the LVRT requirement of wind farm can be achieved.

Figs. 3.36 and 3.37 show responses of load angle of SG1 and SG 2, respectively. It is seen that PMSG with the proposed controller can enhance the transient stability of synchronous generator as well as wind generators when the severe 3LG fault occurs in the power system.

3.4. Chapter Summary

In this chapter a new control strategy of direct-drive permanent magnet wind generator for stabilization of wind farm composed of fixed speed wind generator is presented. The controllers for two levels back-to-back converter embedded with DC-link protection circuit are investigated.

In power system model 1, the terminal voltage of wind farm can be recovered effectively during and after the asymmetrical (1LG and 2LG) faults and the symmetrical (3LG) fault and thus the transient stability of fixed speed wind generator can be enhanced. It is also demonstrated that the DC link voltage can be maintained almost constant by the proposed protection controller during the fault condition. Moreover, the steady state performance of the proposed system is analyzed using real wind speed data, and it is demonstrated that the voltage fluctuation of wind farm under randomly varying wind speed can be reduced, and the active power of wind farms can be delivered to the grid effectively.

In power system model 2, the control strategy of variable speed permanent magnet wind generator for improving LVRT capability of wind farm composed of fixed speed induction generator has been investigated. The controller for two levels back-to-back converter for VSWT-PMSG is also developed. From these results, it is clear that PMSG with the proposed controller can enhance the LVRT capability of wind farms during symmetrical three-line-to-ground fault condition. Moreover, the active and reactive power delivered to the grid system can be controlled effectively; hence the overall system performances can be improved significantly.

Chapter 4

Application of LCL Filter to PMSG based Wind Generator to Enhance Dynamic Stability of Wind Farm

In this chapter a new control scheme for variable speed permanent magnet wind generator connected to grid through LCL filter is proposed in order to enhance stability of wind farms including fixed speed induction generators. Design and control approaches of back to back converters are developed in order for both active and reactive powers delivered to a power grid system to be controlled effectively. The stability performances of the controller system such as characteristics of dynamic response and good margin are also investigated based on the Bode diagram. To evaluate the controller system capabilities, simulation analyses for both transient and steady state conditions are performed on a power system model in which the wind farms are connected to a grid system.

4.1. Introduction

Combined installation of VSWT-PMSG and FSWT- SCIG in a wind farm can be efficient due to reduced system investment cost. The LVRT capability of FSWT-SCIG during network disturbances can be augmented by using VSWT-PMSG installed in the same wind farm as reported in [35]. The grid side converter of PMSG is controlled in such a way that the required reactive power of FSWT-SCIG can be supported when a fault occurs in the grid system. The converter of the PMSG permits flexible control of active and reactive power flows to the grid system. However, the converter is operated at high switching frequencies between 2-15 kHz resulting high order harmonics which can disturb devices on the grid and generate power losses [38], [39].

Attenuation of the current harmonics around switching frequency of the converter is important to get high performance of the converters, which fulfills the standards (IEEE 519-1992, IEC 61000-3-2/IEC 61000-3-4) [74]. Large value of input inductance allows achieving this purpose; however, it reduces dynamics and operation range of PWM rectifier [75]. Therefore, third order low-pass LCL filter is an attractive solution because of its many potential advantages such as higher harmonic attenuation and smaller inductances compared with L filter [40]. In this solution the current ripple attenuation is very effective even for small value of inductance, because capacitor impedance is inversely proportional to frequency of current. However, resonance at high frequency caused by the filter can lead stability problem caused by zero impedance for some higher order harmonics of current. Unstable system can be stabilized using a damping resistor, so-called *passive damping*. This solution can reduce

the filter effectiveness and increase losses in spite of advantages such as simplicity and reliability. Therefore design of LCL filter in industry application has several drawbacks, i.e., increase of losses and decrease of efficiency. Therefore, selection of a damping resistance value should also be taken into account in the controller design of VSC as well as the filter effectiveness and its losses.

Traditionally, the back to back converter of the VSWT- PMSG is controlled through current controlled voltage source converters by using the rotating d-q reference frame control approach. The characteristic of the control system is evaluated through transient and steady state simulation. The PI controller is commonly used in the control of the converter of PMSG. However, determination of the optimal value of gain parameters of the PI controller should be performed carefully in order to obtain good stability control performances. The optimal setting of gain parameters of PI controller is difficult to be achieved by trial and error method. In addition, variation of parameters and operating conditions of plant will change gain margin and phase margin of the control system. Therefore, determination of gain parameters of the converter controller system should be carefully considered.

4.2. Power System Model

The power system model used in this study is shown in Fig. 4.1. Small wind farm consists of three wind generators (a PMSG and two SCIGs) are connected to grid system. The PMSG rated at 5 MW is connected to the grid system bus through a back to back (AC/DC/AC) power

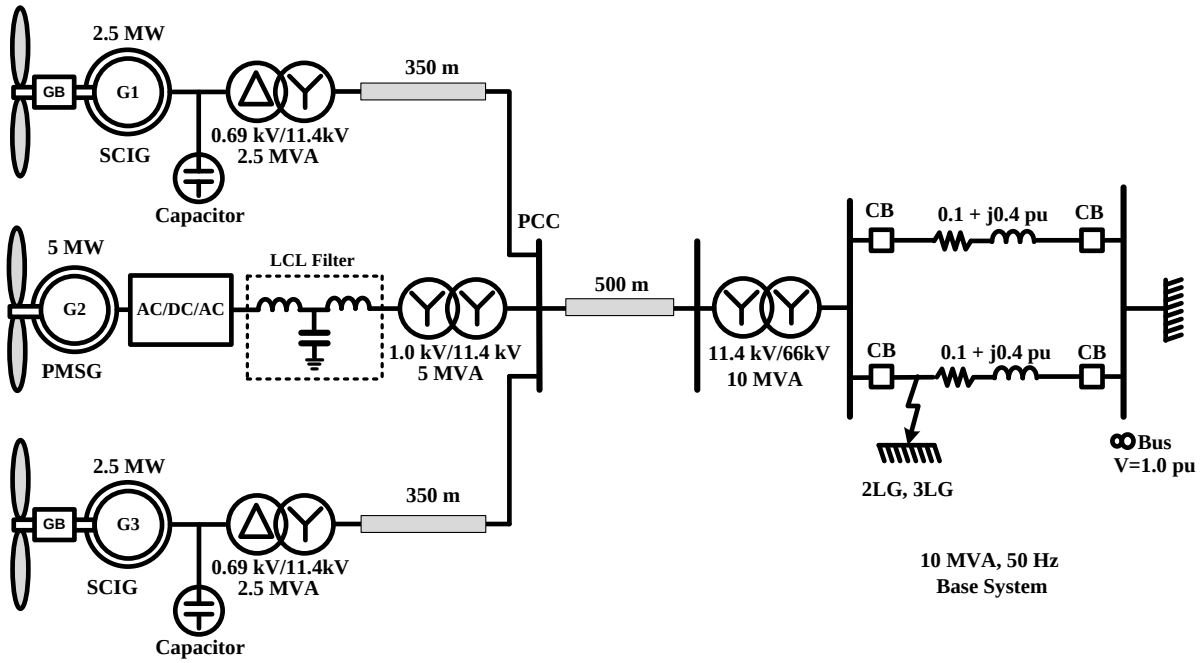

Fig. 4.1. Power system model

converter, a LCL filter, a 1.0/11.4 kV step up transformer, and 500 m underground cable. Two SCIGs rated at 2.5 MW are connected to the Point of Common Connection (PCC) via a 0.69/11.4 kV step up transformer and 350 m underground cables. The wind turbine is connected with the generator through a gear box (GB). In order to reduce reactive power consumption by SCIG from the grid system, a capacitor bank is installed at the generators. The value of the capacitor is determined so that the power factor becomes unity at rated power operation. The resistance and inductance of the transmission line are 0.1 pu and 0.4 pu, respectively. Parameters of PMSG and SCIG are shown in Table 4.1 in which the standard models from PSCAD/EMTDC library are used for both generators. The underground cable parameters are given in [76].The system base is 10 MVA and grid frequency is 50 Hz.

Table. 4.1.

Parameter of generators

Generators	Parameter	Symbol	Value
PMSG	Power rating	*Ps*	5 MW
	Voltage output	*Vs*	1.0 kV
	Frequency	*fe*	20 Hz
	Magnetic Flux	ψ_m	1.4 pu
	Stator Winding Resistance	R_s	0.01 pu
	The d-axis inductance	L_{sd}	0.95 pu
	The q-axis inductance	L_{sq}	0.75 pu
	Inertia constants	*H*	6.0
SCIG	Power output	P_{IG}	2.5 MW
	Voltage output	*Vs*	50 Hz
	Rated Frequency	*fe*	690 V
	Stator Resistance	*Rs*	0.066 (pu)
	First Cage Resistance	*Rr1*	0.298 (pu)
	Second Cage Resistance	*Rr2*	0.018 (pu)
	Stator leakage Reactance	*Ls1*	0.046 (pu)
	Magnetizing Reactance	*Lm*	3.860(pu)
	Mutual Reactance	*Lls*	0.122 (pu)
	Rotor Mutual Reactance	*Ll*	0.105(pu)
	Second Cage Reactance	*Ls2*	0.105 (pu)
	Polar moment inertia	*H*	3.0 s

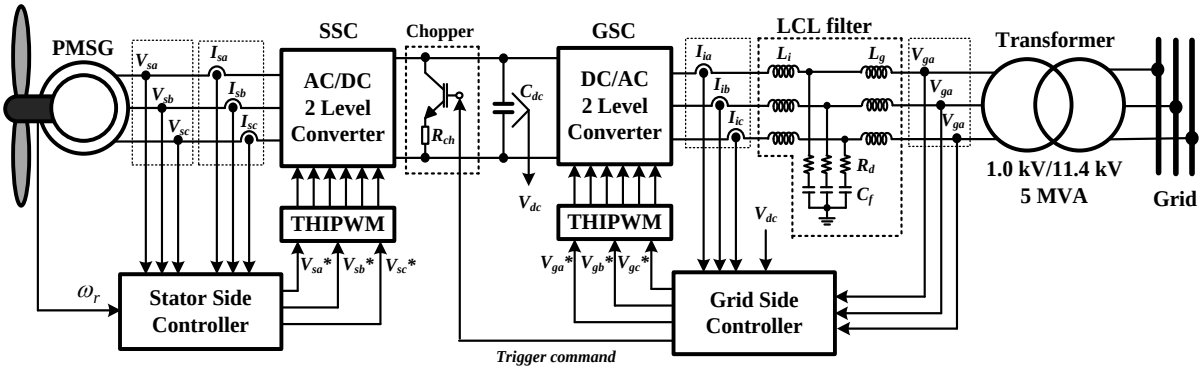

Fig. 4.2. VSWT-PMSG control system

4.3. PMSG based Variable Speed and Its Control Strategy

The block diagram of VSWT-PMSG and its control system proposed in this study is shown in Fig. 4.2. The VSWT-PMSG consists of the following components: a direct drive PMSG, back to back converters based on two levels of IGBT which are composed of stator side converter (SSC) and grid side converter (GSC), a DC-link circuit composed of a chopper with a resistance (R_{ch}) and a capacitor (C_{dc}), stator side controller, and grid side controller. The VSWT-PMSG is connected to utility grid system through LCL filter with a damping resistance (R_d) and step up transformers.

In the SSC, the three phase current and voltage are detected from stator of PMSG. The rotor speed of PMSG is detected from the rotor of wind turbine. Detail of the controller system for stator side converter is shown in Fig. 3.2 in Chapter 3.

In GSC, the converter is connected to the grid system through a LCL filter and a step up transformer. The grid current and the grid voltage are detected on the converter side and grid side of LCL filters, respectively. The DC link voltage (V_{dc}) is detected on the DC capacitor (C_{dc}). When a fault occurs in the grid, V_{dc} increases significantly due to power unbalance between SSC and GSC. In order to protect the DC-link circuit, the grid side controller activates the chopper by a trigger command. Detail of the controller system for stator side converter is shown in Fig. 3.3 in Chapter 3. The DC-link capacitor is 25.000 μF. The rated DC-link voltage is 2.0 kV (1 pu).

In modulation technique, Third Harmonic Injection Pulse Wave Modulation (THIPWM) is used in this work. Injection of third harmonic in the reference voltage makes it possible to utilize the voltage reference without over modulation. In addition, the THIPWM can maximize fundamental amplitude of the output voltage [77]. The switching frequencies (f_s) are selected to 2 KHz for SSC and 4 kHz for GSC.

The transformer converts 1kV output voltage of GCS to 11.4 kV. The total resistance and reactance of the transformer is 0.016 pu and 0.04 pu, respectively.

4.4. Dynamic model of PMSG

As described in Chapter 2, The PMSG dynamic equations are expressed in the d-q reference frame. The model of electrical dynamics in terms of voltage and current can be given as:

$$\frac{d\psi_{sd}}{dt} = -V_{sd} - R_s I_{sd} - \omega_e \psi_{sq} \tag{4-1}$$

$$\frac{d\psi_{sq}}{dt} = -V_{sq} - R_s I_{sq} + \omega_e \psi_{sd} \tag{4-2}$$

with

$$\psi_{sd} = L_{sd} I_{sd} + \psi_m \tag{4-3}$$

$$\psi_{sq} = L_{sq} I_{sq} \tag{4-4}$$

Substituting Eqs. (4-3) and (4-4) into Eqs. (4-1) and (4-2), the deferential equations of PMSG can be expressed as follows:

$$L_{sd} \frac{dI_{sd}}{dt} = -V_{sd} - R_s I_{sd} - \omega_e L_{sq} I_{sq} \tag{4-5}$$

$$L_{sq} \frac{dI_{sq}}{dt} = -V_{sq} - R_s I_{sq} + \omega_e L_{sd} I_{sd} + \omega_e \psi_{sd} \tag{4-6}$$

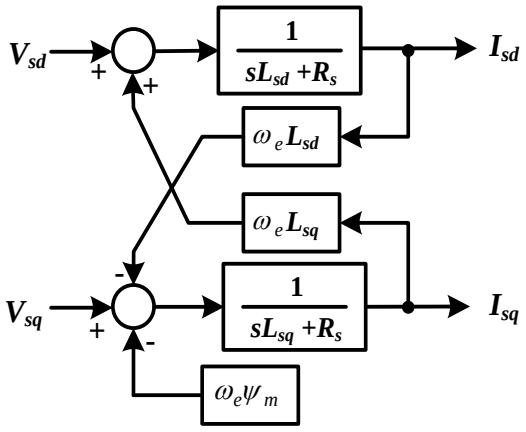

Fig. 4.3. Block diagram of PMSG in the d-q rotating reference frame

A block diagram of the PMSG in the d-q rotating reference frame can be derived as shown in Fig. 4.3, where s denotes a Laplace operator.

4.5. LCL filter Design

4.5.1. Dynamic model of LCL filter

As previously mentioned, utilization of the LCL filter can lead to stability problem due to resonance. To avoid the resonance a passive damping resistance should be allocated in series with a filter capacitor in the filter. However, adopting a damping resistance can cause power losses. Therefore, in designing the voltage source converter controller system, a passive damping resistance should be taken into account in the plant system model.

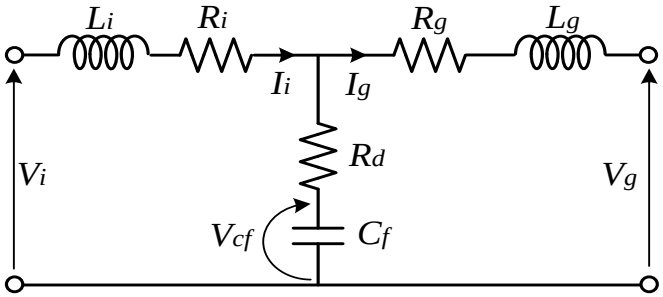

Fig. 4.4. Single phase LC filter equivalent circuit

Single phase LCL filter equivalent circuit is shown in Fig. 4.4. The LCL filter is composed of an inverter side inductance (L_i) and its parasitic resistance (R_i), a grid side inductance (L_g) and its parasitic resistance (R_g), a filter capacitor (C_f) and a damping resistance (R_d). V_i and I_i are voltage and current on the converter side of the LCL filter. V_g and I_g are voltage and current on the grid side of the LCL filter. It should be noted that V_{cf} is a voltage on the filter capacitor (C_f). The differential equations of LCL filter in stationary reference frame can be written as follows:

$$L_i \frac{dI_i}{dt} = V_i - V_{cf} - (R_i + R_d)I_i + R_d I_g \tag{4-7}$$

$$L_g \frac{dI_g}{dt} = V_{cf} - V_g - (R_i + R_d)I_g + R_d I_i \tag{4-8}$$

$$C_f \frac{dV_{cf}}{dt} = I_i - I_g \tag{4-9}$$

From eqs. (4-7) to (4-9) deferential equations in the d-q rotating reference frame are obtained:

$$L_i \frac{dI_{id}}{dt} = V_{id} - V_{cfd} - (R_i + R_d)I_{id} + L_i \omega I_{iq} + R_d I_{gd} \tag{4-10}$$

$$L_i \frac{dI_{iq}}{dt} = V_{iq} - V_{cfq} - (R_i + R_d)I_{iq} - L_i \omega I_{id} + R_d I_{gq} \tag{4-11}$$

$$L_g \frac{dI_{id}}{dt} = V_{cfd} - V_{gd} - \left(R_g + R_d\right)I_{gd} + L_g \omega I_{gq} + R_d I_{id} \tag{4-12}$$

$$L_g \frac{dI_{iq}}{dt} = V_{iq} - V_{cfq} - (R_i + R_d)I_{iq} - L_g \omega I_{gd} + R_d I_{iq} \tag{4-13}$$

$$C_f \frac{dV_{cfd}}{dt} = I_{id} - I_{gd} + \omega C_f V_{cfq} \tag{4-14}$$

$$C_f \frac{dV_{cfq}}{dt} = I_{iq} - I_{gq} + \omega C_f V_{cfd} \tag{4-15}$$

The dynamic block diagram of the grid connected LC filter in the d-q rotating reference frame can be derived as shown in Fig. 4.5.

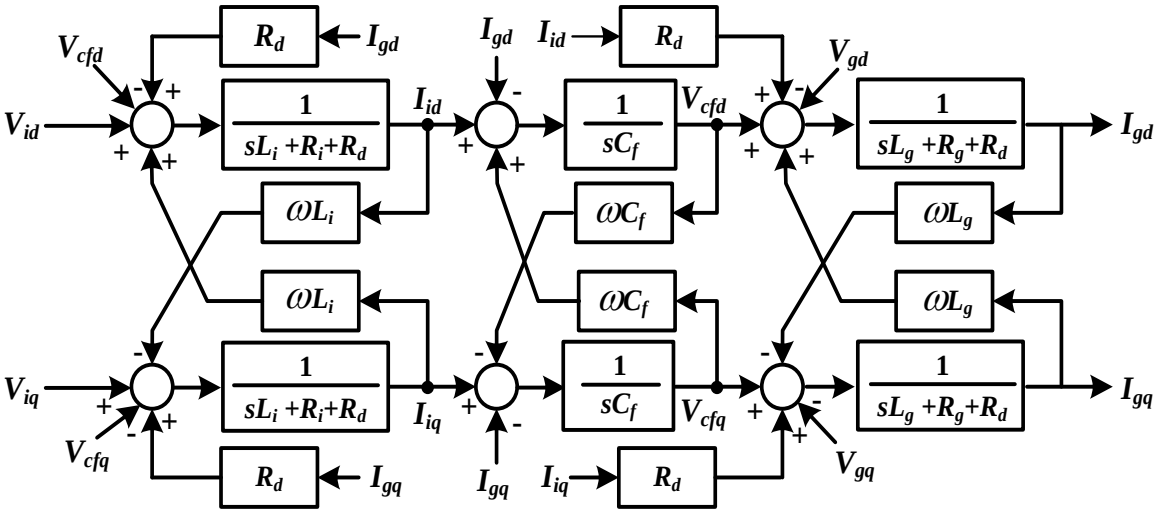

Fig. 4.5. Block diagram of LC filter in the d-q rotating reference frame

The LCL filter shown in Fig. 4.5 can be written in the state space form:

$$\dot{x} = Ax + Bu \tag{4-16}$$

$$y = Cx \tag{4-17}$$

where, $x = [\, I_{id}\ I_{iq}\ I_{gd}\ I_{gq}\ V_{cfd}\ V_{cfq}]^T$ and $u=[V_{id}\ V_{iq}]^T$, and the I_{id} and I_{iq} are chosen as output parameters.

4.5.2. LCL Filter Parameters

The LCL filter aims to reduce high-order harmonics on the grid side, but a poor filter design can cause lower attenuation compared to what is expected, or can even cause a distortion increase because of oscillation effects. The current harmonics may cause saturation of the inductors or filter resonance. Therefore, the inductors should be correctly designed considering current ripple, and the filter should be damped to avoid resonances.

There are many methods that may be considered in determining the filter parameters [39], [78]-[81]. However, in this paper procedure and limitations of LCL filter parameters presented in [39] are considered.

a) The value of the capacitance is limited by the decrease of the power factor that has to be less than 5% at the rated power.
b) The total value of the filter inductance should be less than 10 % from rating power of the converter of PMSG**.**
c) The resonance frequency of the filter should be higher than 10 times the grid frequency and then half of the switching frequency.
d) The passive damping resistance should be sufficient to avoid oscillation, but losses cannot be so high as to reduce efficiency.

The procedure for choosing the LCL filter parameters uses the power rating of the converter, the line frequency, and the switching frequency as inputs. The process to calculate the switching ripple attenuation is based on a frequency-domain approach rather than on a time-domain approach. In the following development, the filter values are reported as a percentage of the base values, given by

$$Z_b = \frac{{V_g}^2}{P_g} \tag{4-18}$$

$$C_b = \frac{1}{\omega_g Z_b} \tag{4-19}$$

$$L_b = \frac{Z_b}{\omega_g} \tag{4-20}$$

where V_g is the line-to-line rms voltage, ω_g is the grid angular frequency, and P_g is the active power absorbed by the converter in rated condition.

First the inverter side inductance L_i is designed in order to limit the current ripple generated by the converter. The selection of the ripple current is a trade-off among the size of inductor L_i, IGBT switching and conduction losses, and inductor coil and core losses.

Typically, the ripple current (Δi_{Li}) can be chosen as 25%~35% of rated current. The maximum current ripple can be derived as eq.(4-21) [82]:

$$L_i = \frac{1}{8}\frac{V_{dc}}{f_{sw}\Delta i_{Li}} \tag{4-21}$$

where f_{sw} is switching frequency of the converter.

The selection of the capacitor is a trade-off between reactive power in C_f and inductance L_i. The capacitance cannot be too small either. Otherwise, the inductance will be large in order to meet the attenuation requirements. The larger inductance L_i resulted from smaller capacitance leads to higher voltage drop across the inductor L_i. Taking x as a percentage of the reactive power absorbed, C_f can be calculated by:

$$C_f = xC_b \tag{4-22}$$

where the capacitor value is limited by condition (a) above.

The value of outer inductor L_g can then be determined as a function of L_i, using the index r for the relation between the two inductances

$$L_g = rL_i \tag{4-23}$$

The frequency resonance (ω_{res}) can be calculated as:

$$\omega_{res} = \sqrt{\frac{L_i + L_g}{L_i L_g C_f}} \tag{4-24}$$

The ripple attenuation (h_{sw} is harmonics around the switching frequency), calculated neglecting losses and damping of the filter, is defined by (4-25) and can be written, considering (4-22) and (4-23), as

$$\frac{I_g(h_{sw})}{I_i(h_{sw})} = \frac{1}{|1 + r(1 - ax)|} \tag{4-25}$$

where $a = L_i C_f(\omega_{res})^2$ is a constant.

The passive damping resistance is selected according to condition (d) above. At the resonant frequency the impedance of the filter is zero. The aim of the damping is to insert impedance at this frequency to avoid oscillation. Hence, the damping value is set to a similar order of magnitude as the series capacitor impedance at the resonant frequency [83].

If the filter attenuation is not adequate, the multiplication coefficient x should be increased taking into account the decrease of the filtering action due to losses. If this is not sufficient, higher value of the reactive power should be selected by changing the value of C_f. The filter attenuation should be verified under several load conditions and switching frequencies.

Table 4.2 show the LCL filter parameters obtained by the step by step procedure explained above.

Table 4.2

LCL filter parameters

Components	Symbol	Values
Base impedance	Z_b	0.2 Ω
Base capacitance	C_b	15900 μF
Base inductance	L_b	0.636 mH
Converter side inductance	L_i	43 μH
Parasitic resistance of Li	R_i	0.0011Ω
Grid side inductance	L_g	6.5 μH
Parasitic resistance of Lg	R_g	0.0001 Ω
Filter capacitor	C_f	397uF
Damping resistance	R_d	0.07 Ω

According to the table, 0.2 Ω base impedance, 1.3mH base inductance, and 15900μF base capacitance are calculated. As the inductance on the inverter side (L_i), 6 % of base inductance is adopted. In order to calculate the grid side inductance (L_g), the transformer inductance (L_t) should be considered. 4% of base inductance has been adopted as transformer inductance. Adding a small value of grid side inductance (L_g), total 4.1% of base inductance is obtained. As the filter capacitor (C_f), 2.5% of base capacitance is adopted. The resonance frequency of LCL filter is around 1.855 kHz. The impedance of the filter capacitor (Z_{cres}) at the resonant frequency is 0.21Ω. The damping resistance (Rd) is chosen around one-third of the Z_{cres}.

4.6. Design and Analysis of PMSG Controller System

4.6.1. Current Loop Controller of SSC

In order to achieve good performance of the control system, the dynamic stability of the current loop control system is analyzed based on frequency responses in Bode diagram. A block diagram of the current loop control is shown in Fig. 4.6. The controller system is composed of two PI controllers (PI 2 for d-axis current and PI 4 for q-axis current), sampling time transfer function ($1/sT_s+1$), inverter transfer function ($1/sT_{inv}+1$), and PMSG transfer function. The sampling time transfer function is caused by switching frequency ($T_s=1/f_s$) and inverter transfer function is caused by the dead time of PWM converter ($T_{inv}=1/T_s$), where switching frequency (fs) of SSC is 2 kHz. The transfer function of PMSG is obtained from Eqs. (4-5) and (4-6).

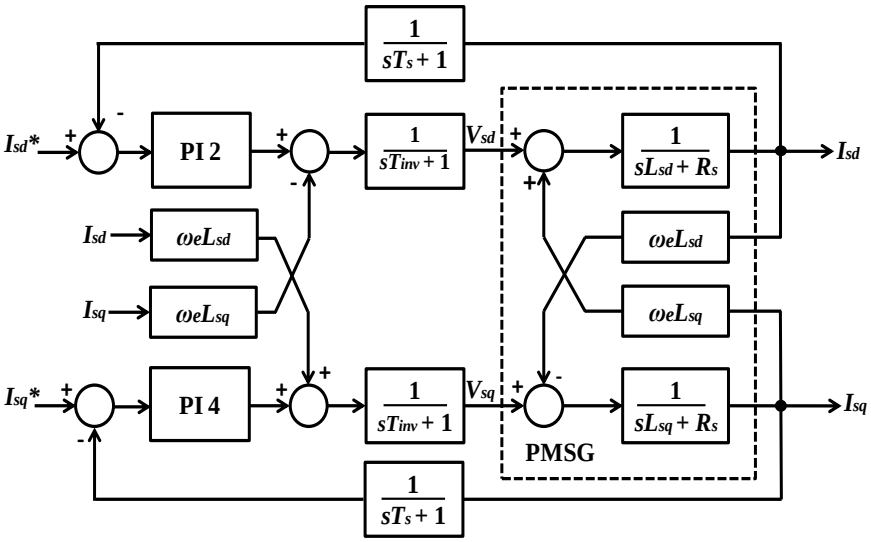

Fig. 4.6. Current control loop of SSC controller

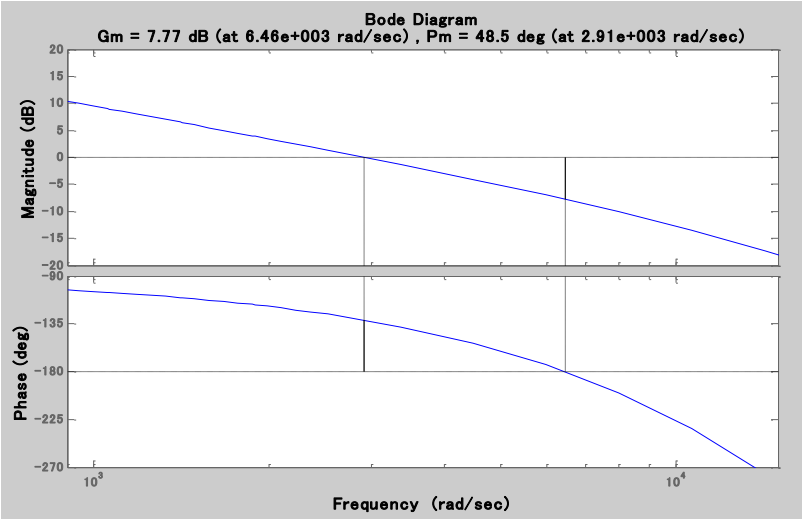

Fig. 4.7. The Bode diagram of open loop current control of SSC

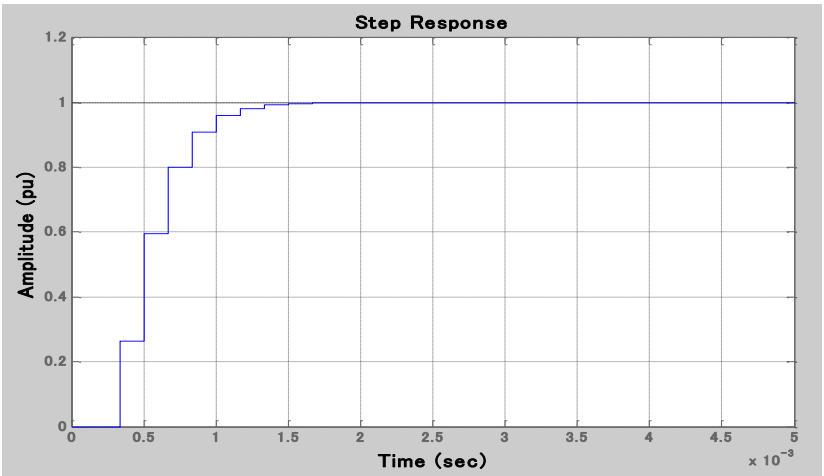

Fig. 4.8. The step response of closed loop current control of SSC

In this study T_i of PI controller is set equal to the plant system time constant, (L_s/R_s) [9], and K_p is obtained through the frequency response on Bode diagram analysis. In order to stabilize the current loop control, gain margin (Gm) larger than 6 dB and phase margin (Pm) larger than 45 deg are required. Fig. 4.7 shows the Bode diagram of the open loop current control of the SSC with K_p = 4.77 and K_i = 6.00, where $K_i = K_p/T_i$, where the initial gain is obtained by using modulus criterion method. It is seen that the loop can be stable with a gain margin of 7.77 dB and a phase margin of 48.5 deg. Finally, step response of the closed loop current control in discrete system is depicted in Fig. 4.8. It is seen that the settling time of response is less than 0.004 sec.

4.6.2. Current Loop Controller of GSC

Fig. 4.9 shows a block diagram of the current control loop for GSC. The switching frequency for GSC is chosen at 4 kHz. T_s and T_{inv} for GSC can be determined by using $T_s=1/f_s$ and $T_{inv}=1/T_s$, respectively. The dynamic block diagram of the grid connected LCL filter in the d-q rotating reference frame is shown in Fig. 4.5

In this study, the d-axis and the q-axis components are assumed identical, and hence the plant system can be analyzed by using d axis component only, where the cross coupling and grid voltage are neglected. It should be noted that the inductance (L_t) and resistance (R_t) of transformer are included in L_g and R_g. For PI controller usually the integral time constant (T_i) is set equal to the plant system time constant, (L_{tot}/R_{tot}) [9], where L_{tot} and R_{tot} are total of series inductances and its parasitic resistances of the plant system, respectively.

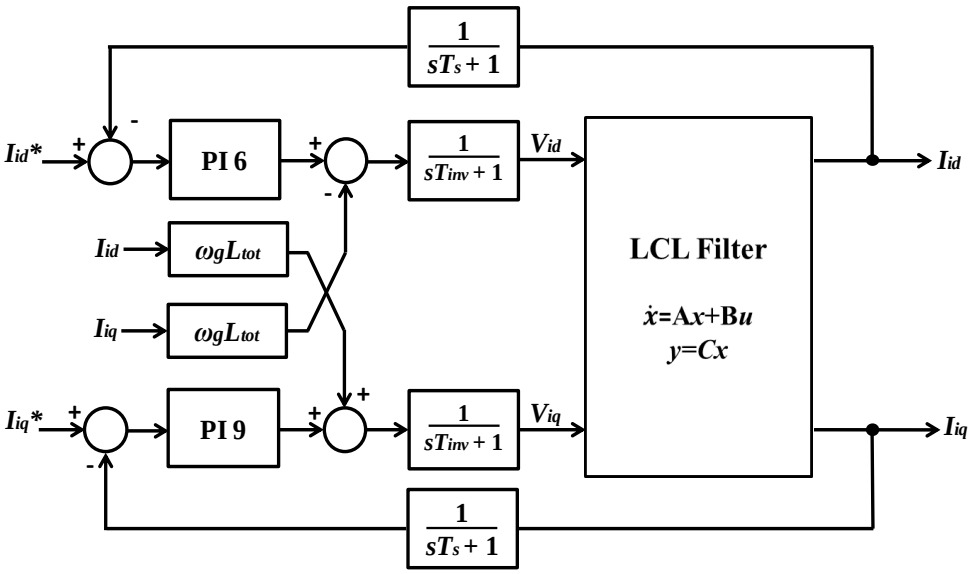

Fig. 4.9. Current control loop of SSC controller

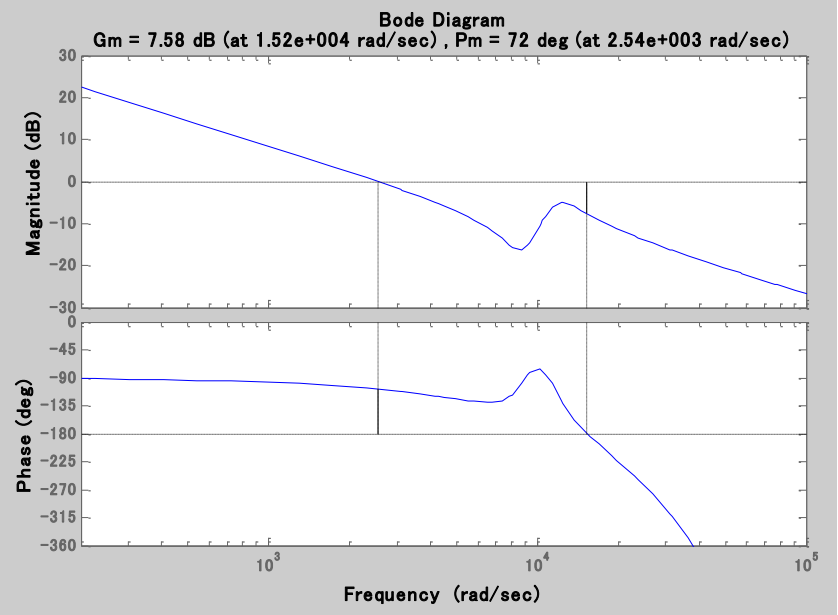

Fig. 4.10. The Bode diagram of open loop current control of GSC

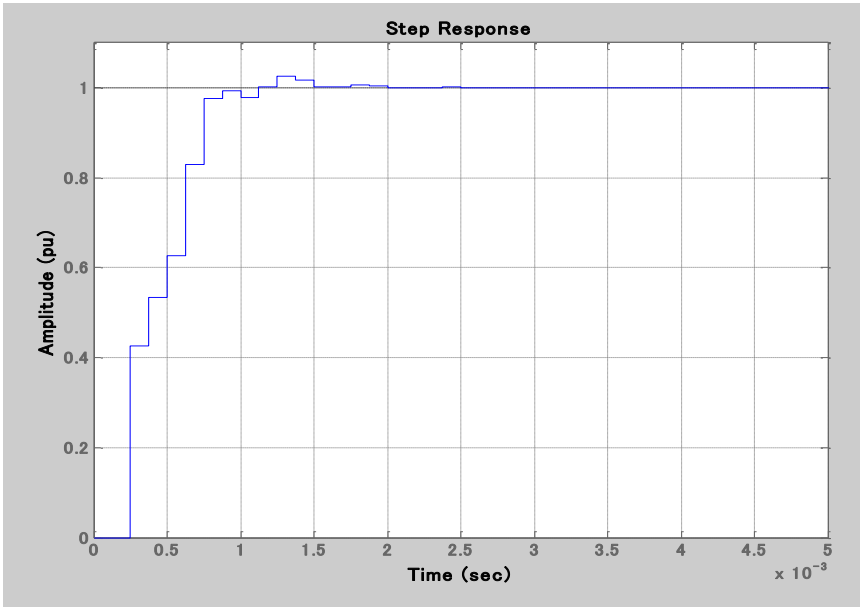

Fig. 4.11. The step response of closed loop current control of GSC

In this study, in order to stabilize the current controller, gain margin (Gm) larger than 6 dB and phase margin (Pm) larger than 45 deg are required for step response with settling time less than or equal to 2.5 msec and 3% maximum overshoot. With K_p=0.20 and K_i = 5.02, stable loop with a gain margin of 7.58 dB and a phase margin of 72 deg is obtained as shown in Fig. 4.10. Step response of the current control loop in discrete system is depicted in Fig. 4.11. It is seen that settling time of the response is less than 2.5 msec and the maximum overshoot is less than 3%.

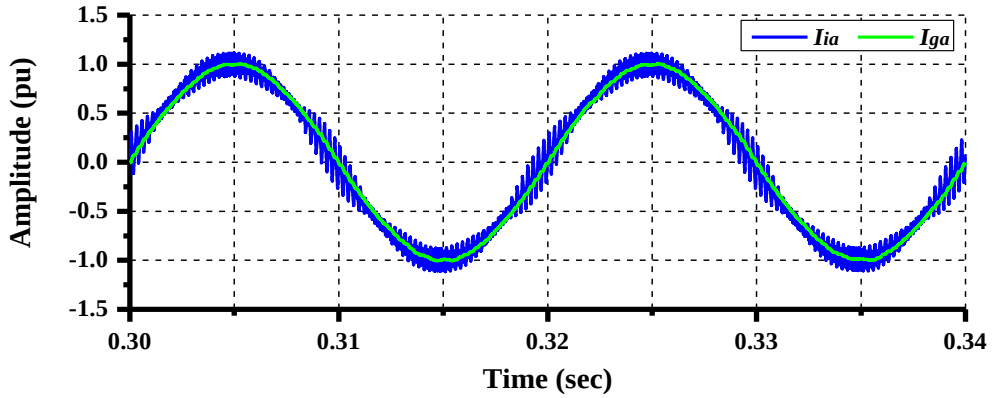

Fig. 4.12. Current observed on phase A

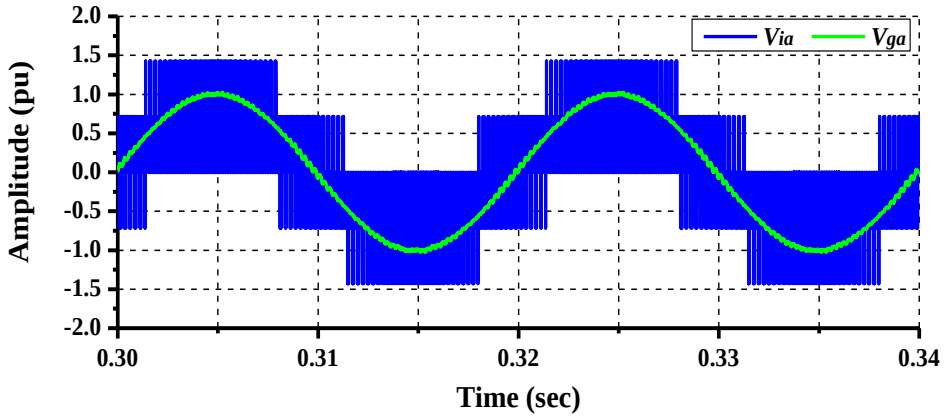

Fig. 4.13. Voltage observed on phase A

The current controller performance and effectiveness of the LCL filter have been verified by using power system blockset of Matlab/Simulink. The current and voltage responses on the converter side and grid side of the LCL filter are shown in Figs. 4.12 and 4.13, respectively. It is seen that the filter attenuates the harmonic distortion very effectively. The THD (total harmonic distortion) is measured by using Fast Fourier Transform (FFT) tool in Matlab. The THD of the grid side current is 1.17%, while the THD of the grid side voltage is 2.29%.

4.7. Simulation and Analysis

In this paper, the behavior of the combined wind farm with variable speed and fixed speed wind generators is analyzed in transient and steady state conditions. Two cases shown in Table 4.3 are considered in the transient and steady state simulation analyses to demonstrate the effectiveness and performance of the proposed strategy. In Case 1, a model system shown in Fig. 4.1 is analyzed. The controls are mainly performed by the power converters of VSWT-PMSG. The full-rating power converter of variable speed PMSG wind turbine system is

Table 4.3.

Cases studied

Case	G1 (2.5 MW)	G2 (5MW)	G3 (2.5 MW)
Case 1	SCIG	PMSG	SCIG
Case 2	SCIG	SCIG	SCIG

controlled in such a way that the grid voltage at the point of common connection (PCC) can be maintained at desired reference level (1 pu). In Case 2, simulation study is performed using the modified model system of Fig. 4.1 in which all of wind generators are installed with FSWT-SCIG only. Simulations were performed by using PSCAD/ EMTDC.

4.7.1. Transient Analysis

In the transient analysis, the unsymmetrical double line to ground (between phase A, B, and ground) fault (2LG) and the symmetrical three line to ground fault (3LG) at the transmission line are considered as network fault as shown in Fig. 4.1. The fault occurs at 0.1 s, then the circuit breakers (CBs) only on the faulted line are opened at 0.2 s, and the CBs are re-closed at 1.0 s assuming the fault has been cleared. During the simulation period from 0.0 s through 5.0 s, the wind speeds for both wind farms are assumed to be constant at rated speed (12 m/sec).

As the responses of G1 and G3 are same, the responses of G1 are shown in the figures for each simulation result. Figs. 4.14 to 4.21 show simulation results during 2LG. Figs. 4.14 to 4.15 show responses of reactive power output of each wind generator in Case 1 and Case 2, from which it is seen that the PMSG can provide necessary reactive power during the fault. In Case 2 all wind generators required large reactive power. Figs. 4.16 to 4.17 show the rotor speed response of wind generators. It is seen that the rotor speed of wind generator become stable in Case 1. Terminal voltages at the PCC can return back to the rated value quickly in Case 1 as shown in Fig. 4.18. Figs. 4.19 to 4.20 show the active power output of wind generators. It is seen that the active power supplied to the grid system can be recovered quickly after fault clearing in Case 1. Fig. 4.21 shows the DC-link circuit voltage of PMSG. By the DC link protection, the DC link voltage can be maintained almost constant.

Simulation results for 3LG are shown in Figs. 4.22 to 4.29. It can be understood that the wind farms can be stable in Case 1. On the other hand, the wind generators in both wind farms become unstable in Case 2 as shown in the simulation results.

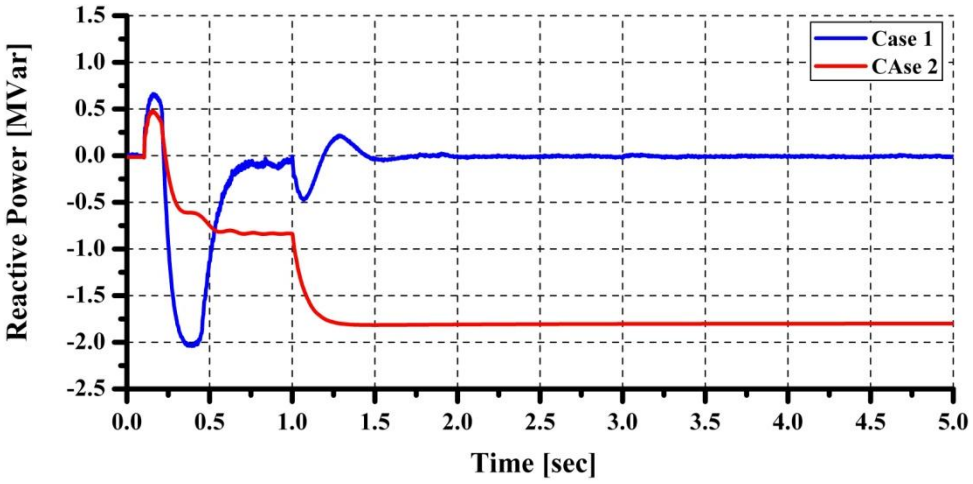

Fig. 4.14. Reactive power output of G1(G3) in 2LG

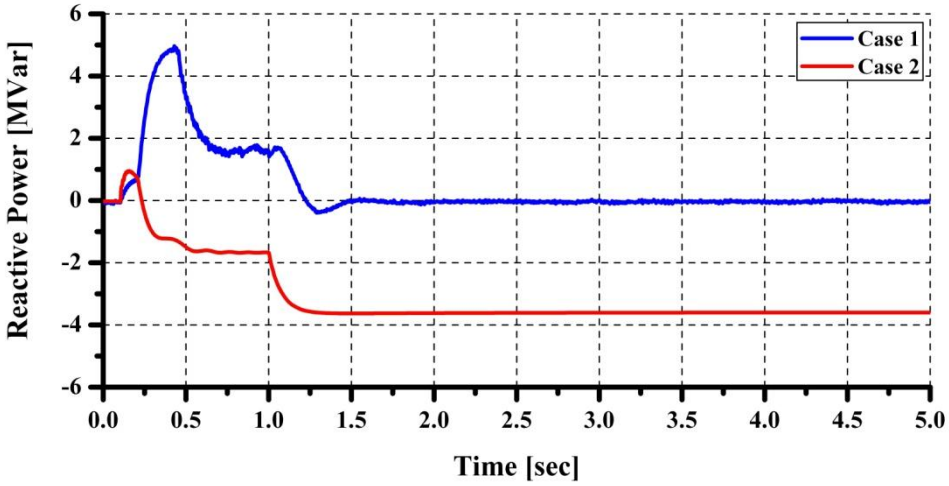

Fig. 4.15. Reactive power output of G2 in 2LG

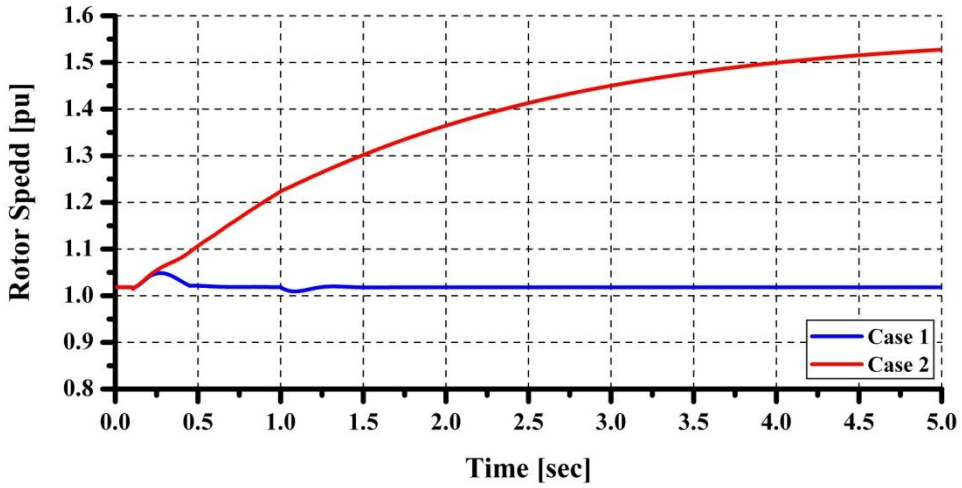

Fig. 4.16. Rotor speed of G1(G3) in 2LG

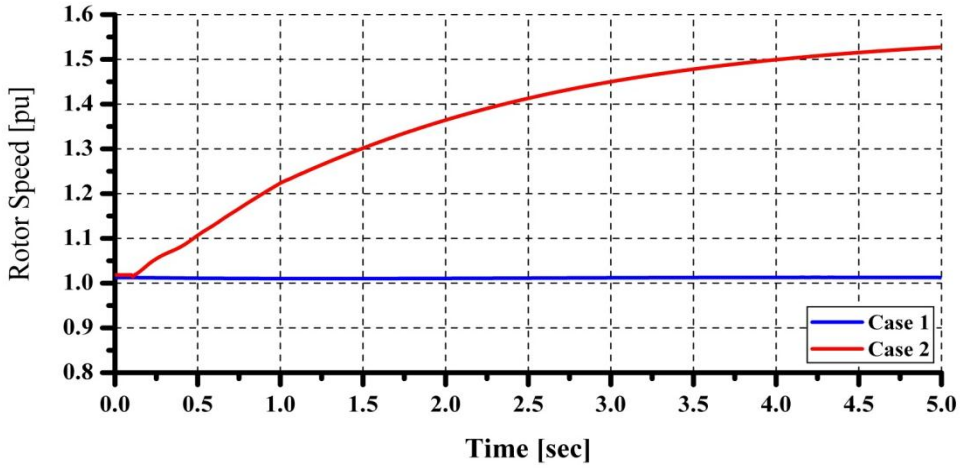

Fig. 4.17. Rotor speed of G2 in 2LG

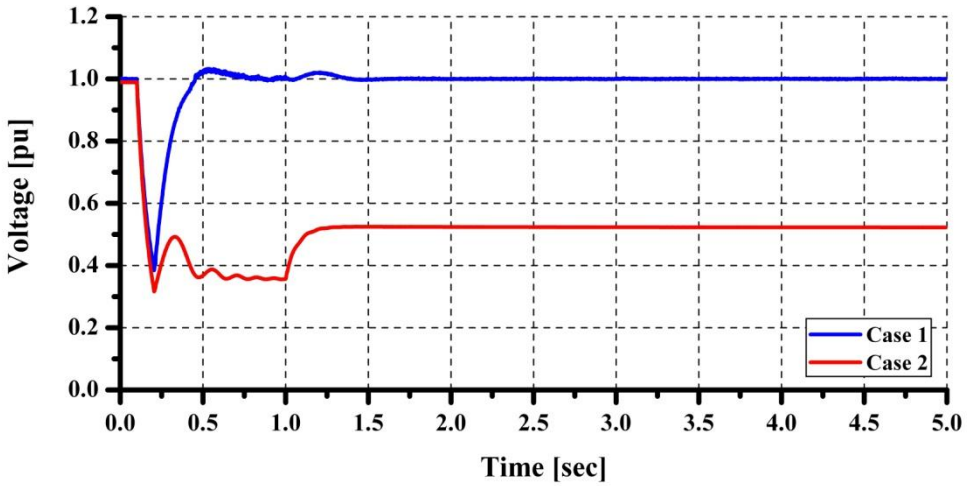

Fig. 4.18. Terminal voltage at PCC in 2LG

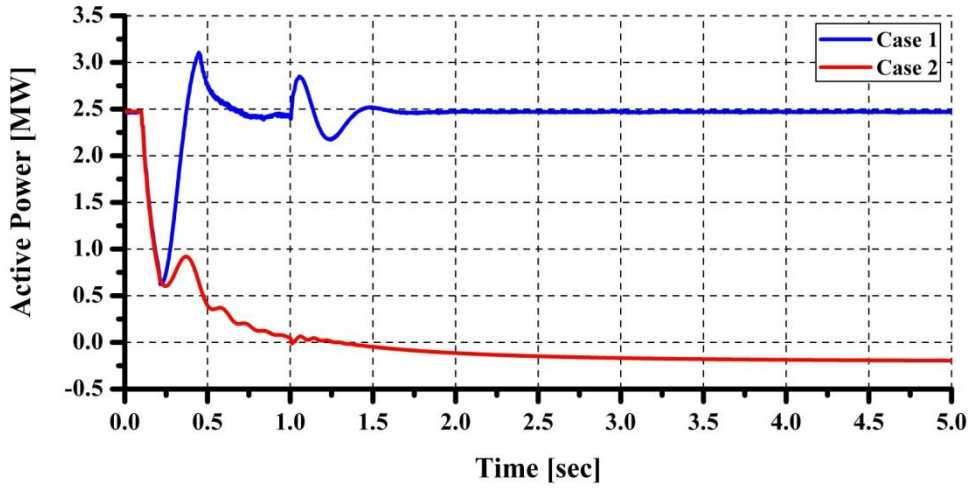

Fig. 4.19. Active power output of G1(G3) in 2LG

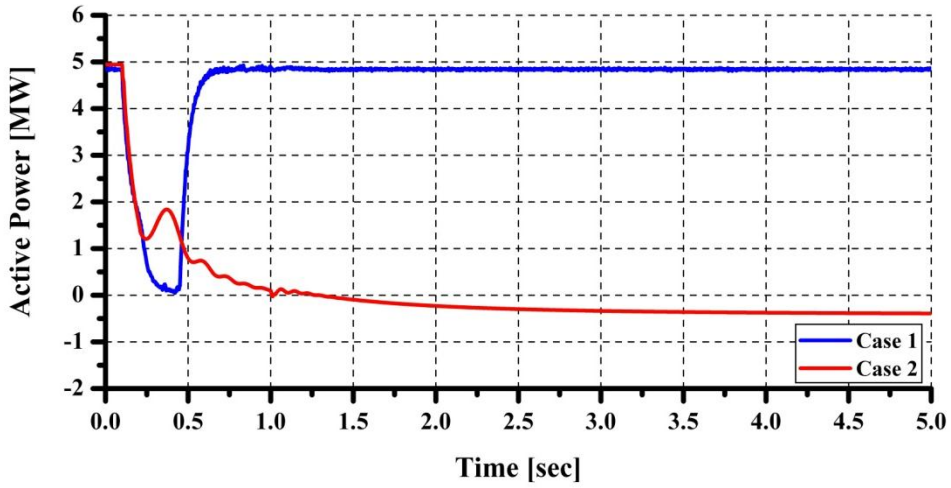

Fig. 4.20. Active power output of G2 in 2LG

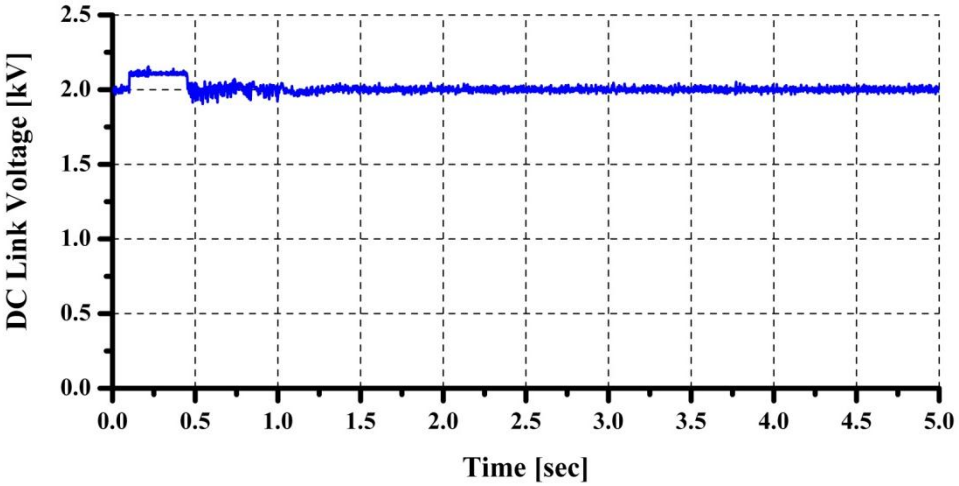

Fig. 4.21. DC link voltage of PMSG in 2LG

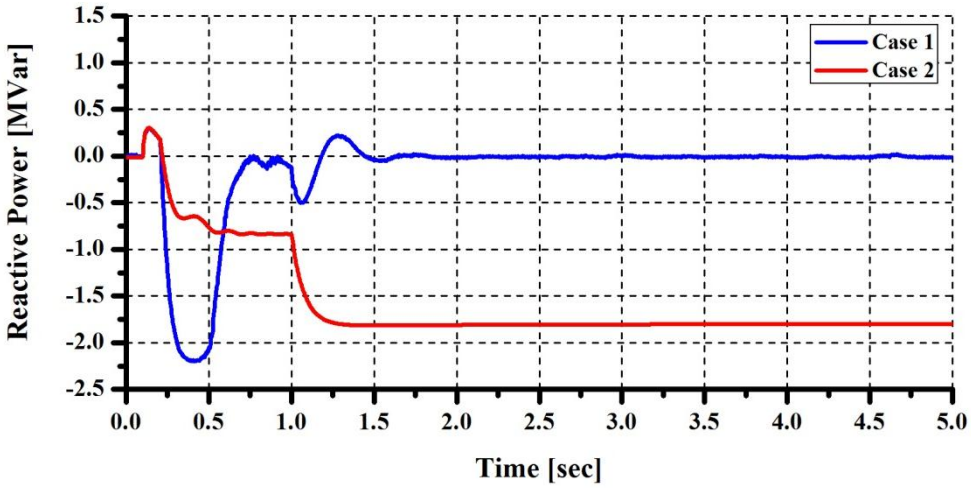

Fig. 4.22. Reactive power output of G1 (G3) in 3LG

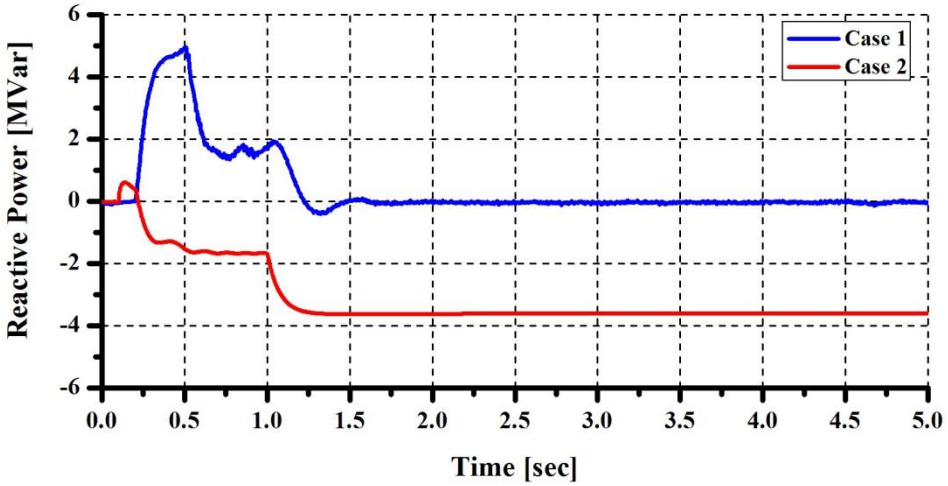

Fig. 4.23. Reactive power output of G2 in 3LG

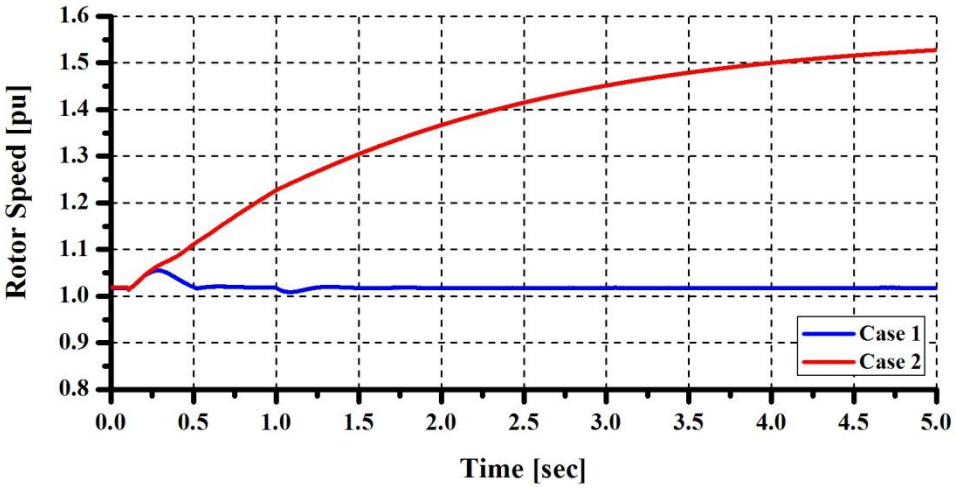

Fig. 4.24. Rotor speed of G1(G3) in 3LG

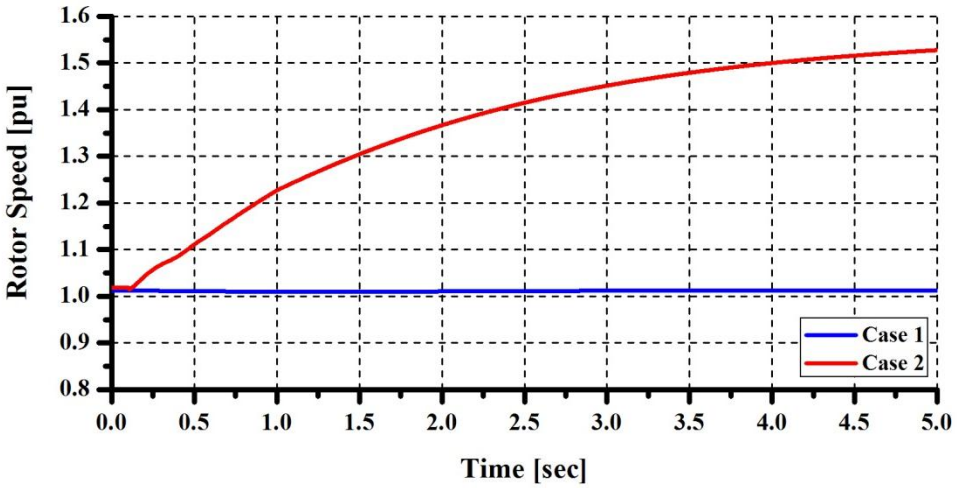

Fig. 4.25. Rotor speed of G2 in 3LG

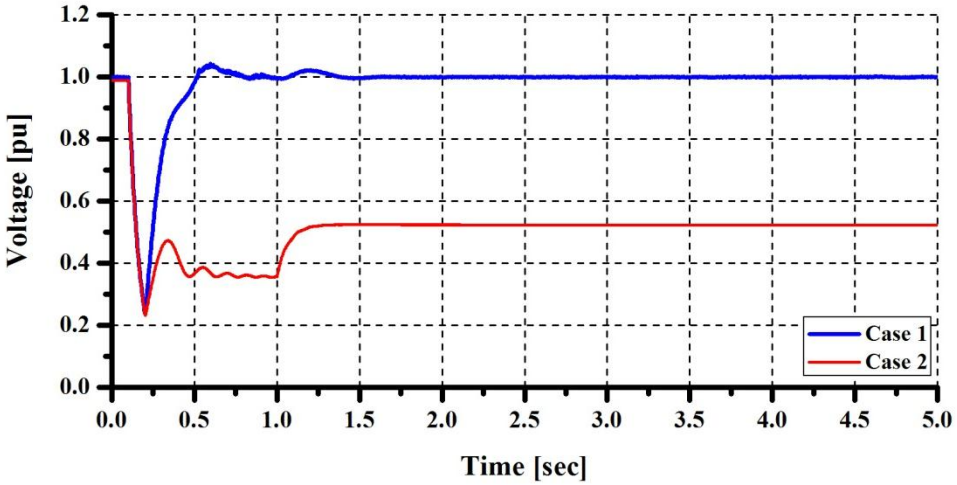

Fig. 4.26. Terminal voltage at PCC in 3LG

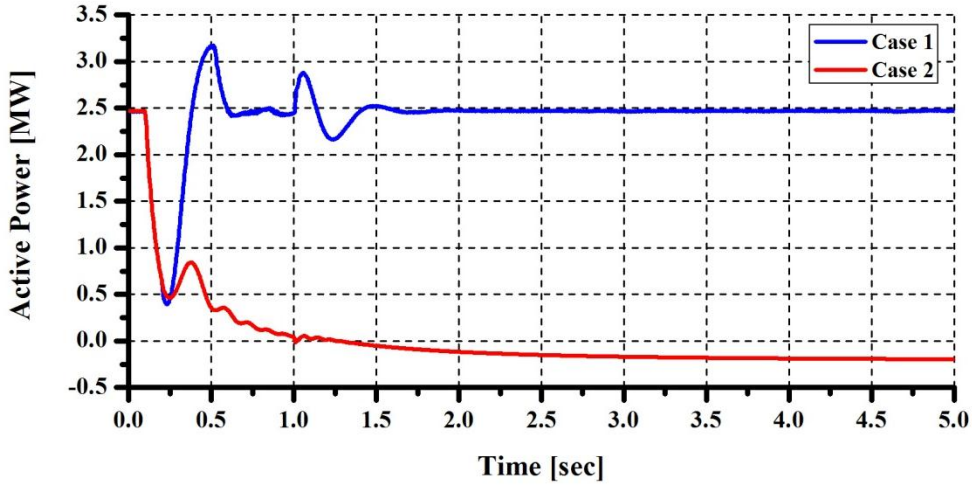

Fig. 4.27. Active power output of G1(G3) in 3LG

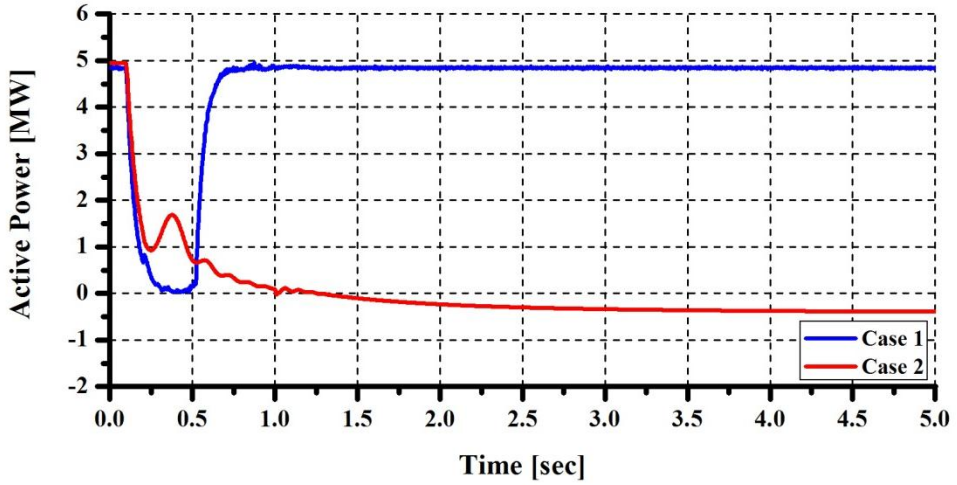

Fig. 4.28. Active power output of G2 in 3LG

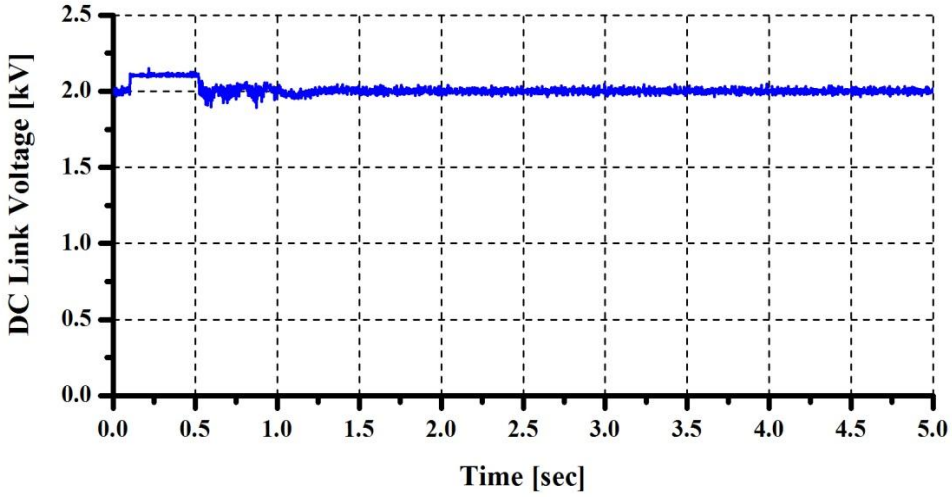

Fig. 4.29. DC link voltage of PMSG in 3LG

4.7.2. Steady State Analysis

The steady state performances of the proposed system are evaluated by using real wind speed data measured in Hokkaido Island, Japan, shown in Fig. 4.30. Fig. 4.31 shows the reactive power output of wind generators in Case 1. It is seen that the reactive power from the grid side converter of the VSWT-PMSG (G2) compensates the reactive power of FSWT-SCIG in G1 and G3 in order to maintain terminal voltage at PCC. Fig. 4.32 shows the terminal voltage at PCC in Case 1 and 2. It is seen that the voltage is controlled almost constant in Case 1.

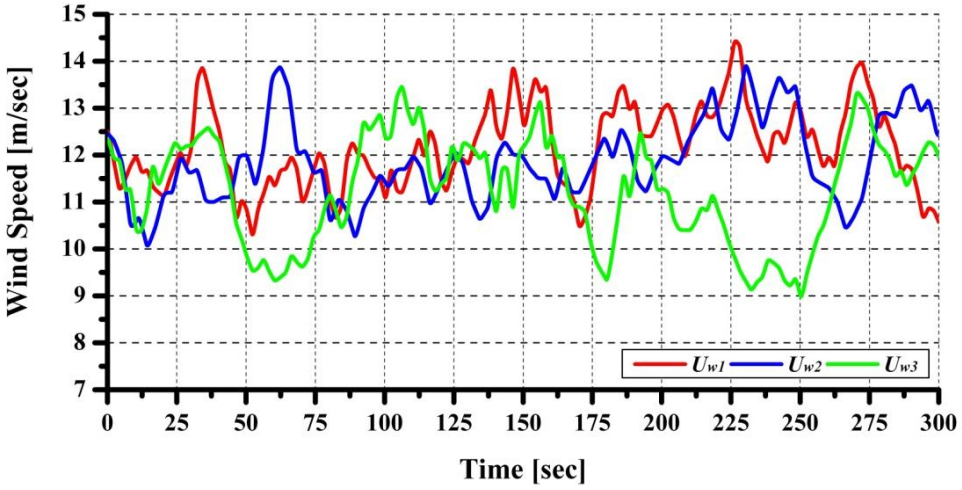

Fig. 4.30. Wind speed data

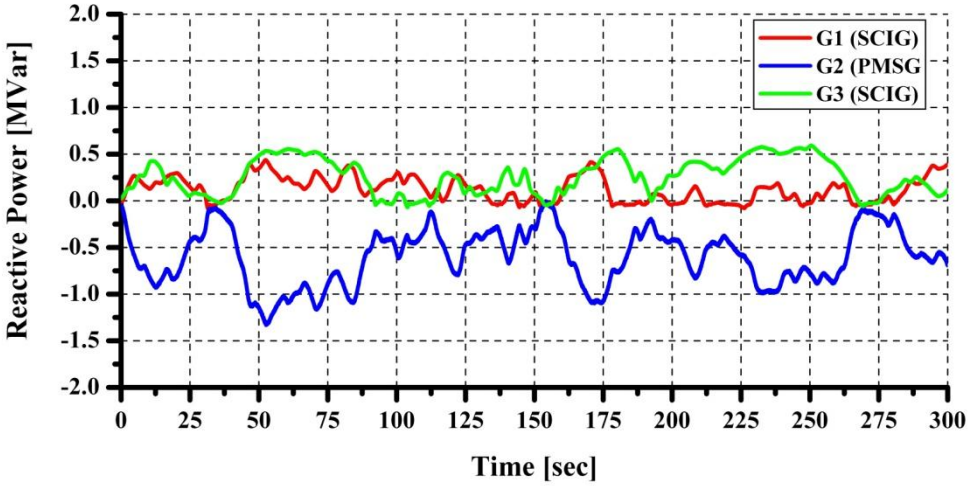

Fig. 4.31. Reactive power output of wind generators (Case 1)

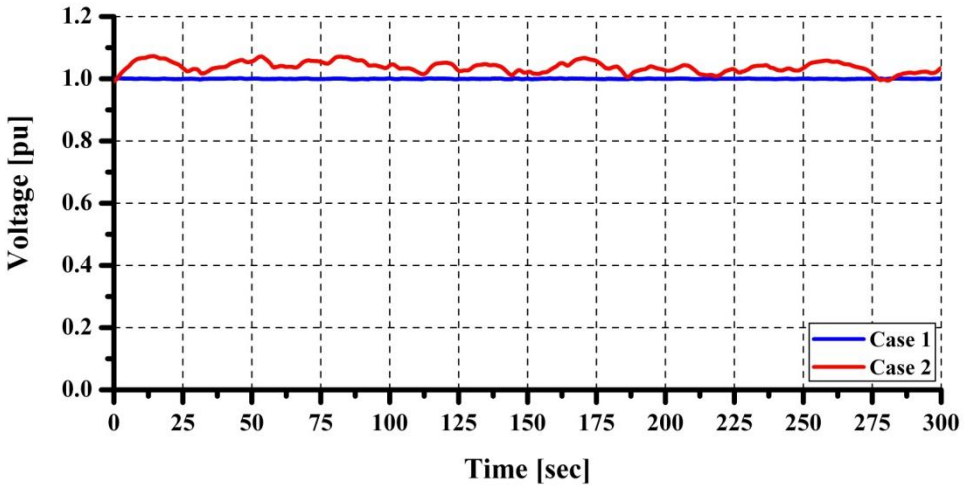

Fig. 4.32. Terminal voltage of wind farm at PCC

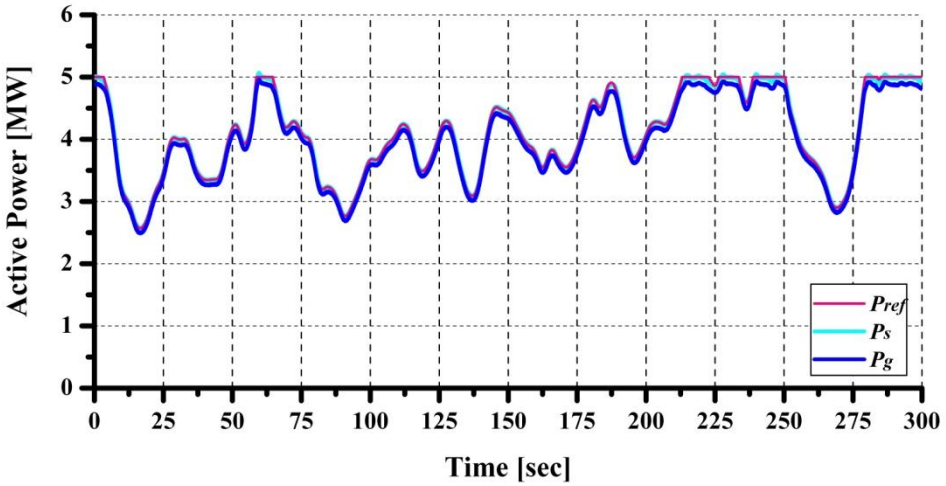

Fig. 4.33. Active power output of PMSG (Case 1)

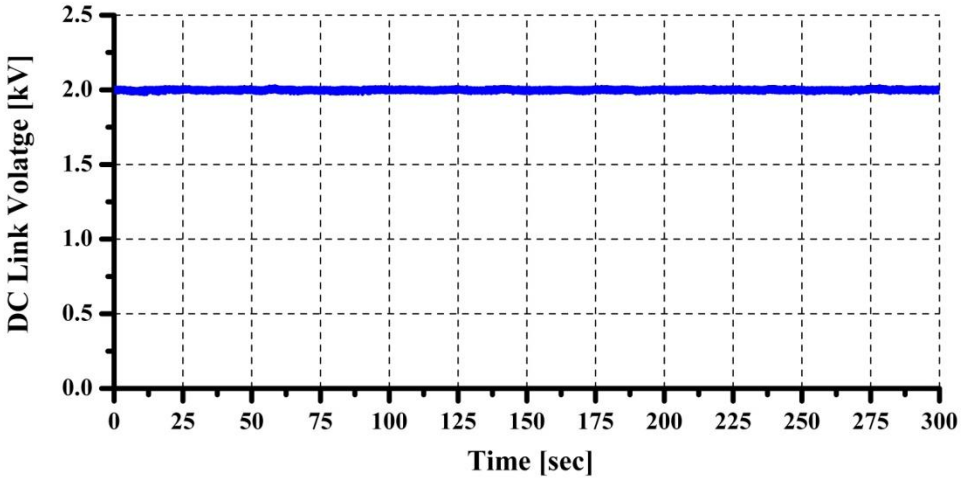

Fig. 4.34. DC link Voltage of PMSG (Case 1)

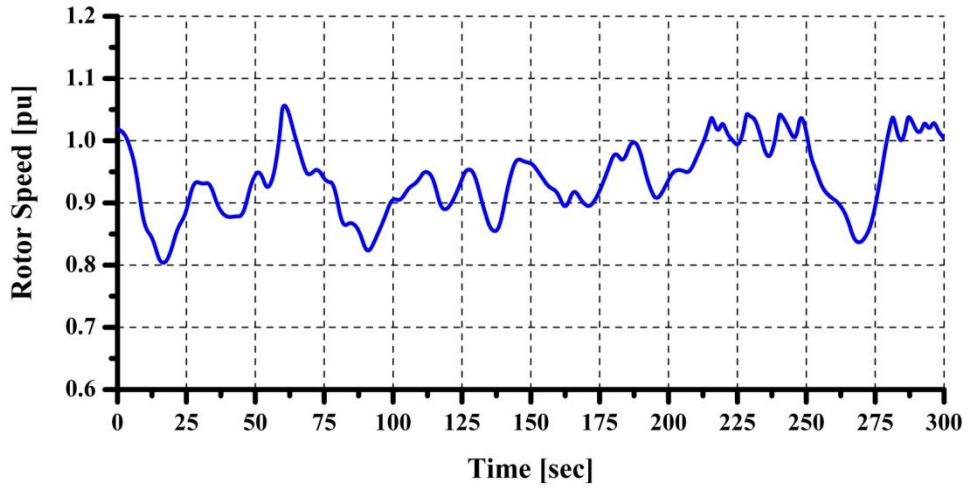

Fig. 4.35. Rotor speed response of PMSG (Case 1)

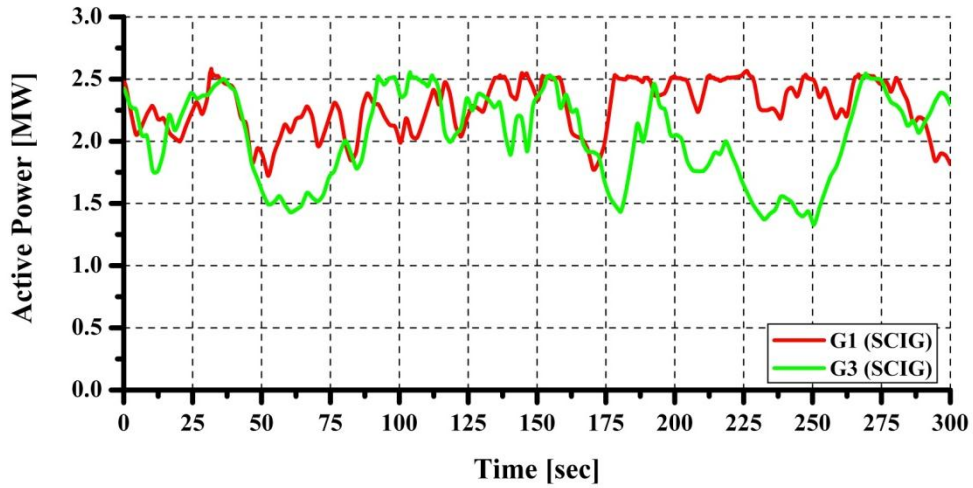

Fig. 4.36. Active power output of SCIGs (Case 1)

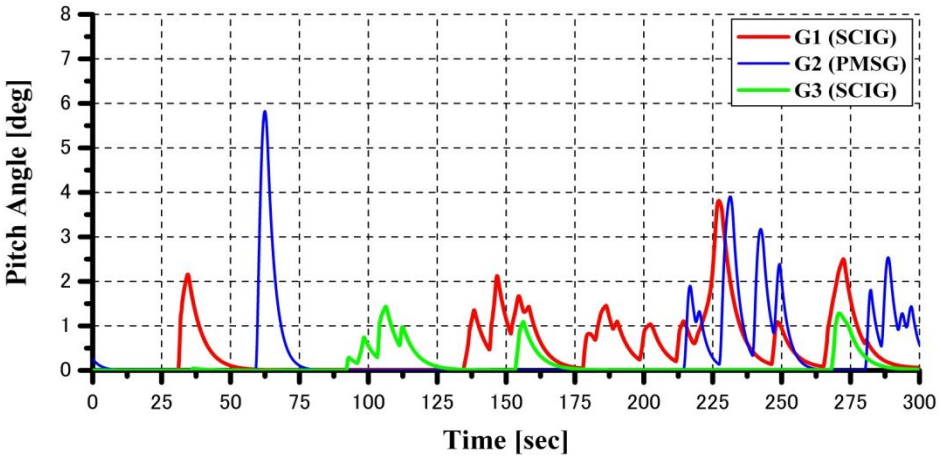

Fig. 4.37. Pitch angle response of wind generators (Case 1)

Fig. 4.33 shows the active power output of the PMSG, where P_{ref}, P_s and P_g are active power reference, active power output of SSC and active power output of GSC of PMSG, respectively. It can be noted that the power output of SSC and GSC can be tracking the reference very well. In Fig 4.34, the DC link voltage of PMSG is also remained constants. The rotor speed response of PMSG is shown in Fig. 4.35. The active powers of the SCIGs (G1 and G3) are shown in Fig. 4.36. Finally the pitch angle responses of wind generators are shown in Fig. 4.37.

4.8. Chapter Summary

In this chapter new control scheme of variable speed permanent magnet wind generator connected to grid system through LCL filter is proposed to enhance the stability of wind farm including fixed speed wind turbine based squirrel cage induction generator. The current controlled voltage source converter of PMSG system is developed based on the d-q rotating reference frame, in which the dynamic stability of the control system is analyzed based on frequency response of the Bode diagram. The control strategies of overall wind farm have been investigated in transient and steady state analyses to show the capability and effectiveness of the proposed method. The results show that the terminal voltage of wind farm can be recovered effectively during and after the unsymmetrical and the symmetrical faults, and thus the transient stability of fixed speed wind generator can be enhanced. In addition, the steady state performances show that the voltage fluctuation of wind farm under varying wind speed can be controlled almost constants at rated value and the active power of wind farms delivered to the grid can be controlled effectively. Moreover, it is also shown that the proposed LCL filter can attenuate the harmonic distortions of current and voltage output very effectively.

Chapter 5

Design of Fuzzy Logic Controller for Permanent Magnet Wind Generator to Enhance Dynamic Stability of Wind Farm

In this chapter, design method of fuzzy logic controller for variable speed permanent magnet wind generator connected to a grid system is proposed. A new current control method of grid side converter is developed with integrating the fuzzy controller, in which both active and reactive power delivered to a power grid system are controlled effectively. The fuzzy logic controller is designed to adjust the gain parameters of the PI controllers under any operating conditions for the dynamic stability to be enhanced. A simple method based on frequency response of Bode diagram is proposed in the design of the fuzzy logic controller. To evaluate the controller system capabilities, simulation analyses are performed on wind farm model system including induction wind generator connected to an infinite bus and multi-machine power system. The simulations have been performed using PSCAD/EMTDC. Simulation results show that the proposed control scheme is more effective to enhance the stability of wind farms during network disturbances and randomly fluctuating wind speed compared with that with conventional PI controllers.

5.1. Introduction

The back to back converter of PMSG consists of stator side converter and grid side converter linked by dc circuit. Since the VSWT-PMSG is applied to stabilise the FSWT-SCIG in a wind farm system, design of the grid side converter of the PMSG is very important. The grid side converter controller is most essential, because it can dominate the performance of the PMSG connected to a grid system. The grid side converter is required to ensure the power delivery to the network system effectively. Parameter change in the grid system can lead significant impact on the stability of the control system performance especially under fault condition. The deviation of grid system impedances can cause change in the stability gain margin and phase margin of the control system. In addition, the converter is operated at high switching frequencies between 2-15 kHz resulting high order harmonics which can disturb sensitive load on the grid and generate power losses [38],[39]. To reduce harmonic currents injected to the grid, LC filter is an attractive solution because of its many potential advantages such as higher harmonic attenuation and smaller inductances compared with L filter [40]. However, resonance frequency of the filter can cause stability problem on the control system

performance. Hence, determination of gain parameters should be performed carefully in the design process.

Traditionally, the conventional PI controller is very common in the control of the converter because of their simple structure and good performances in a wide range of operating conditions. The PI controllers are simple but cannot always effectively control systems with changing parameters or strong nonlinearities, and they may need frequent online retuning of their parameters [41].

On the other hand, fuzzy logic controller has attracted the attention of researchers because it can deal with nonlinear systems and does not need precise mathematical modeling of the system [42]-[44]. Compared with conventional PI controller, fuzzy logic controller has the potential to provide an improved performance even for a system with wide parameter variations [45]. The fuzzy logic controller has advantages of robust, simple, easily to be modified, usable for multi input and output sources, and to be implemented very quickly and cheaply. The fuzzy logic controller can take the place of conventional PI controller. Integration of fuzzy logic control with conventional PI controller can be an effective way to solve the problem of system parameter change. The fuzzy logic control can be used to adjust the gain parameters of PI controller for any operating conditions. Hence, a good control performance can be achieved. However, the membership function of the fuzzy set should be carefully determined in the controller design. It is difficult to achieve an optimal controller performance by using trial and error method.

5.2. Overview Fuzzy Logic System

The artificial intelligence techniques have been applied to convert human experience into a form understandable by computers. Advanced control based on artificial intelligence techniques is called intelligent control. Intelligent systems are usually explained by analogies, for example, how human beings perform control tasks, recognize patterns, or make decisions. There exists a mismatch between humans and machines. Human's reason is uncertain, imprecise, fuzzy ways, while machines and the computers are based on binary reasoning. Fuzzy logic is a way to make machines more intelligent enabling them to reason in a fuzzy manner like humans [84].

Fuzzy logic was first proposed by Lotfi A. Zadeh of the University of California at Berkeley in 1965. He elaborated on his ideas in the paper in 1973 that introduced the concept of *linguistic variables*, which in this article equate to a variable defined as a fuzzy set [85]. Fuzzy logic emerged as a tool to deal with uncertain, imprecise, or qualitative decision-making problems. Controllers that combine intelligent and conventional techniques are commonly used in the intelligent control of complex dynamic systems. Therefore, embedded fuzzy controllers automate what has traditionally been a human control activity. Other research with

the first industrial application, a cement kiln built in Denmark, came on line in 1975 [86]. Interest in fuzzy systems was sparked by Seiji Yasunobu and Soji Miyamoto of Hitachi. In 1985, they provided simulations that demonstrated the superiority of fuzzy control systems for the Sendai railway. Their ideas were adopted, and fuzzy systems were used to control accelerating, braking, and stopping when the line was opened in 1987 [86].

Traditional control approach requires modeling of the physical reality. Three methods may be used in the description of a system [84], [87]:

1. Experimental Method: By experimenting and determining how the process reacts to various inputs, one can characterize an input-output table. Graphically the method is equivalent to plotting some discrete points of the input-output curve, using the horizontal axis for input and the vertical axis for output. The disadvantages are that the process equipment may not be available for experimentation, the procedure would usually be very costly, and for a large number of input values it is impractical to measure the output and then interpolation between measured outputs would be required.
2. Mathematical Modeling: Control engineering requires an idealized mathematical model of the controlled process, usually in the form of differential or difference equations. Laplace transforms and z-transforms are respectively used. In order to make mathematical models simple enough, certain assumptions are made, one of which is that the process is linear, that is, its output is proportional to the input. Linear techniques are valuable because they provide good insight. Besides, there exists no general theory for the analytic solution of nonlinear differential equations and consequently no comprehensive analysis tools for nonlinear dynamic systems. The following problems arise in developing a meaningful and realistic mathematical description of an industrial process: poorly understood phenomena, inaccurate values of various parameters, and model complexity.
3. Heuristics Method: The heuristic method consists of modeling and understanding in accordance with previous experience, rules-of-thumb and often-used strategies. A heuristic rule is a logical implication of the form: If <condition> Then <action>. Rules associate with conclusions with conditions. Therefore, the heuristic method is actually similar to the experimental method of constructing a table of inputs and corresponding output values instead of having crisp numeric values of input and output variables. The advantages of the heuristic method are: (1) the assumption of linearity is not required, and, (2) heuristic rules can be integrated to the control strategies of human operators.

Fuzzy control strategies come from experience and experiments rather than from mathematical models and, therefore, linguistic implementations are much faster accomplished.

Fuzzy control strategies involve a large number of inputs, most of which are relevant only for some special conditions. Such inputs are activated only when the related condition prevails. In this way, little additional computational overhead is required for adding extra rules. As a result, the rule base structure remains understandable, leading to efficient coding and system documentation.

5.3. VSWT-PMSG Control System

The VSWT-PMSG and its controller systems are shown in Fig. 5.1. The VSWT-PMSG system consists of a direct drive PMSG, blade pitch controller, AC/DC/AC converters based on two levels of IGBT which are composed of stator side converter (SSC) and grid side converter (GSC), a DC-link circuit composed of a chopper with a resistance (R_{ch}) and a capacitor (C_{dc}), two voltage source converter controllers (stator side controller and grid side controller), and LC filter with passive damping resistance (R_d).

The SSC is connected to the stator of PMSG, and it converts the three phase AC voltage generated by PMSG to DC voltage. The three phase voltage and current of PMSG are detected on the stator terminal. The rotor speed of PMSG is detected from the rotor of the generator. All outputs of the sensors are fed to the stator side controller as input signals in order to control the voltage references of the stator side converter for modulation.

In the GSC, the converter converts the DC voltage into three phase AC voltage of the grid frequency. The converter is connected to the grid system through a LC filter and a step up transformer. The grid current and the grid voltage are detected on the converter side of LC filter and the high voltage side of the transformer, respectively. The DC voltage (V_{dc}) is detected on the DC capacitor. The voltage reference of grid side voltage source converter for modulation is controlled by using the grid side controller. When a fault occurs in the grid, the V_{dc} increases significantly due to power unbalance between SSC and GSC. In order to protect the DC-link circuit, the controller activates the chopper by a trigger command (*Ctrl*).

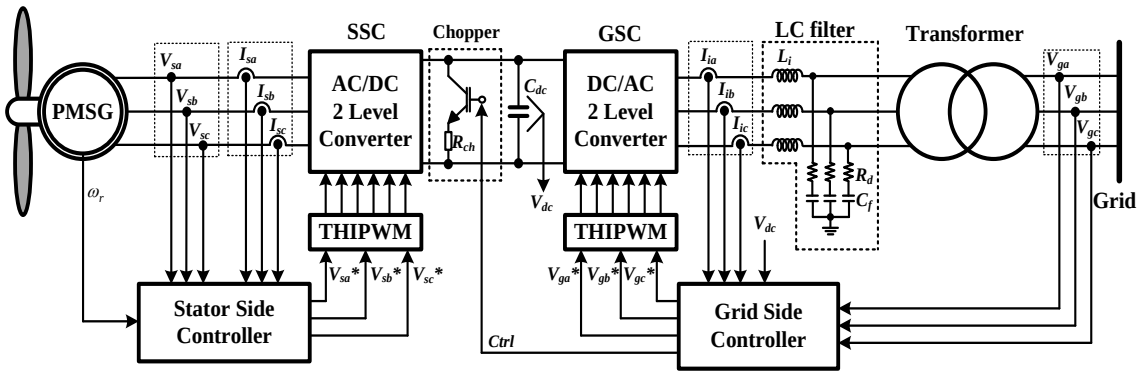

Fig. 5.1. The VSWT-PMSG Control System

Table 5.1.

System parameters

Component	Parameter	Symbol	Value
Wind Turbine	Blade Radius	R	40 m
	Rated Wind Speed	V_w	12 m/s
	rated rotation speed	ωr	2.43 rad/s
	Maximum Power Coefficient	Cp_{opt}	0.48
	Optimum Tip Speed Ratio	λ_{opt}	8.1
	Air density	ρ	1.225 Kg/m3
	Inertia	J_{wt}	10,137,000 Kgm2
PMSG	Rated Voltage	V	1.0 kV
	Rated Frequency	fe	20 Hz
	Magnetic Flux	ψ_m	1.4 pu
	Stator Winding Resistance	R_s	0.01 pu
	The d-axis inductance	L_d	0.95 pu
	The q-axis inductance	L_q	0.75 pu
	Pole pairs	p	52
AC/DC/AC Power Converter	SSC frequency Switching	fs	2 kHz
	GSC frequency Switching	fs	4 kHz
	Grid Frequency	fg	50 Hz
	DC Link capacitor	C_{dc}	25000 μF
	DC Link voltage	V_{dc}	1.75 kV
LC Filter	Inverter side inductance	L_i	0.07 pu
	Inverter side parasitic resistance	R_i	0.0056 pu
	Filter capacitor	C_f	0.05 pu
	Damping Resistance	R_d	0.3 pu
Step Up Transformer	Transformer inductance	L_g	0.04 pu
	Transformer resistance	R_g	0.015 pu
	Low voltage	V_{TL}	1.0 kV
	High voltage	V_{TH}	66 kV

Output power of a wind generator always fluctuates due to the wind speed variations. To maintain the output power of generator under the rated level, a pitch controller is used to regulate rotational speed of PMSG under its rated value.

In modulation technique, Third Harmonic Injection Pulse Wave Modulation (THIPWM) is used in this work. Injection of third harmonic in the reference voltage makes it possible to

utilize the voltage reference without over modulation. In addition, the THIPWM can maximize fundamental amplitude of the output voltage [77].

In this paper 2.5 MVA class of VSWT-PMSG is considered. Table 1 presents the system parameters of the grid connected VSWT-PMSG. In order to determine the LC filter parameters, step by step procedures and limitations of the filter parameters presented in [39] are adopted.

5.3.1. Stator Side Controller

Detail of the stator side controller system is presented in a block diagram shown in Fig. 5.2. The active power (P_s) and reactive power (Q_s) of the generator are controlled by the d-axis current (I_{sd}) and the q-axis current (I_{sq}), respectively. The value of active power reference (P_{ref}) is determined by MPPT method. For unity power factor operation, the reactive power reference (Q_s*) is set to zero. The cross couplings, $I_{sd}\omega_e L_{sd}$ and $I_{sd}\omega_e L_{sq}$, should be compensated at the output of the current controllers in order to improve tracking capability of the control system. Finally, V_{sd}* and V_{sq}* are voltage reference output of current controller which is used to generate the three phase reference voltage (V_{sa}*, V_{sb}*, V_{sc}*) to control stator currents of the PMSG.

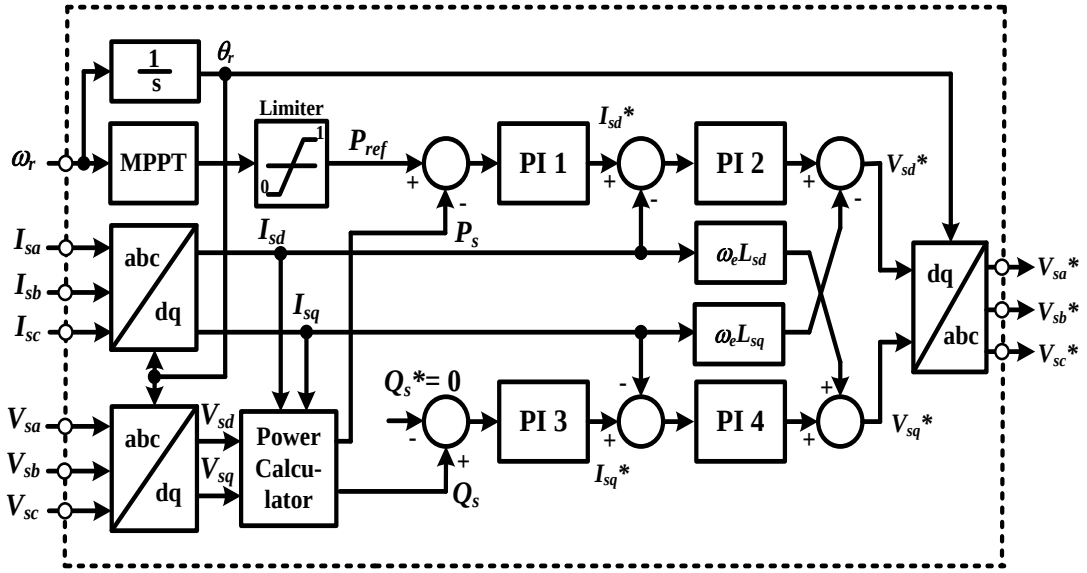

Fig.5.2. Stator side controller system

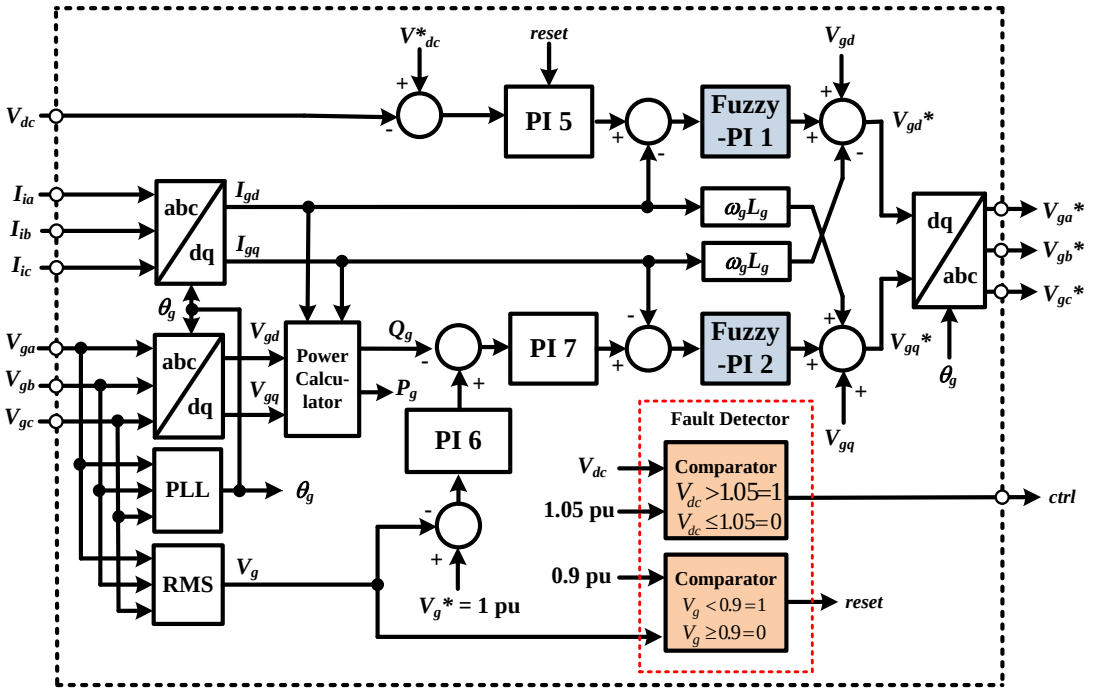

Fig.5.3. Grid side controller

5.3.2. Grid Side Controller

Fig. 5.3 shows a block diagram of the grid side controller system. In this control strategy, the control system based on the d-q rotating reference frame is implemented which has same rotational speed as the grid voltage. The three phase currents of converter side of LC filter (I_{ia}, I_{ib}, I_{ic}) and the grid voltages (V_{ga}, V_{gb}, V_{gc}) are transformed into the d-q rotating reference frame by using Park transformation. The Phase Locked Loop (PLL) [15] is used to extract the grid side phase angle (θ_g). The active and reactive power delivered to the grid are controlled separately by the d-axis current (I_{gd}) and the q-axis current (I_{gq}), respectively. To improve tracking capability of control system, the cross coupling should be canceled by adding $I_{gd}\omega L_g$ and $I_{gq}\omega L_g$ at the output of the current controllers. For d-axis and q-axis current loop regulation, in this study the Fuzzy-PI controllers are applied. The control strategy for the Fuzzy-PI controller will be explained in Section 5.4. The output of current controller (V_{gd}* and V_{gq}*) is transformed into the stationery reference frame (V_{ga}*, V_{gb}*, V_{gc}*) which is used as reference signal for pulse wave modulation.

In normal mode operating condition, the voltage of DC-link capacitor (V_{dc}) is maintained constant in order to transfer the active power generated by PMSG to the grid. The d-axis current reference signal is determined from output of the DC-voltage controller, and the q-axis current reference signal is obtained from reactive power controller output. The reactive power reference (Q_g*) is set so that the terminal voltage at the high voltage side of the transformer

remains constant. In grid fault condition, the active power transfer to the grid is set to zero by trigger reset command to PI 5. By using this way supplying reactive power to the grid can be maximized. At the same time the detector send the control signal command (*ctrl*) to trigger the DC link protection. The *reset* command is activated when the grid voltage decreases under 0.9 pu. The *ctrl* command is activated when the DC link voltage exceeds the predefined limit (1.75 kV, 1.05 pu).

5.4. Fuzzy-PI Controller Design

In order to design fuzzy logic controller (FLC) for the current control loop, the equivalent circuit of single-phase LC filter including transformer impedance shown in Fig. 5.4 is modeled as plant system. The LC filter is composed of an inverter side inductance (L_i) and its parasitic resistance (R_i), a filter capacitor (C_f), and a damping resistance (R_d). Transformer impedance consists of leakage inductance (L_g) and resistance (R_g). V_i and I_i are voltage and current on the converter side of the LC filter. V_g and I_g are voltage and current on the grid side of the transformer. It should be noted that V_{cf} is a voltage on the filter capacitor (C_f).

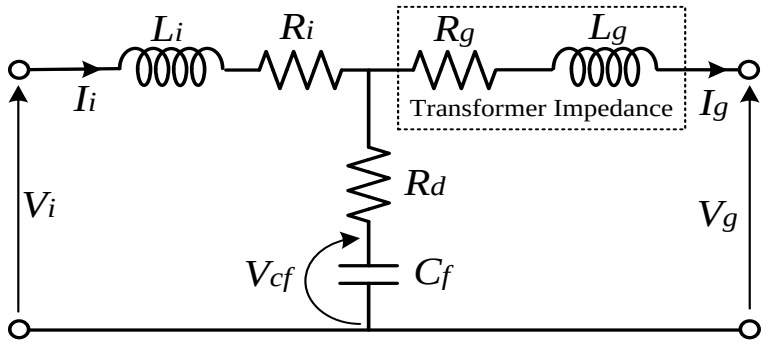

Fig. 5.4. Single phase LC filter with transformer equivalent circuit

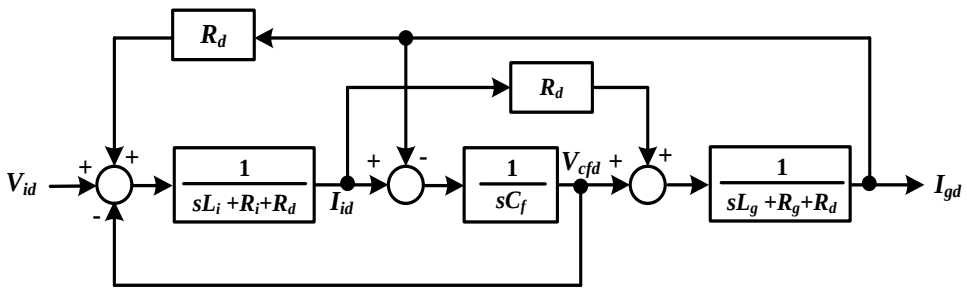

Fig. 5.5. The LCL filter in d-axis component only

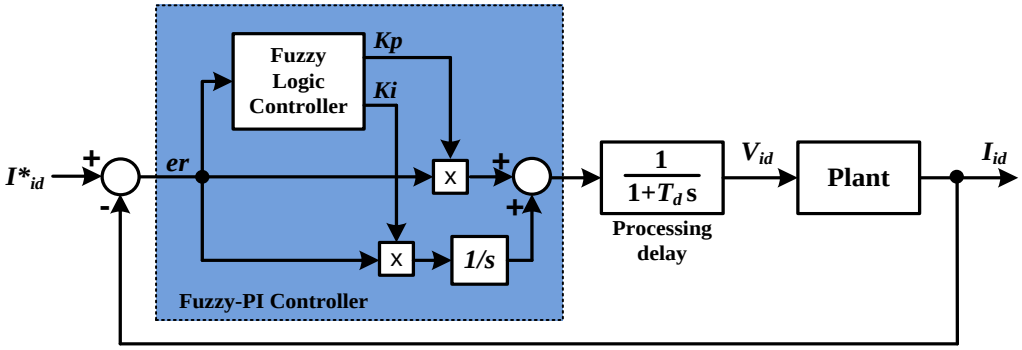

Fig. 5.6. Current control loop of GSC

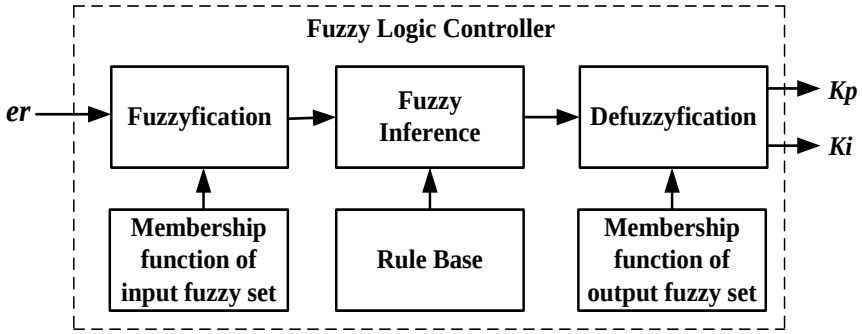

Fig. 5.7. Block diagram of fuzzy logic controller

Additional transformer parameters in output of LC filter in the d-q rotating reference frame shown in Fig. 4.5 (in Chapter 4) can be considered as a plant system. The plant system can be modelled by using the d-axis component only as shown in Fig. 5.5, where the cross coupling and the grid voltage are neglected. Fig. 5.6 shows a block diagram of the current control loop for GSC. The control system is composed of a Fuzzy-PI controller, a processing delay, and plant system, using the converter side voltage (V_{id}) as input and the converter side current (I_{id}) as output. The FLC is used to adjust the PI parameters according to the input signal error (*er*). To determine control signal for proportional gain (K_p) and integral gain (K_i), inference engine with rule base having if-then rules in the form of "If *er*, then K_p and K_i" is used.

The general structure of the fuzzy logic control is shown in Fig 5.7. The FLC is composed of fuzzification, membership function, rule base, fuzzy inference and defuzzification. The fuzzification comprises the process of transforming crisp values into grades of membership for linguistic terms of fuzzy sets. The membership function is used to associate a grade with each linguistic term. For fuzzification of the three variables of the FLC, the error (*er*) have five

triangle membership functions and the gain outputs, *Kp* and *Ki*, have three triangle membership functions. The variables fuzzy subsets for input are Negative Big (NB), Negative Small (NS), Zero (Z), Positive Small (PS), and Positive Big (PB). The variables fuzzy subsets for output are Small (SM), Medium (MD), and Big (BG). Fig. 5.8 shows the membership function for input *er*. The interval input of the membership function is set at [-1 to 1] due to the variation of the d-axis or q-axis current between -1 to 1 pu.

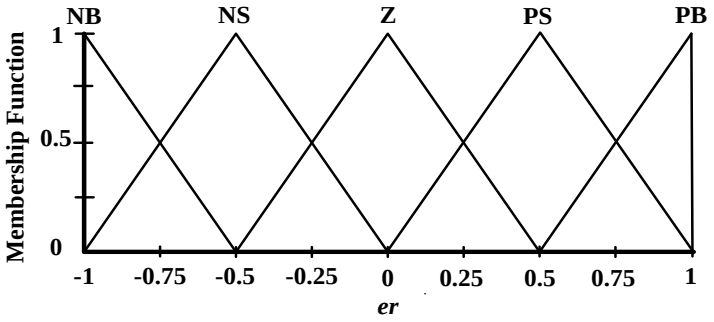

Fig. 5.8. The membership function for input *er*

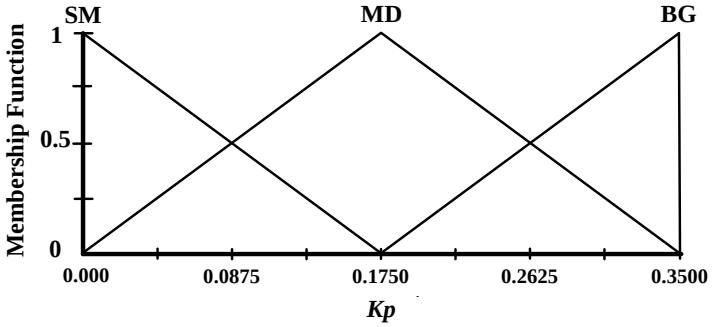

Fig. 5.9. The membership function for output *Kp*

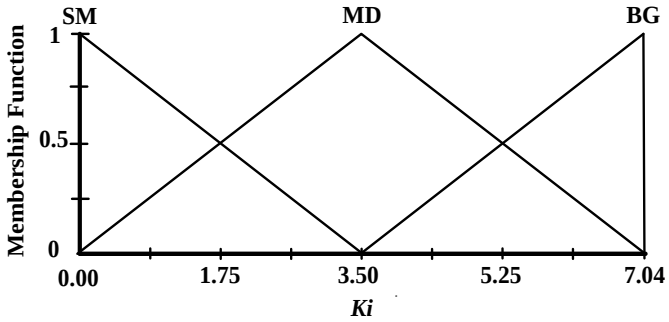

Fig. 5.10. The membership function for output *Ki*

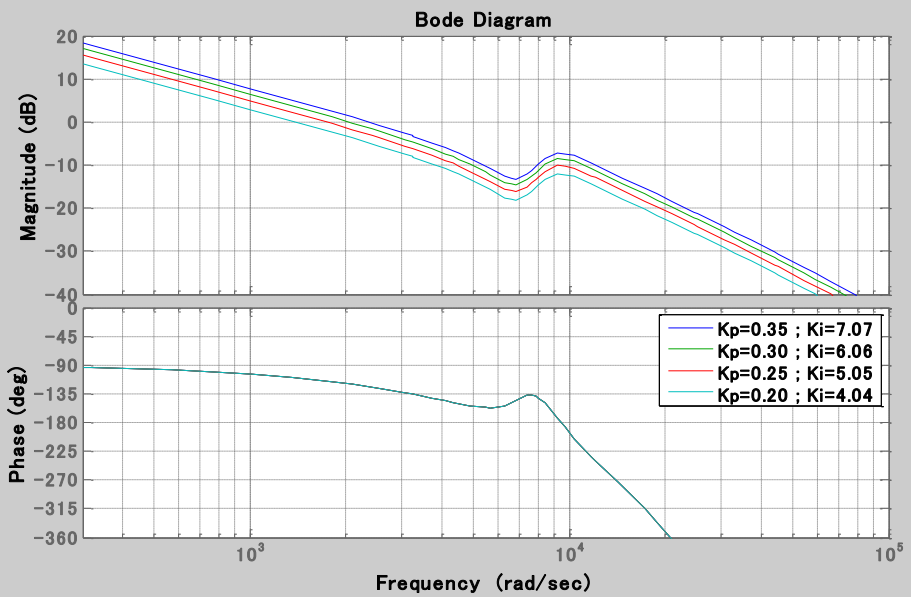

Fig. 5.11. Bode diagram of current control loop of GSC

Figs. 5.9 and 5.10 show the membership functions of output for *Kp* and *Ki*, respectively. The membership functions are designed based on frequency response of the Bode diagram of the current control loop. In this paper the initial gain K_p is obtained by using optimum modulus criterion. The integral time constant (T_i) of controller system is set equal to the plant system time constant (L_{tot}/R_{tot}). L_{tot} and R_{tot} are total of series inductances and its parasitic resistances of the plant system, respectively. The integral gain can be calculated by using $K_i = K_p/T_i$.

Fig. 5.11 shows frequency response of the Bode diagram of the current loop control of GSC for four different values of K_p and K_i. It is seen that maximum gain with gain margin (Gm) larger than 6 dB and phase margin (Pm) larger than 45 deg is obtained with K_p= 0.35 and K_i =7.07. Therefore, the interval of membership function for output *Kp* and *Ki* can be set at [0.0 to 0.35] and [0.00 to 7.04] as shown in Figs. 5.9 and 5.10, respectively.

The rules are set based upon the knowledge and working of the system. The gain values of *Kp* and *Ki* for PI controller of the current regulator are calculated for the changes in the input of the FLC according to the rule base. The number of rules can be set as desired. A rule in the rule base can be expressed in the form:

If (*er* is NB), then (*Kp* is BG) and (*Ki* is BG)
If (*er* is NS), then (*Kp* is MD) and (*Ki* is MD)
If (*er* is ZE), then (*Kp* is SM) and (*Ki* is SM)
If (*er* is PS), then (*Kp* is MD) and (*Ki* is MD)
If (*er* is PB), then (*Kp* is BG) and (*Ki* is BG)

The rule base includes five rules, which are based upon the five membership functions of the input variables to achieve the desired *Kp* and *Ki*. In this work, Mamdani's max-min method is used for inference mechanism. The centre of gravity method is used for defuzzification to obtain P_{er} and I_{er}, which is given by the following equation:

$$K_p \text{ and } K_i = \frac{\sum_{i=1}^{n} \mu_i C_i}{\sum_{i=1}^{n} \mu_i} \tag{5-1}$$

where, n is the total number of rules, μ_i is the membership grade for the i-th rule, and C_i is the coordinate corresponding to respective output or consequent membership function.

To analyse the dynamic performance of current control loop, the linear block model as shown in Fig. 5.6 is used. The analysis has been performed by using Matlab/Simulink. Fig. 5.12 shows step response of the current control loop. The reference for the d-axis current has been varied four times at every 100 msec. It is seen that good performance can be achieved by using proposed Fuzzy-PI controller. The three phase current on the grid side as well as I_{id} have been observed by using power system blockset as shown in Fig. 5.13. It can be seen that the three phase current tracks the reference very well.

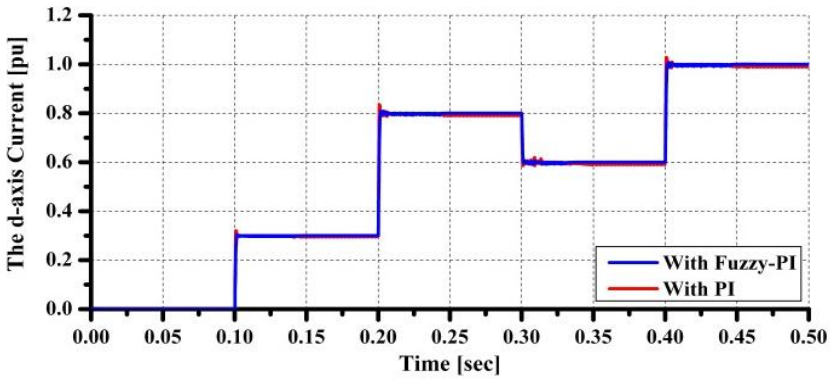

(a) Step response

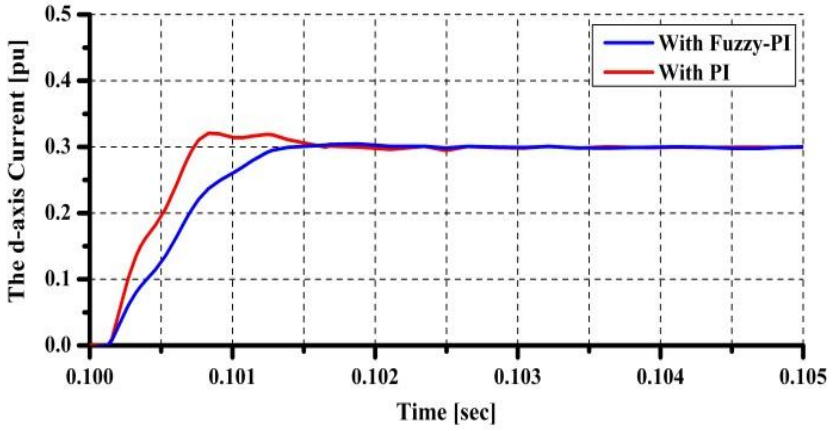

(b) Zoom of step response at 0.1 sec

Fig. 5.12. Linear block model analysis

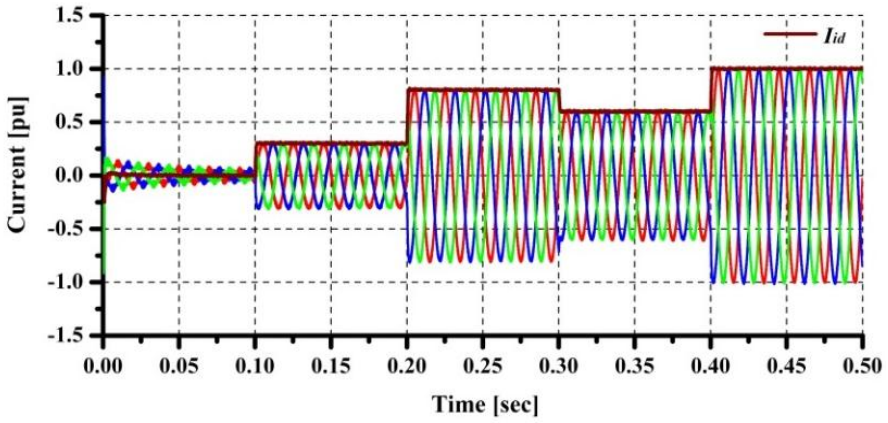

Fig. 5.13. Power system blockset model analysis

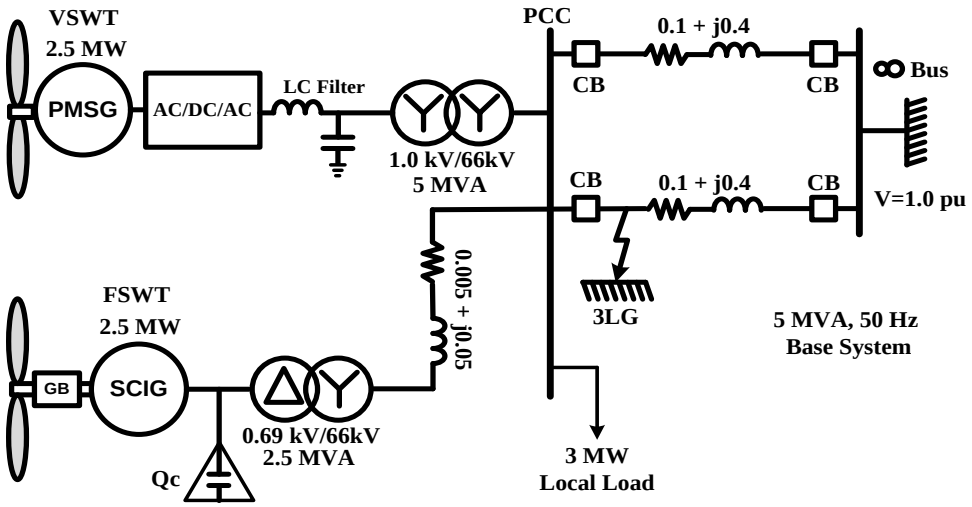

Fig. 5.14. Power system model

5.5. Simulation Analysis

5.5.1. Stabilization of Small Wind Farm Connected Infinite Bus

In order to investigate the performance of the proposed control system, a model system shown in Fig. 5.14 where VSWT-PMSG and FSWT- SCIG are installed in neighboring small wind farms connected to an infinite bus is analyzed in this study, where the VSWT-PMSG is connected to the infinite bus through AC/DC/AC power converter, LC filter, a 1.0/66 kV step up transformer and a double circuit transmission line. The FSWT-IG rated at 2.5 MW is also connected to the infinite bus via a 0.69/66 kV step up transformer and a single circuit and double circuit transmission lines. The FSWT-SCIG is controlled only by a pitch angle controller in order to regulate power output of IG under the rated power. The both wind generators are connected at point of common connection (PCC), to which a local load is also connected. In order to compensate reactive power consumption by IG, a capacitor bank (Qc) is

installed at the terminal of SCIG. The value of the capacitor is determined so that the power factor becomes unity at rated power operation. The resistance and reactance of the transmission line is represented in the form of R+jX in per unit as shown in the figure, respectively. The simulation analyses have been performed by using PSCAD/ EMTDC.

5.5.1.1. Transient Analysis

In the transient stability analysis, a symmetrical three line to ground (3LG) fault at the transmission line is considered as network disturbance, as shown in Fig. 4.14. Temporary fault (Case 1) and permanent fault (Case 2) are considered in the simulation study to show the effectiveness of the proposed control. In Case 1, the fault occurs at 0.1 sec; the circuit breakers (CBs) on the faulted line are opened at 0.2 sec, and at 1.0 sec the CBs are re-closed. In Case 2, the fault occurs at 0.1 sec; the CBs on the faulted line are opened at 0.2 sec, and at 1.0 sec the CBs are re-closed, and at 1.1 sec the CBs are opened again because the fault is still continuing. In this transient analysis, the wind speeds for the wind generators are kept constant at the rated speed (12 m/s), assuming that the wind speed does not change in the short time duration.

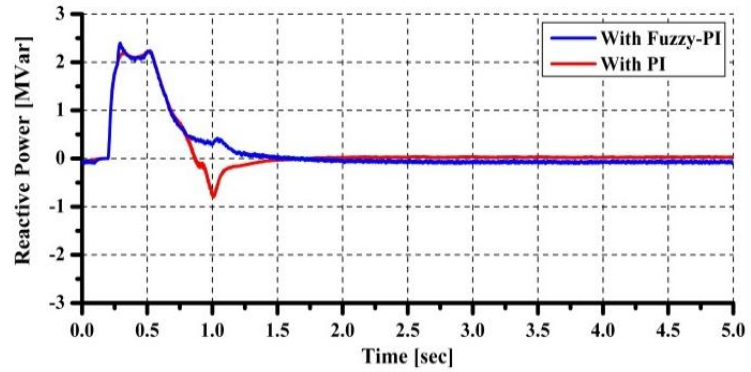

(a) Case 1

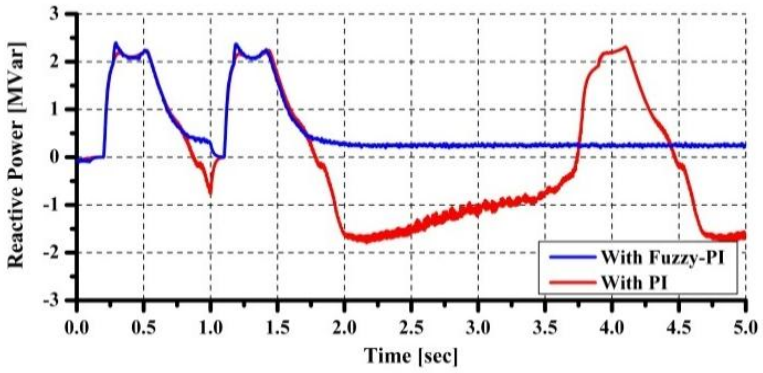

(b) Case 2

Fig. 5.15. Reactive power output of PMSG

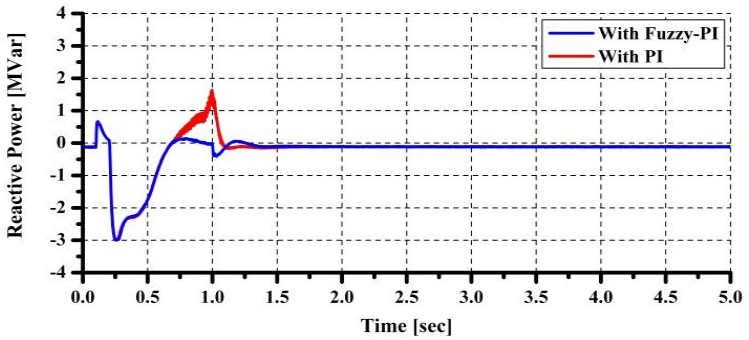

(a) Case 1

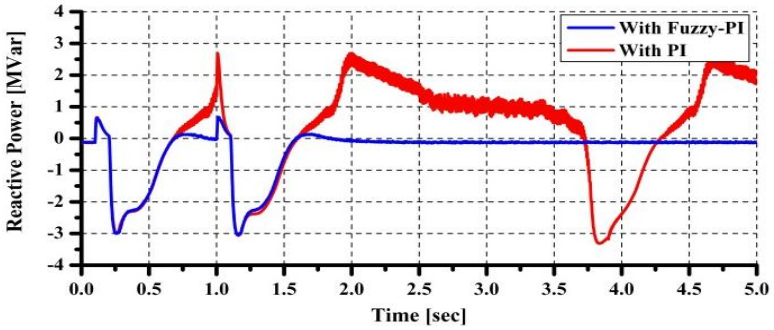

(b) Case 2

Fig. 5.16. Reactive power output of SCIG

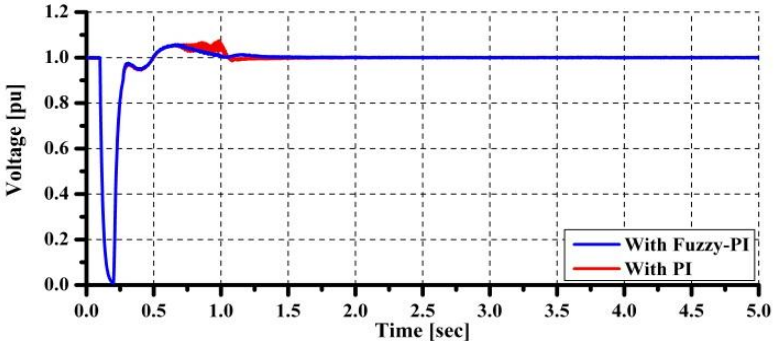

(a) Case 1

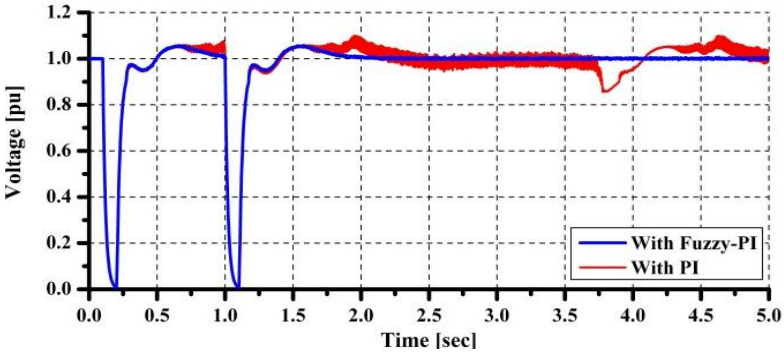

(b) Case 2

Fig. 5.17. Terminal voltage at PCC

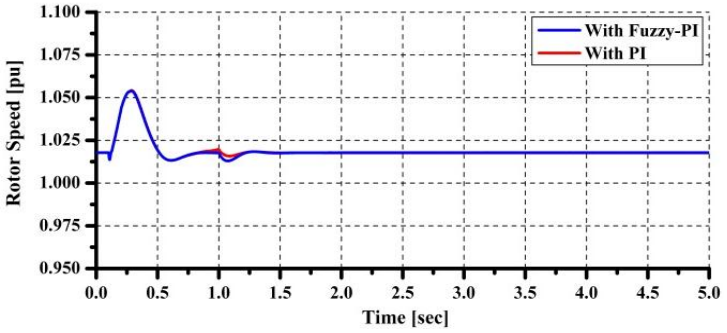

(a) Case 1

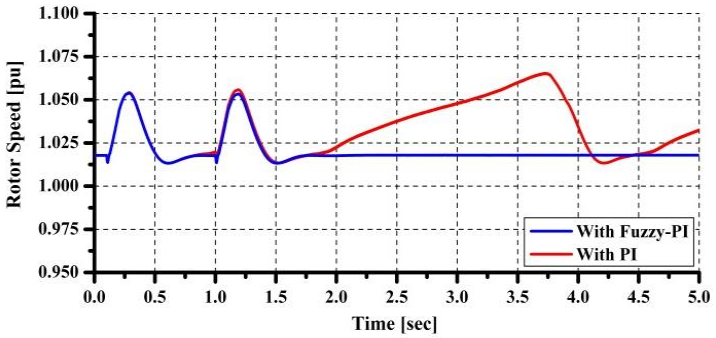

(b) Case 2

Fig. 5.18. Rotor speed of SCIG

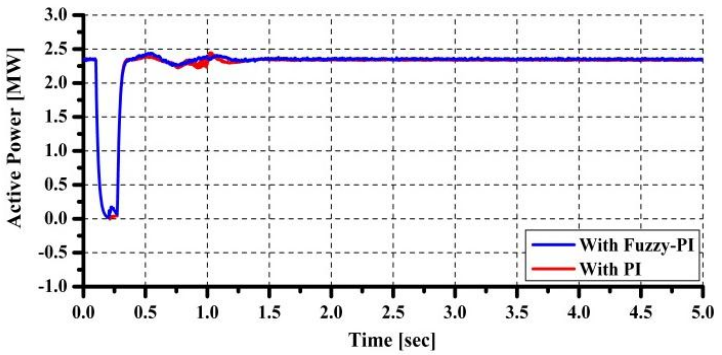

(a) Case 1

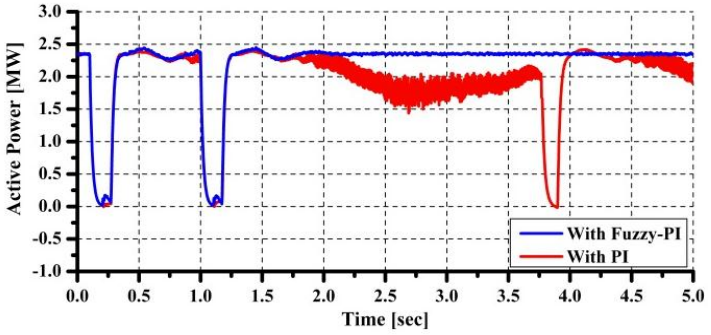

(b) Case 2

Fig. 5.19. Active power output of PMSG

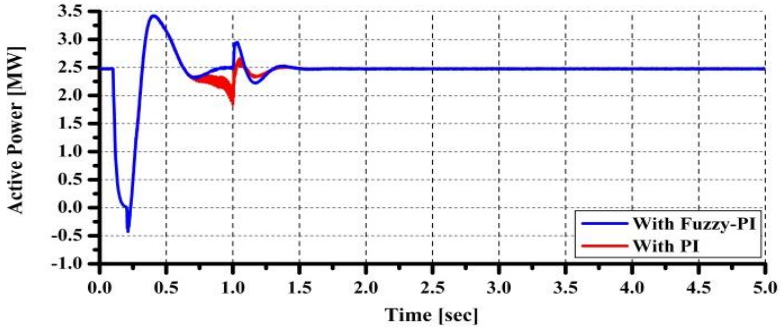

(a) Case 1

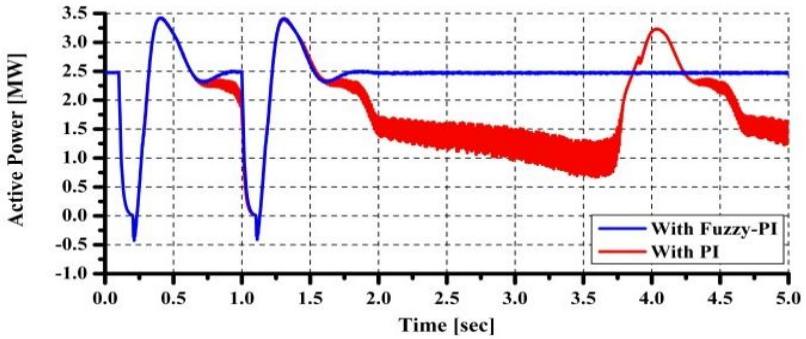

(b) Case 2

Fig. 5.20. Active power output of SCIG

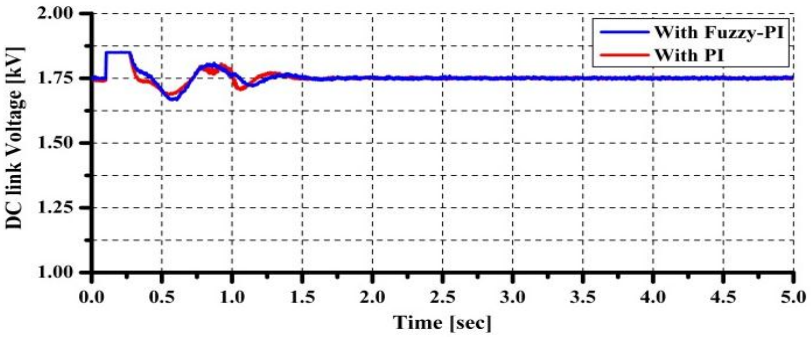

(a) Case 1

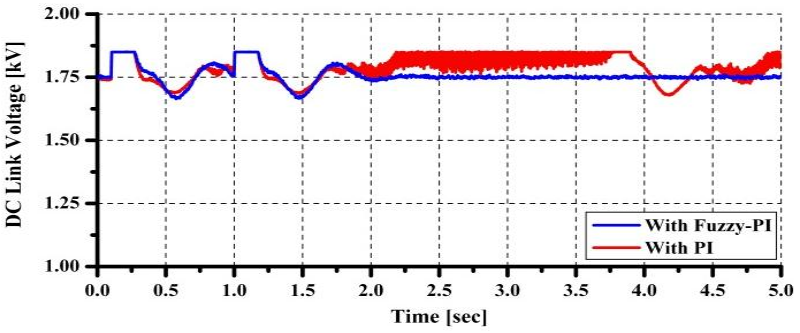

(b) Case 2

Fig. 5.21. DC link voltage of PMSG

The simulation results for the transient stability analysis in Case 1 and Case 2 are shown through Figs. 5.15- 5.21. Figs. 5.15 and 5.16 show responses of reactive power output of PMSG and SCIG, respectively. It is seen that, by using the proposed controller for PMSG, the grid side converter of PMSG can provide necessary reactive power during 3LG fault. Therefore, the terminal voltage at PCC can return back to the rated value quickly as shown in Fig. 5.17. The rotor speed of SCIG can also become stable as shown in Fig. 5.18. Figs. 5.19 and 5.20 show responses of the active power output of PMSG and SCIG, respectively. The active power can be controlled more effectively by using Fuzzy-PI Controller. Fig. 5.21 shows the DC-link voltage response of the PMSG during the fault. From these results, it is clear that the stability performances of the wind farms can be improved more effectively in the case of PMSG with the Fuzzy-PI controller than that with normal PI controller. Moreover, in Case 2, the system becomes unstable when the converter with PI Controller is used for PMSG.

5.5.1.2. Steady State Analysis with Fuzzy-PI Controller

To evaluate the steady state performance of the proposed system, responses for wind speed data shown in Fig. 5.22 are evaluated for the cases of FSWT-SCIG and the Fuzzy-PI controlled VSWT-PMSG. Fig 5.23 shows the active power output of both wind generators. It can be seen that the active power of the wind generators can be delivered to the grid effectively. The blade pitch angle responses are shown in Fig. 5.24. Fig. 5.25 shows the reactive power output of both wind generators. It is seen that the reactive power from the grid side converter of VSWT-PMSG provides reactive power compensation for FSWT-SCIG for voltage regulation. Therefore the voltage at the PCC is controlled almost constant as shown in Fig 5.26.

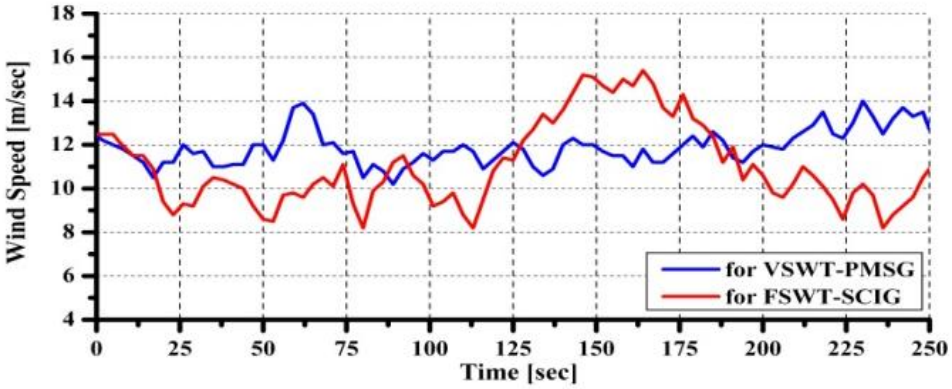

Fig. 5.22. Wind speed data

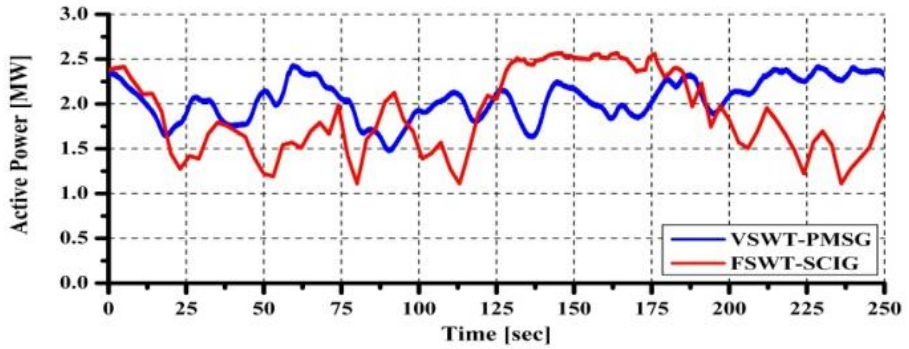

Fig. 5.23. Active power output of wind generators

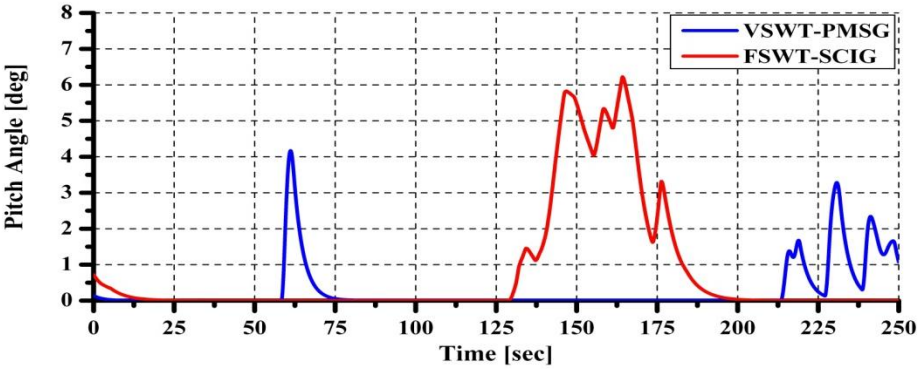

Fig. 5.24. Pitch Angle of wind turbines

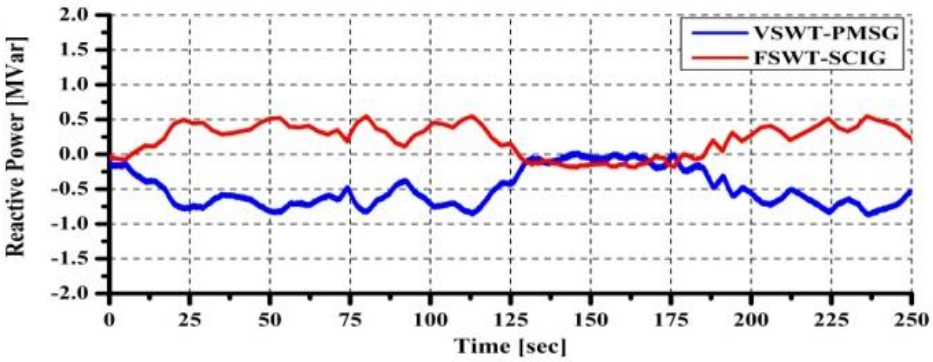

Fig. 5.25. Reactive power output of wind generators

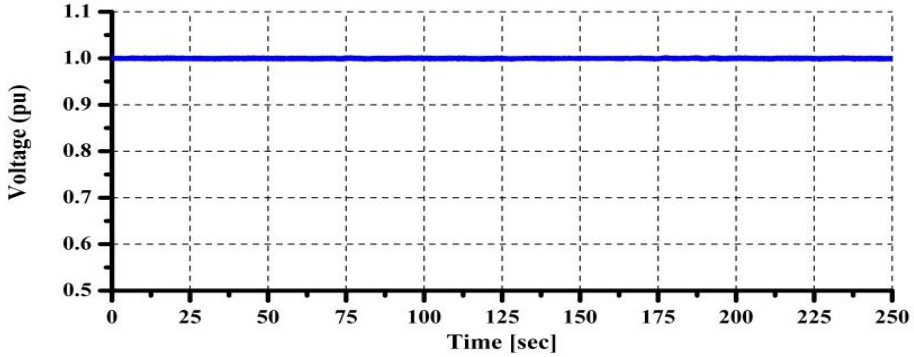

Fig. 5.26. Terminal voltage at PCC

5.5.2. Stabilization of Wind Farm in Multi-machine Power System

Fig. 5.27 shows a model system composed of 9-bus main system and a wind farm. Steam turbine generator (SG1) and hydro turbine generator (SG2) are connected with the main system. Automatic Voltage Regulator (AVR) and governor models in PSCAD/EMTDC package [9] are used here. The IEEE type SCRX solid state exciter is considered for all synchronous generators as exciter model. In SG1, the generic steam turbine model equipped with approximate mechanical-hydraulic controls of governor is used. In SG2, the hydro turbine with non-elastic water column without surge tank model and the hydro governor with PID controls including pilot and servo dynamics model are used.

Wind farm is connected to Bus 9 through double circuit transmission lines. The wind farm power capacity is 50 MVA composed of one 10 MW VSWT-PMSG and four 10 MW FSWT-SCIGs. A capacitor bank, C, is used for reactive power compensation of SCIGs. The value of capacitor C is chosen so that the power factor of each wind generator becomes unity at rated condition. The grid system frequency is 50 Hz and the system base is 100 MVA. Parameters of generators are shown in Table 5.2.

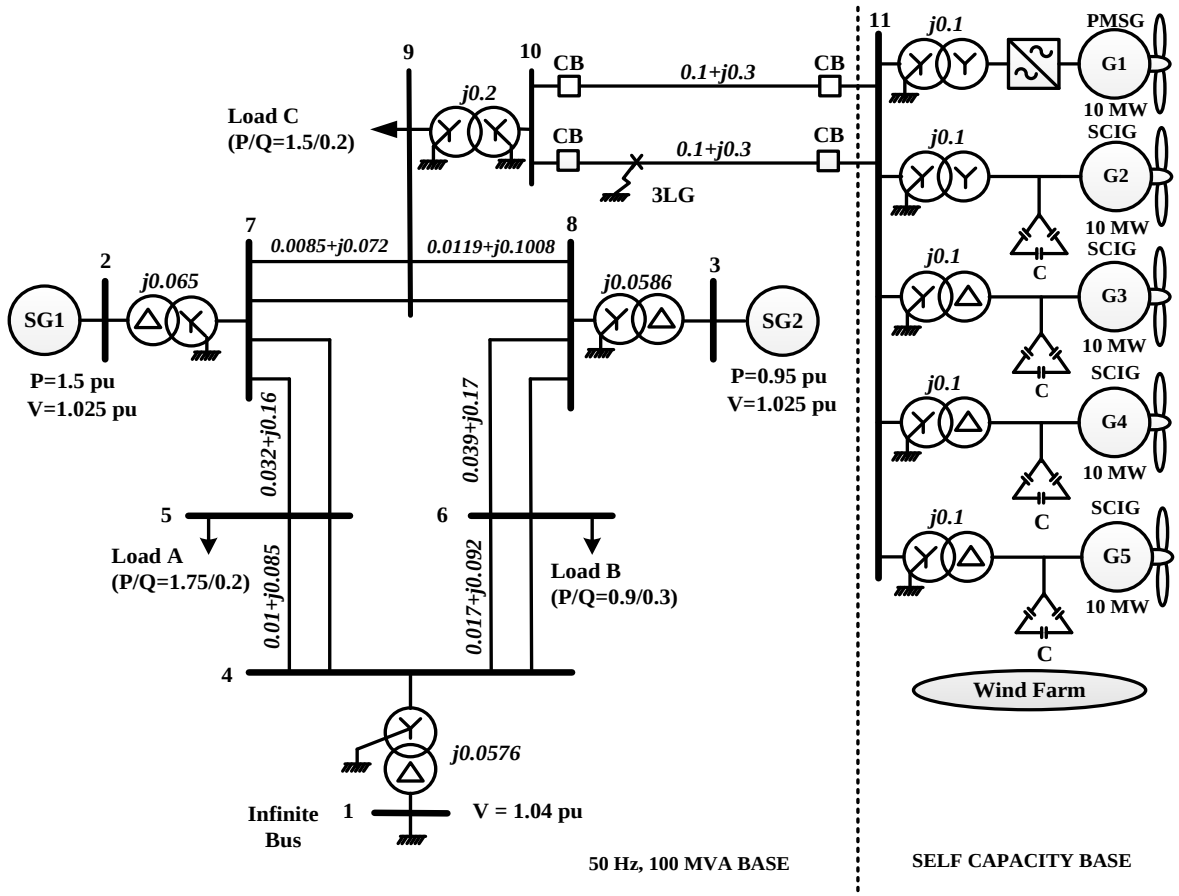

Fig. 5.27. Power System Model

Table 5.2.

Generator parameters

	Synchronous Generators		SCIG		PMSG	
	SG1	SG2				
MVA	200	150	MVA	10	MVA	10
ra (pu)	0.003	0.004	R1 (pu)	0.01	Rs (pu)	0.01
Xa (pu)	0.102	0.078	X1 (pu)	0.1	Ls (pu)	0.064
Xd (pu)	1.651	1.22	Xm (pu)	3.5	Xd (pu)	0.9
Xq (pu)	1.59	1.16	R21 (pu)	0.035	Xq (pu)	0.7
X'd (pu)	0.232	0.174	R22 (pu)	0.014	Flux (pu)	1.4
X'q (pu)	0.38	0.25	X21 (pu)	0.03	H	3.0 s
X"d (pu)	0.171	0.134	X22 (pu)	0.089		
X"q (pu)	0.171	0.134	H	1.5 s		
T'do (sec)	5.9	8.97				
T'qo (sec)	0.535	1.5				
T"do (sec)	0.033	0.033				
T"qo (sec)	0.078	0.141				
H	6.2 s	6.0 s				

5.5.2.1. The VSWT-PMSG Control Strategy

The control strategy for the VSWT-PMSG is shown in Fig. 5.28. The SSC is directly connected with the stator of PMSG. The GSC is connected to the grid system through a step up transformer. Three phase voltage is detected at the high voltage side of transformer and three phase current is detected at the output side of GSC. All controller systems (stator side and grid side controllers) are based on the models shown in Figs. 5.2 and 5.3 for stator side and grid side controllers, respectively.

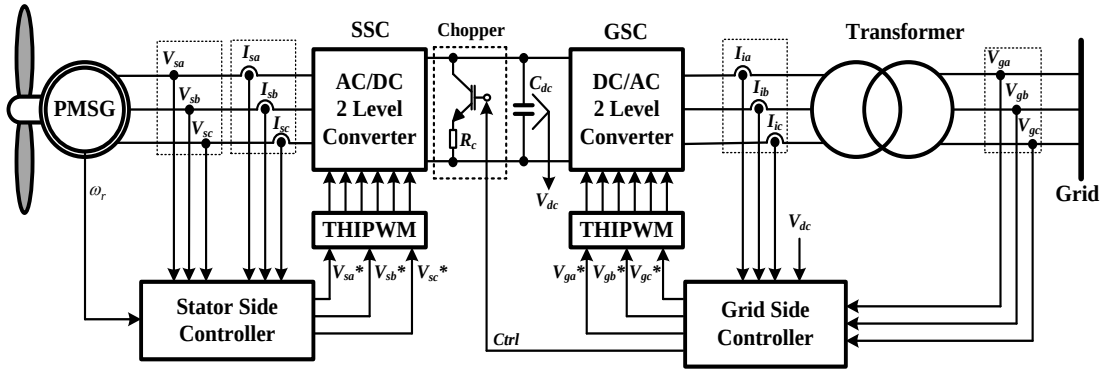

Fig. 5.28. Control Strategy for VSWT-PMSG

5.5.2.2. The membership function and rule base of FLC

For fuzzification of the three variables of the FLC, the error (*er*) have seven triangle membership functions. Fuzzy subsets for input are Negative Big (NB), Negative Medium (NM), Negative Small (NS), Zero (ZE), Positive Small (PS), Positive Medium (PM) and Positive Big

(PB). The gains output, *Kp* and *Ki*, have four triangle membership functions respectively. Fuzzy subsets for output are Very Small (VS), Small (SM), Big (BG), and Very Big (VB).The basic fuzzy sets of membership functions for the variables are shown in the Figs. 5.29, 5.30 and 5.31.

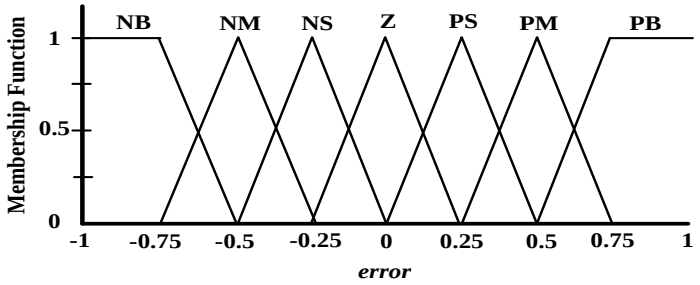

Fig. 5.29. Membership function of error

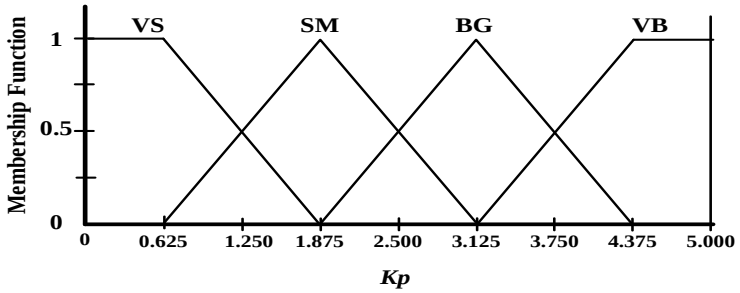

Fig. 5.30. Membership function of *Kp*

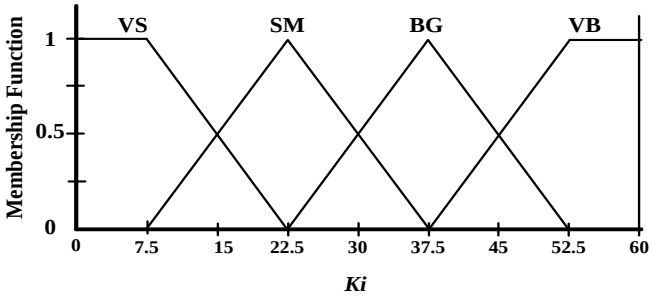

Fig. 5.31. Membership function of *Ki*

The number of rules can be expressed in the form:

If (*er* is NB) then (*Kp* and *Ki* is VB).
If (*er* is NM) then (*Kp* and *Ki* is BG).
If (*er* is NS) then (*Kp* and *Ki* is SM).
If (*er* is ZE) then (*Kp* and *Ki* is VS).
If (*er* is PS) then (*Kp* and *Ki* is SM).
If (*er* is PM) then (*Kp* and *Ki* is BG).
If (*er* is PB) then (*Kp* and *Ki* is VB).

In this work, Mamdani's max-min method is used for inference mechanism. The center of gravity method is used for defuzzification to obtain *Kp* and *Ki*.

5.5.2.3. Case Study and Simulation Results

The model system shown in Fig. 5.27 is analyzed, which includes a wind farm connected with multi-machine power system. The wind farm is composed of VSWT-PMSG and FSWT-SCIG. Symmetrical three-line-to-ground fault (3LG) is considered as network disturbance. The fault occurs at 0.1 sec, the circuit breakers (CBs) on the faulted line are opened at 0.2 sec, and at 1.0 sec the CBs are reclosed.

Table 5.3.

Case Study

Case	Generator Type				
	G1	G2	G3	G4	G5
Case 1	SCIG	SCIG	SCIG	SCIG	SCIG
Case 2	PMSG with PI Controller	SCIG	SCIG	SCIG	SCIG
Case 3	PMSG with Fuzzy-PI Controller	SCIG	SCIG	SCIG	SCIG

Three cases shown in Table 5.3 are considered in the simulation study to verify the stabilization effect of the proposed controller for the VSWT-PMSG. In Case 1, all of wind generators in the wind farm are SCIG. In Case 2 and Case 3 the generator number 1 (G1) is PMSG where the current control of the grid side converter is performed by PI or Fuzzy-PI controller, respectively. In Case 2 and 3, when the fault occurs in the grid system, the full-rating power converter of VSWT-PMSG wind turbine system is controlled in such a way to maintain the grid voltage (voltage at Bus 11) at desired reference level. To maximize the reactive power support to the grid system, the active power reference is set to zero during the fault. Simulations were performed by using PSCAD/EMTDC.

Fig. 5.32 shows the wind speed data for each wind generator considered in the simulation analysis. Responses of reactive power outputs of the generators in Case 1, Case 2 and Case 3 are shown in Fig. 5.33 (a), (b) and (c), respectively. From these figures it is seen that the grid side converter of G1 can support necessary reactive power during fault condition in Case 2 and Case 3. The rotor speeds of all wind generators become stable in Case 2 and Case 3 as shown in Fig. 5.34. The terminal voltage at Bus 11 can return back to the rated value quickly in Case 2 and Case 3 as depicted in Fig. 5.35. It is seen that the wind farm voltage can be stabilized to the nominal value more effectively in the case of the Fuzzy-PI controller than in the case of the PI controller. The active power output of wind generators are shown in Fig. 5.36. It is seen that, the active power of PMSG is controlled to be decreased to zero during the fault effectively in Case 2 and 3, and then to be recovered after the reactive power compensation returns to the initial level. From Figs. 5.33 through 5.36, it is seen that the proposed Fuzzy-PI controller is very effective in improving the voltage stability of wind farm during a fault condition.

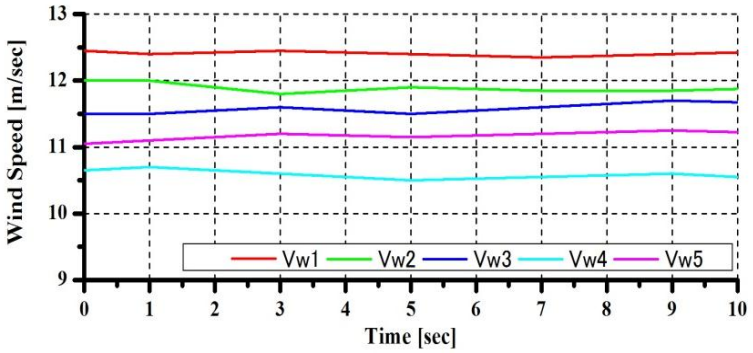

Fig. 5.32. Wind speed data

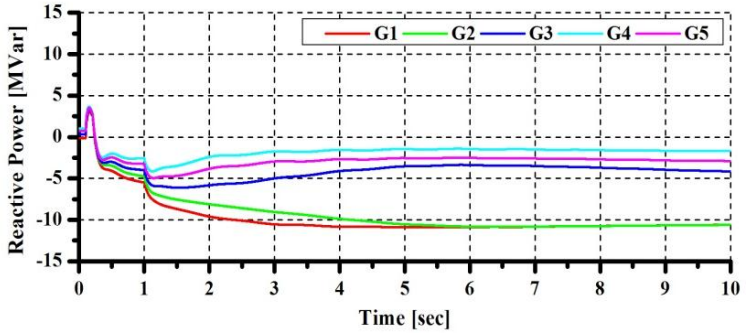

(a) Case 1

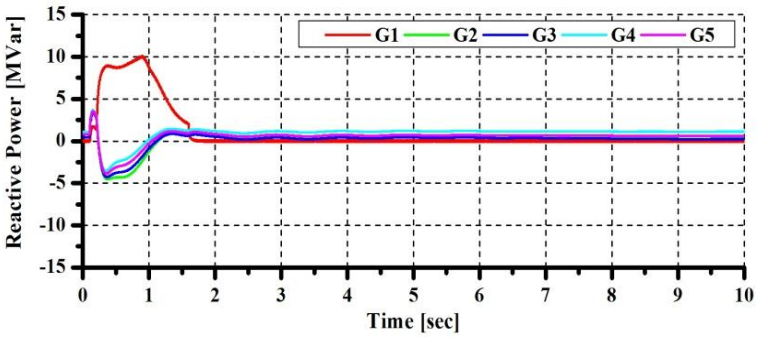

(b) Case 2

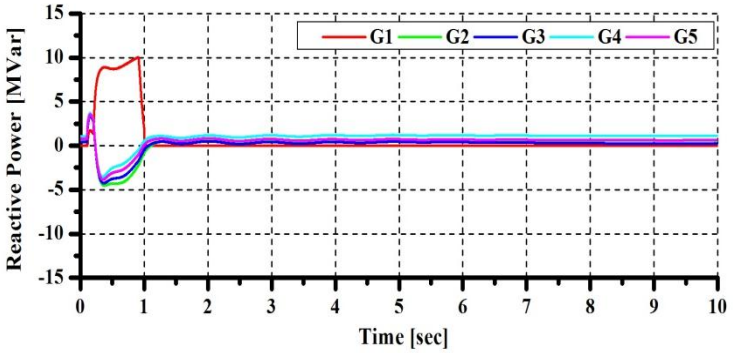

(c) Case 3

Fig. 5.33. Reactive power output of wind generators

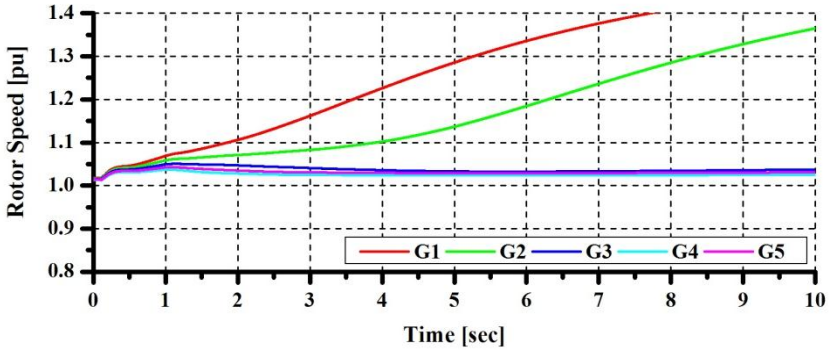

(a) Case 1

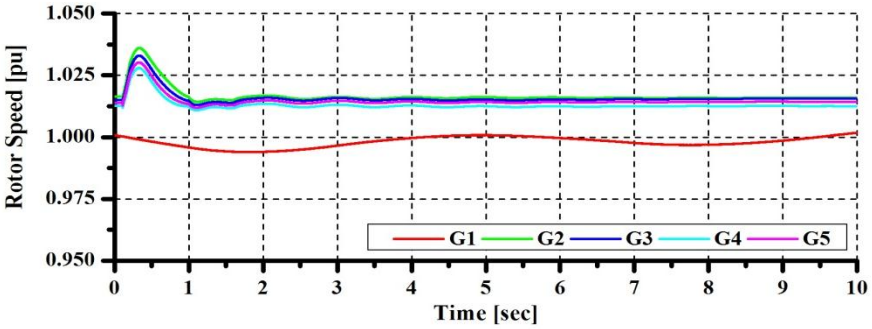

(b) Case 2

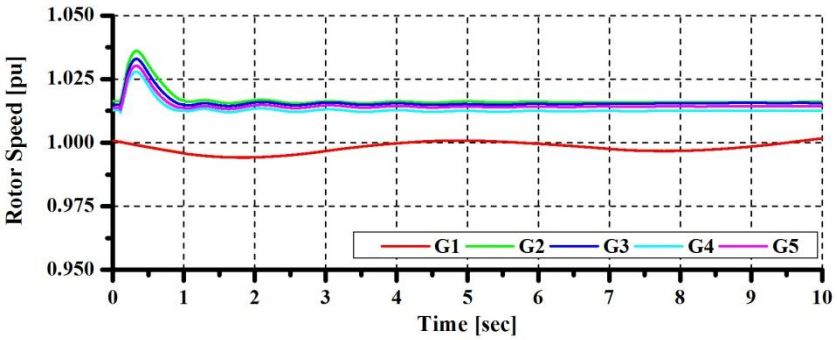

(c) Case 3

Fig. 5.34. Rotor speed response of wind generators

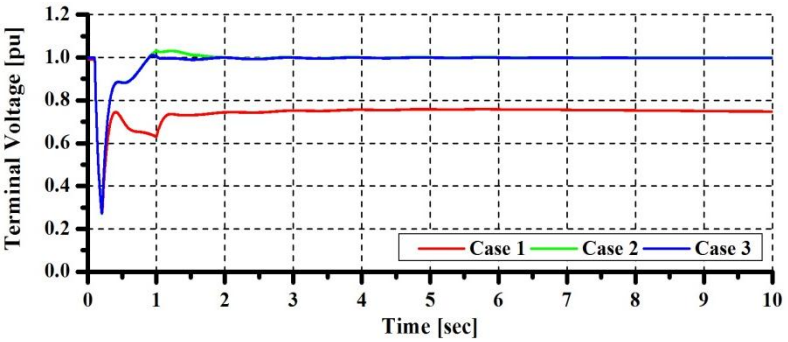

Fig. 5.35. Terminal voltage at Bus 11

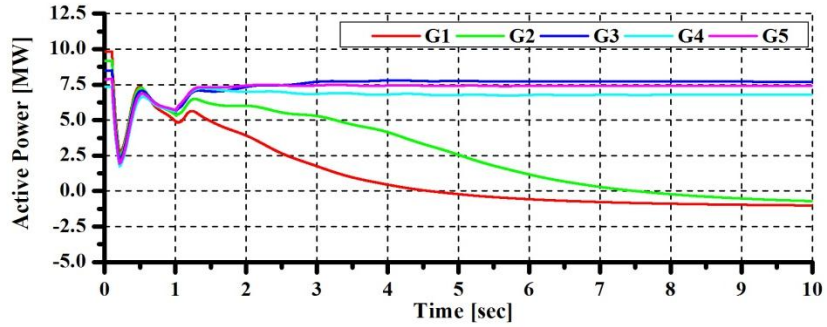

(a) Case 1

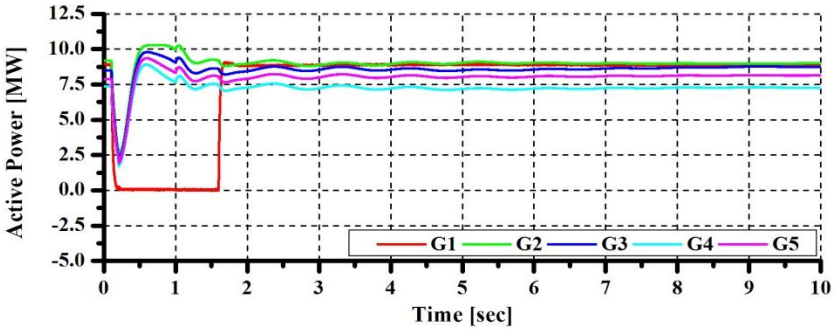

(b) Case 2

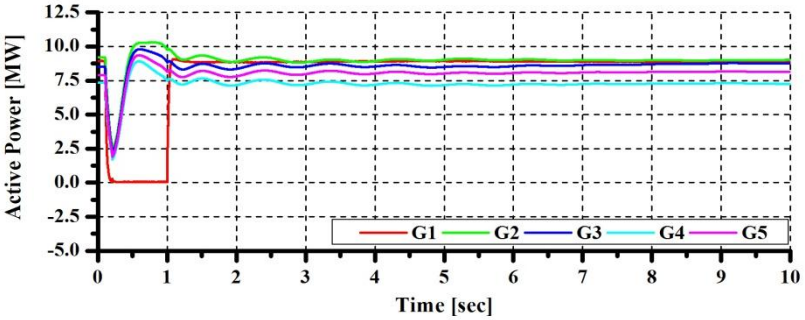

(c) Case 3

Fig. 5.36. Active power output of wind generators

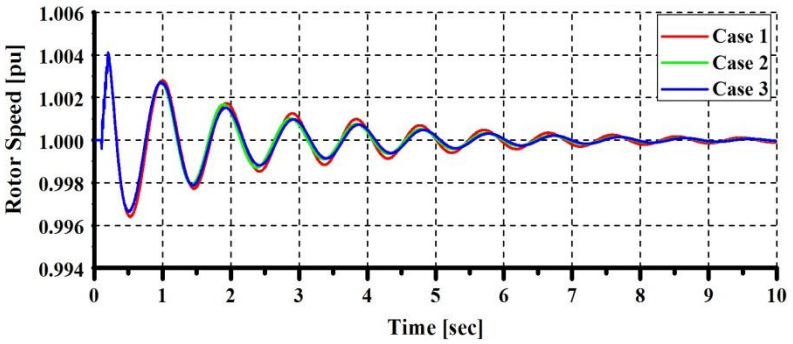

Fig. 5.37. Rotor speed of SG1

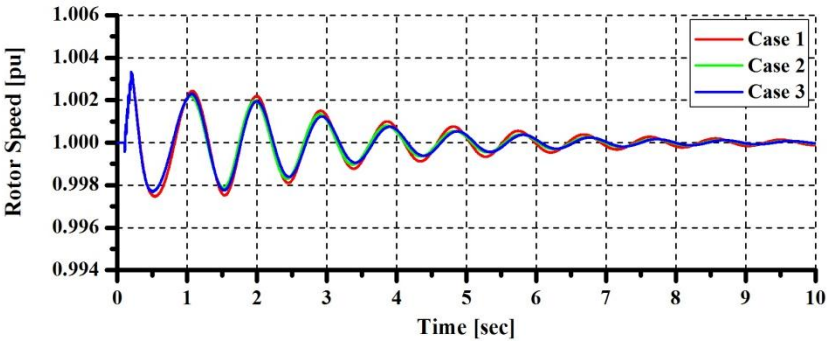

Fig. 5.38. Rotor speed of SG2

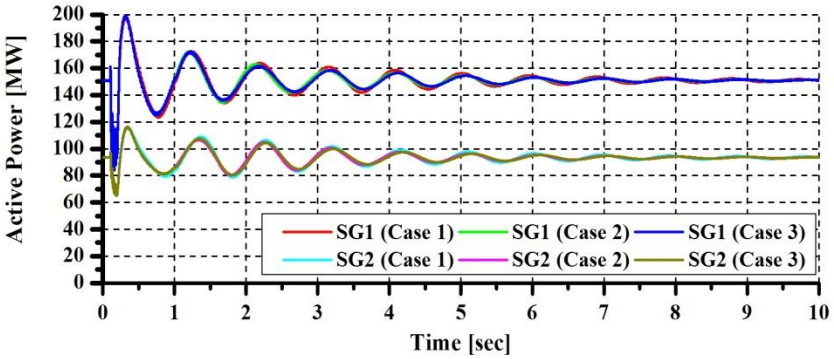

Fig. 5.39. Active power output of synchronous generators

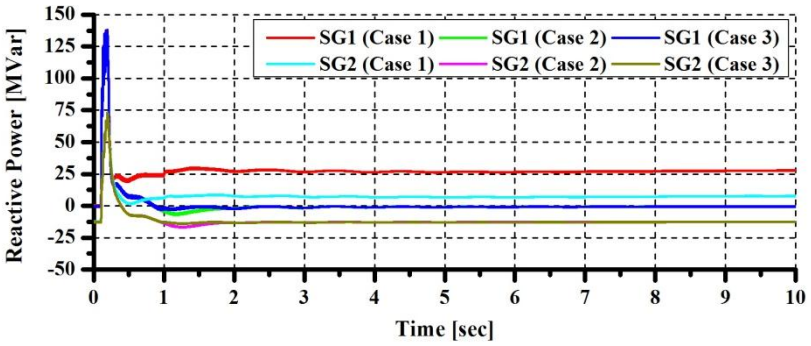

Fig. 5.40. Reactive power output of synchronous generators

Figs. 5.37 and 5.38 show responses of rotor speed of SG1 and SG 2, respectively. Figs. 5.39 and 5.40 show the active power and the reactive power output of SG1 and SG2, respectively. It can be seen that VSWT-PMSG can also improve the transient behavior of synchronous generator in some degree.

5.6. Chapter Summary

In this chapter a new Fuzzy-PI controller for variable speed permanent magnet wind generator connected to a power grid through a LC filter is proposed and its effect on enhancing

dynamic (transient stability and steady state behavior) performances is investigated. The membership function of fuzzy logic control system is designed based on frequency response of the Bode diagram. The controller combines fuzzy logic to classical PI controller to adjust the PI gains online. Stabilizing effect of the proposed PMSG system on the fixed speed wind generators is also investigated. The results show that the proposed Fuzzy-PI controller is very effective in improving the transient stability of overall wind farm system during temporary and permanent fault conditions. The significant effect of proposed control system has been demonstrated especially in the permanent fault analysis. Moreover, the steady state performance of the proposed system is analyzed using variable wind speed data, and it is demonstrated that the terminal voltage of wind farm under randomly varying wind speed can be controlled constant.

In addition, the effect of Variable Speed Wind Turbine with Permanent Magnet Synchronous Generator (VSWT-PMSG) on stabilizing wind farm connected to a multi-machine power system is also analyzed. The results show that VSWT-PMSG with the proposed Fuzzy-PI controller can enhance the transient stability as well as the voltage stability of the wind farm when a severe 3LG fault occurs in the power system.

Chapter 6

Artificial Immune System Based Design of Current Controlled Voltage Source Converter for PM Wind Generator

In this chapter a novel design method of current controlled voltage source converter for variable speed permanent magnet wind generator is proposed. The method is based on optimum tuning of PI gain parameters of voltage source converter control system with the artificial immune system (AIS) algorithm considered. The analytical simulation studies have been performed using mfile/Matlab. In order to verify the effectiveness of the proposed method, the simulation studies using PSCAD/EMTDC have also been performed. Simulation results show that the proposed method is very effective in enhancing the dynamic stability of the wind generator system.

6.1. Introduction

In industrial applications, PI controllers are most widely used in back to back power converter controller system of PMSG because of simple structure and good performances in a wide range of operating conditions. In fixed gain controllers, these parameters are determined by methods such as the Zeigler and Nichols, optimum modulus criterion, pole placement, etc. However a common disadvantage of the methods are that the resulting closed loop system is often more oscillatory than that desired [46]. In order to provide closed loop responses with a damping ratio of 25%, Cohen and Coon technique is proposed [47]. However this technique sometimes brings about oscillatory responses [48], [88]. In addition, for the strong nonlinear system the global optimum solution is difficult to be achieved by using these methods.

Over the last ten years, interests in studying biologically inspired systems such as genetic algorithm, artificial neural network, and artificial immune systems, have been increased. The immune system of human body is a complex of cells, molecules and organs and has the ability to perform multiple tasks like pattern recognition, learning, distributed detection, optimization, etc. [49]. Artificial immune system (AIS) is computational techniques based on immunological principles. The computation with AIS technique has some merits: the feasibility and diversity of spaces can be better ensured, the method operates on a big population of antibodies simultaneously, hence stagnation in computation process can be eliminated, and the global optimum can be achieved easily [50].

In this work, the artificial immune system (AIS) is proposed to tune PI controller parameter of current controlled voltage source converter of the VSWT-PMSG. In the AIS method, the objective function and constraints are represented as antigen. The method is followed to produce antibody as candidate solution on a feasible space through clonal selection operations. Through an affinity maturation and hyper-mutation, a specific antibody that most fits the antigen become a solution.

6.2. Artificial Immune System

The interests in studying the immune system have been increasing since more than ten years ago. Computer scientists, engineers, mathematicians, philosophers and other researchers are particularly interested in the capabilities of this system, whose complexity is comparable to that of the brain. A new field of research called Artificial Immune Systems has been arisen since 1996 [89]-[94]. The immune system is a complex of cells, molecules and organs that represent an identification mechanism capable of perceiving and combating dysfunction from our own cells and the action of exogenous infectious microorganisms.

Many properties of the immune system are of great interest for computer scientists and engineers [49]:

1. Uniqueness: each individual possesses its own immune system, with its particular vulnerabilities and capabilities;
2. Recognition of foreigners: the (harmful) molecules that are not native to the body are recognized and eliminated by the immune system;
3. Anomaly detection: the immune system can detect and react to pathogens that the body has never encountered before;
4. Distributed detection: the cells of the system are distributed all over the body, and most importantly, are not subject to any centralized control;
5. Imperfect detection (noise tolerance): an absolute recognition of the pathogens is not required, hence the system is flexible;
6. Reinforcement learning and memory: the system can “learn” the structures of pathogens, so that future responses to the same pathogens are faster and stronger.

An immune system can detect and eliminate the nonself materials such as viruses and cancer cells that originate from inside or outside of the living system. Therefore, it must possess the functions to distinguish self and nonself materials (antigens). There are various sets of antibodies that can be produced in an immune system. However, like key and lock relations, an antibody can only specifically recognize an antigen. For the operation of an immune system, the role of antibody lies in eliminating the antigen, while the lymphocyte helps to produce the antibody through the clonal proliferation.

The clonal selection principle is the algorithm used by the immune system to describe the basic features of an immune response to an antigenic stimulus. Fig. 6.1 depicts the clonal selection principle [50]. It establishes the idea that only those cells that recognize the antigens proliferate, thus being selected against those which do not. Clonal selection operates on both T cells and B cells. In the lymphocyte structure, the B-lymphocytes and T-lymphocytes are two main components. The B-lymphocytes are the cells produced by bone marrow, and the T-lymphocytes are the cells produced by thymus. A B-lymphocyte can be programmed to make only one antibody that is placed on the outer surface of the lymphocyte to act as a receptor. Control mechanisms of antibody productions are then regulated by use of T-lymphocytes. The lymphocytes receive triggering signals when their receptors have bound antigens. These triggering signals can activate the clonal proliferation to form a large clone of plasma cells. Since the lymphocytes are programmed to make only one body, the antibody secreted by the plasma cell will be identical with that originally acting as the lymphocyte receptor. Lymphocytes are proliferating or differentiating into plasma cells, can differentiate into long-lived B memory cells. Memory cells circulate through the blood, lymph and tissues, probably not manufacturing antibodies, but when exposed to a second antigenic stimulus commence differentiating into large lymphocytes capable of producing high affinity antibody, preselected for the specific antigen that had stimulated the primary response [95], [96].

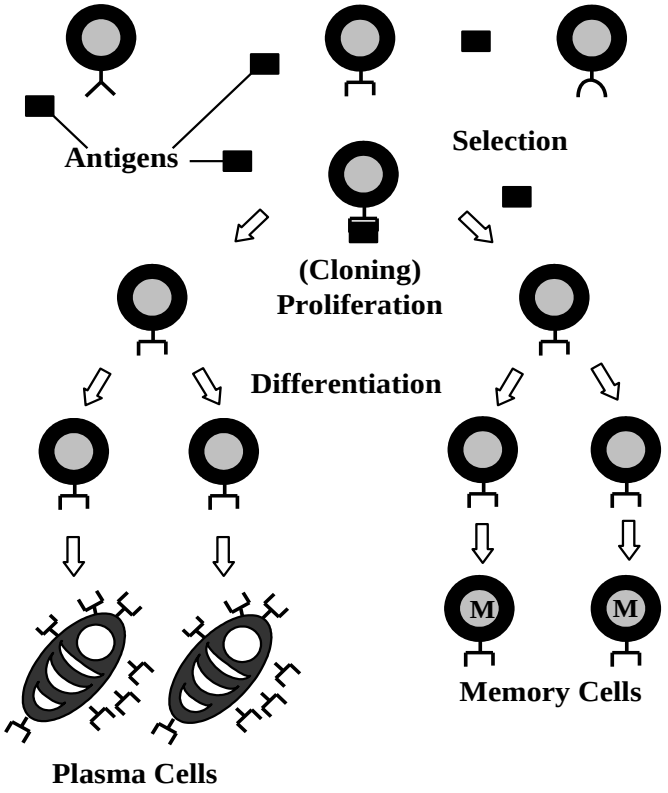

Fig. 6.1. Artificial immune system with clonal selection algorithm [50]

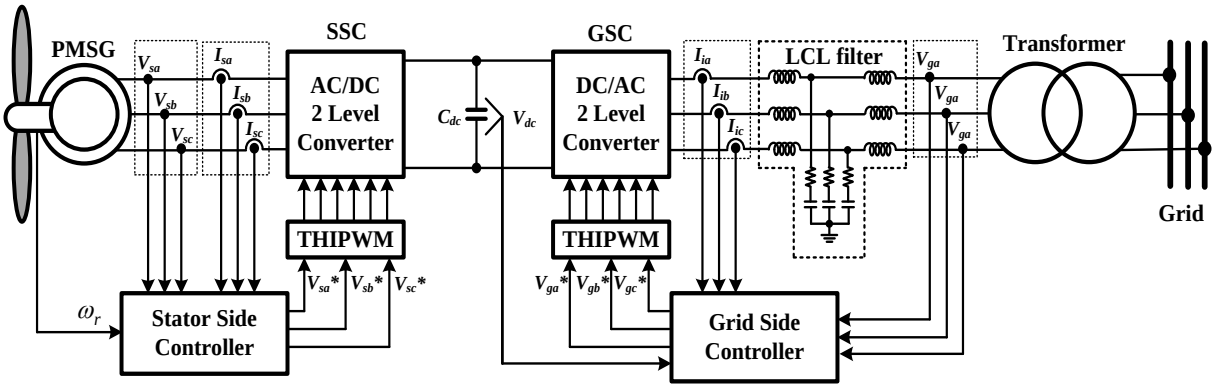

Fig. 6.2. The VSWT-PMSG control system

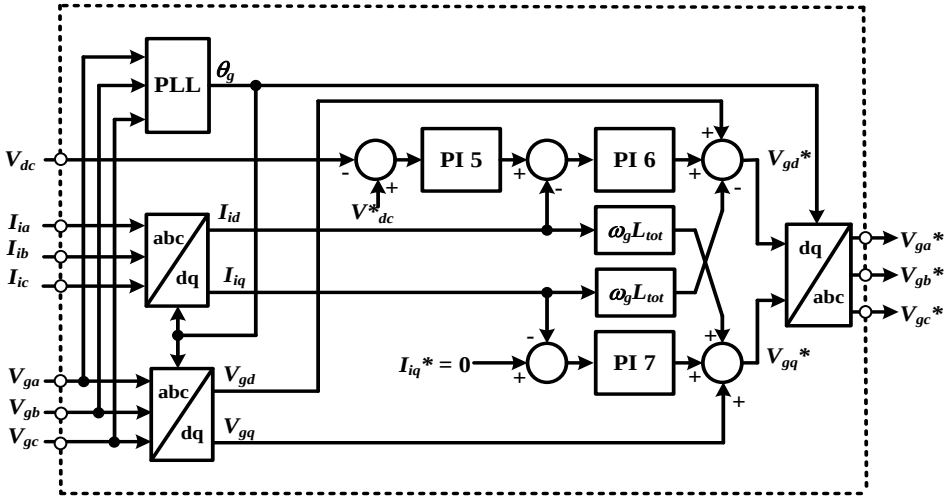

Fig. 6.3. Grid side controller of the VSWT-PMSG

6.3. Grid Connected VSWT-PMSG Control System

Fig. 6.2 shows the VSWT-PMSG control system considered in this study. The direct driven PMSG is connected to the grid system through two levels AC/DC/AC converter, LCL filter, and a transformers. In SSC, three phase current and voltage are detected on the stator winding terminal of PMSG. In GSC, three phase current and voltage are detected on the converter side and grid side of the LCL filter, respectively. The stator side controller system is adopted from Fig. 3.2 in Chapter 3.

Fig. 6.3 shows a block diagram of the grid side controller system. By using the Phase Locked Loop (PLL) [14] the grid side phase angle (θ) for the d-q transformation is obtained. When grid voltages on the stationary reference frame are transformed into the d-q rotating reference frame, V_{gd} becomes constant and V_{gq} becomes zero. Therefore, the active and reactive power delivered to the grid can be controlled separately by the d-axis current (I_{id}) and the q-axis current (I_{iq}), respectively. In order to deliver active power produced by PMSG to the grid, the

voltage of DC-link capacitor (V_{dc}) is maintained constant. Hence, the d-axis current reference signal (I_{id}*) is determined from output of the DC-voltage controller. For unity power factor operation, the q-axis current reference signal (I_{iq}*) is also set to zero.

The Table 6.1 shows the system parameters of the grid connected VSWT-PMSG considered in this study. In order to determine the LCL filter parameters, step by step procedures and limitations of the filter parameters presented in [15] are adopted.

Tabel 6.1.

The VSWT-PMSG parameters

Component	Parameter	Value
Turbine	*R*	40 m
	ρ	1.225 kg/m3
	Vw	12 m/sec
	Cp	0.48
	λ	8.1
	ρ	1.225 kg/m3
	Jt	7.67×⟦10⟧^6 Nm
PMSG	*Rs*	0.01 pu
	Ld	1.0 pu
	Lq	0.7 pu
	ψm	1.4 pu
	ω*e*	125.664 rad/sec
	pole pair	52
	H (inertia constant)	3.0 s
AC/DC/AC Power Converter	SSC frequency Switching	1 kHz
	GSC frequency Switching	5 kHz
	Grid Frequency	50 Hz
	DC Link capacitor	25000 μF
	DC Link voltage	2.0 kV
LCL Filter	*Li*	0.048 pu
	Ri	0.004 pu
	Lg	0.01 pu
	Rg	0.0004 pu
	Cf	0.05 pu
	Rd	0.23 pu
Transformer	*Lt*	0.04 pu
	Rt	0.0024 pu
	Converter side voltage	1.0 kV
	Grid side voltage	66 kV

6.4. Current Control Loop Design

A block diagram of the current control loop for SSC is shown in Fig. 6.4. The controller system is composed of two PI controllers (PI 2 and PI 4), sampling time transfer function ($1/sT_s+1$), inverter transfer function ($1/sT_{inv}+1$), and PMSG transfer function. The sampling time transfer function is caused by switching frequency ($T_s=1/f_s$) and inverter transfer function

is caused by the dead time of PWM converter (T_{inv}=1/T_s), where switching frequency (fs) of SSC is 2 kHz.

Fig. 6.5 shows a block diagram of the current control loop for GSC. The switching frequency for GSC is chosen at 5 kHz. T_s and T_{inv} for GSC can be determined by using T_s=1/f_s and T_{inv}=1/T_s, respectively. The state space plant of LCL filter shown in the figure is obtained from eqs. (4-1) and (4-17) (see Chapter 4).

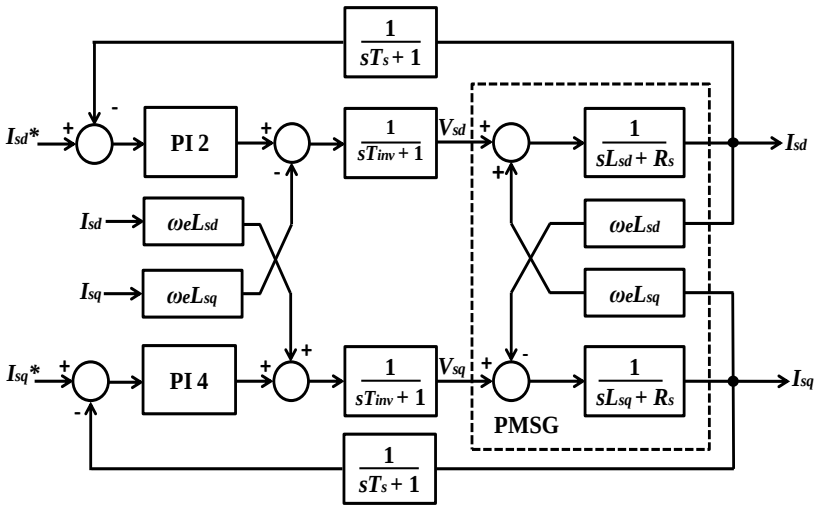

Fig. 6.4. Current control loop of stator side controller

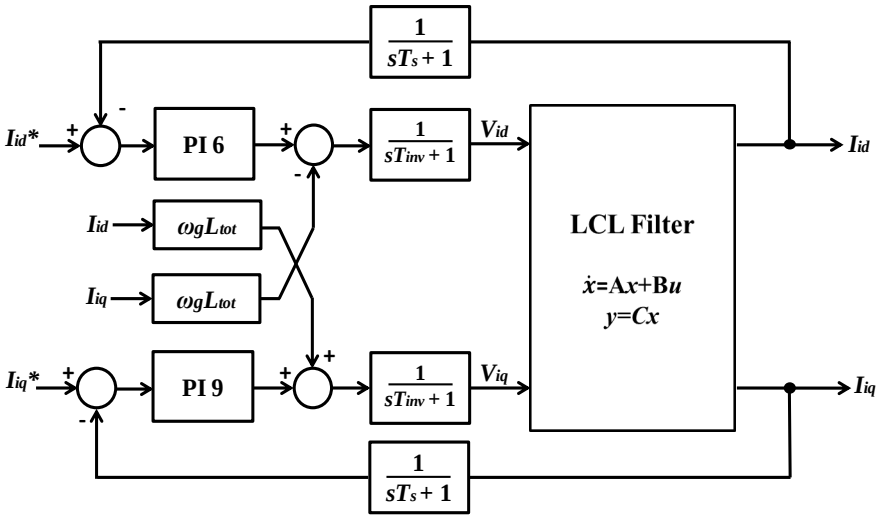

Fig. 6.5. Current control loop of grid side controller

6.5. Implementation of AIS

In this study, a novel method employing the AIS with clonal selection algorithm is introduced to achieve the optimum gains of PI controllers for current loop controllers. The immune system can produce various sets of antibodies. However, only one antibody can

specifically recognize an antigen. An antibody receives triggering signals when their receptors have bound antigens. Through clonal proliferation and affinity maturation, an antibody that most fits the antigen becomes the solution.

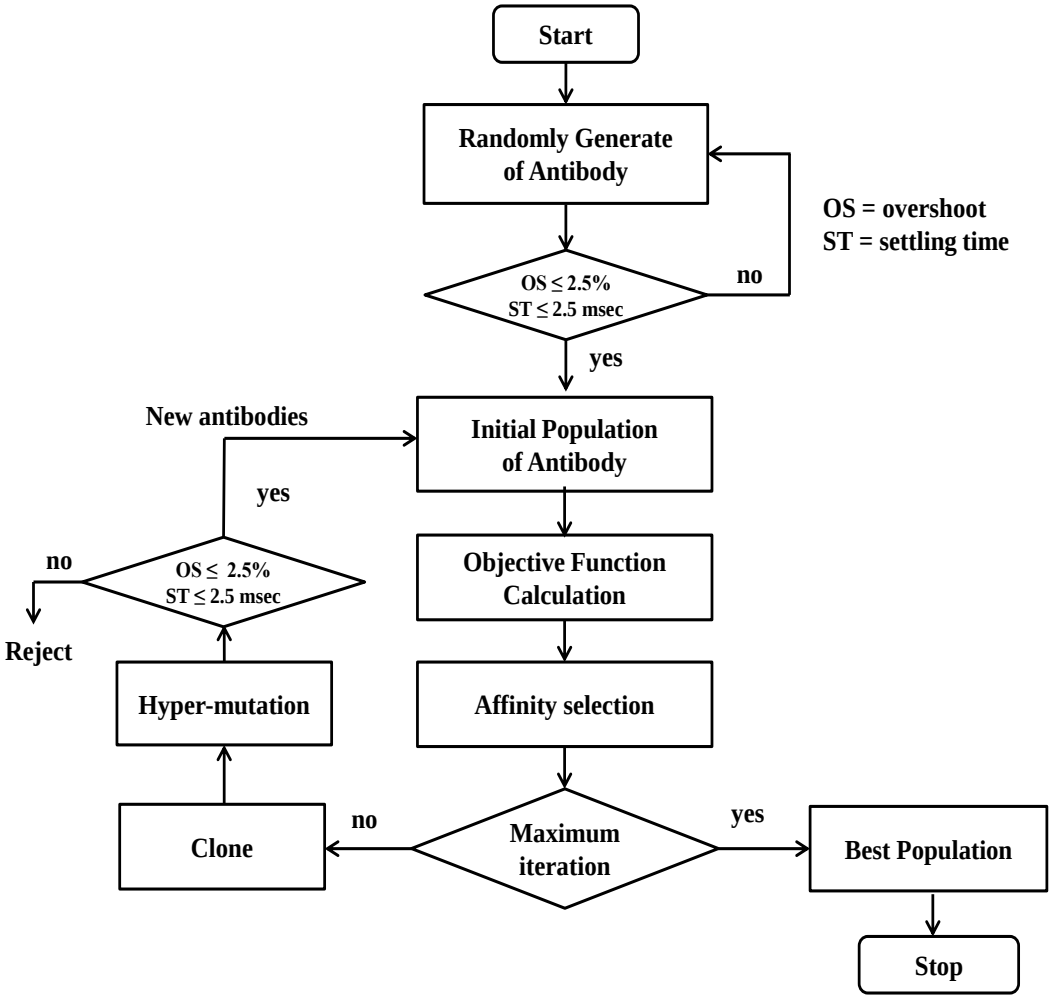

Fig. 6.6. Computation procedure of AIS with clonal selection algorithm

Computation procedure of AIS with clonal selection algorithm to search the optimum gains for PI controller shown in Fig. 6.6 is as follows:

1. *Randomly generate antibodies population*.
2. *Create Initial population of antibody*. Each of antibody is evaluated in which over shoot (OS) should be less than 2.5 % and settling time (ST) should be 2.5 msec. Total number of antibody in a population is 100.
3. *Compute objective function*. The objective function, the integral of the absolute magnitude of error (ITAE) index, is minimized. In this step objective function for each layer is calculated separately. The ITAE performance index is defined as follows:

$$ITAE = \int_0^{\infty} t|er(t)dt| \tag{6-1}$$

4. *Short the antibodies based on their affinity*. Affinity is calculated by 1/ITAE. The best individual of antibody has high affinity.
5. *Clone these n best antibodies of the population*. Probability of clone is proportional to the affinity. The high affinity antibodies have higher probabilities of being cloned.
6. *Submit the population of clones to an affinity maturation scheme*. The affinity maturation (hyper-mutation) is a process for an antibody to improve their receptor in order to obtain a strong bond between antibody and antigen. The lower affinity antibodies have higher probabilities of being hyper-mutated.
7. *Re-select the improved individuals*. In this stage, each antibody is selected again based on OS and ST.
8. *Replace initial population of antibodies by new one.* The lower affinity antibodies have higher probabilities of being replaced. The computation process is repeated until the maximum iteration (100).

6.5.1. Initial population of Antibody

Structure of an antibody is shown in Fig. 6.7. An antibody is composed of three layers. Layer 1 and Layer 2 represent PI 2 and PI 4, respectively. PI 6 and PI 7 is represented in single layer (Layer 3) because of the LCL filter parameters in d-q axis are identical. Each layer consists of 16 bit of cell, where 8 bit for K_p and 8 bit for T_i. The population of antibodies structure of antibodies is shown in Fig. 6.8. In this study, the total number of antibody (Ab) in a population is 100.

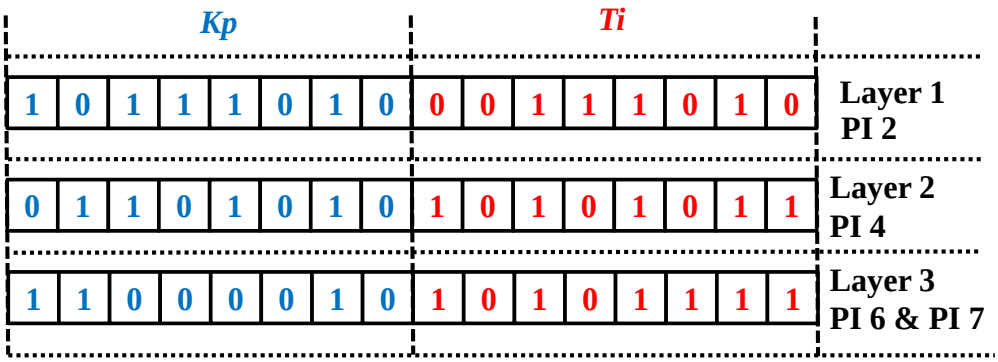

Fig. 6.7. An antibody (Ab) Structure

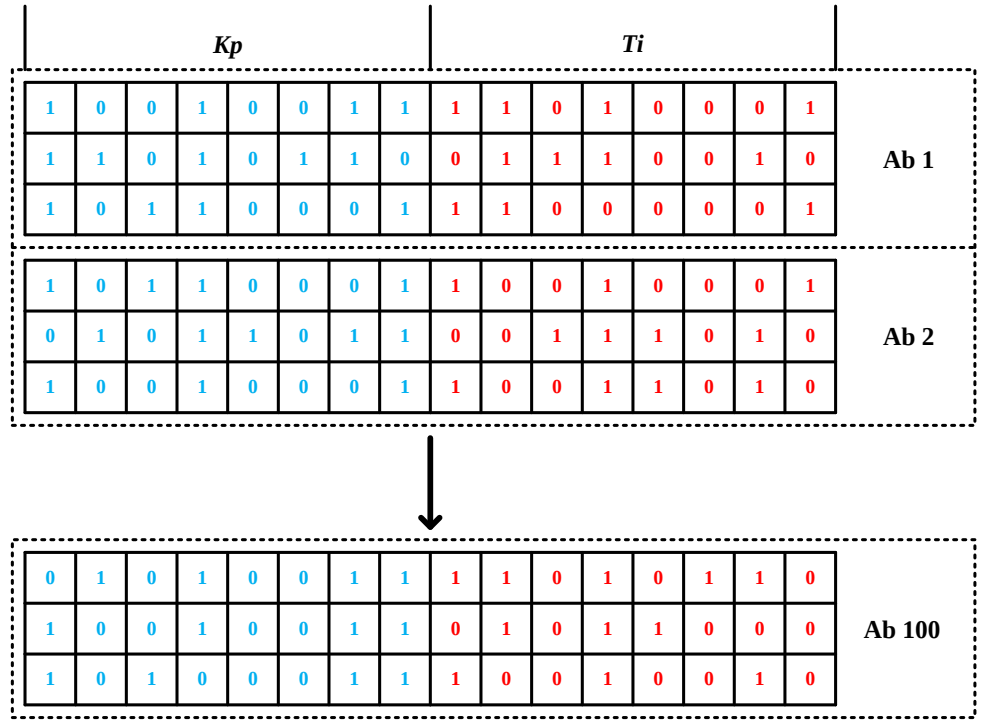

Fig. 6.8. Population of antibodies

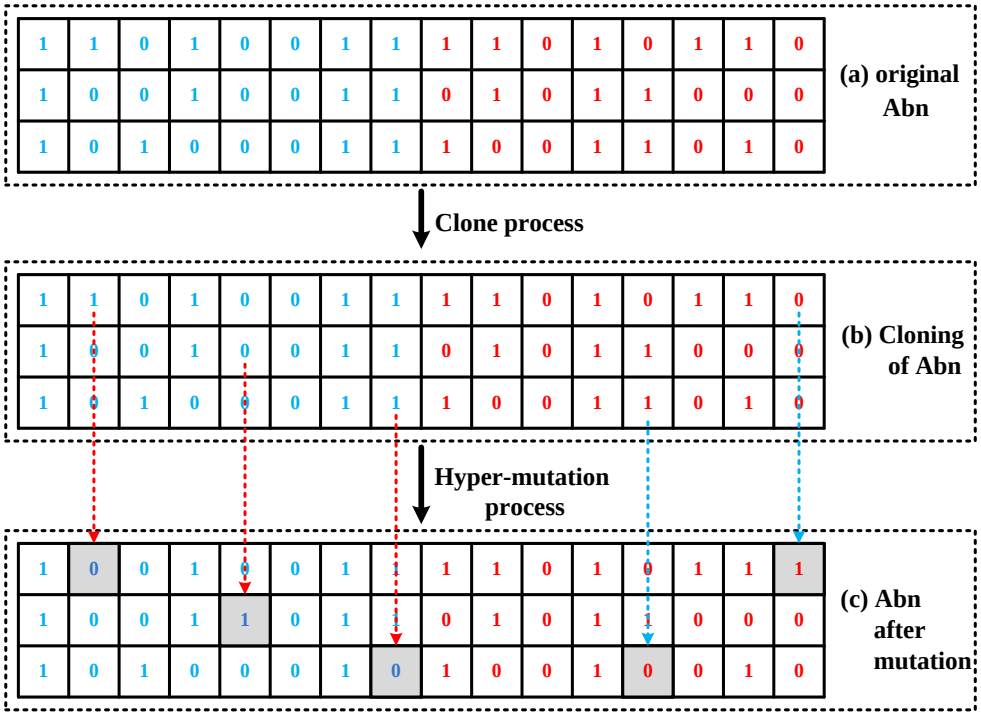

Fig. 6.9. An antibody in cloning and hyper-mutation process

6.5.2. Clone and hyper-mutation

The clone selection is the main characteristic of the property that the immunological cells can reproduce themselves when stimulated by antigens, and subsequently mutate and differentiate into variety effectors cell. Clone selection parallels with a process of affinity mutation, namely a cell with low affinity toward the antigens, driven by mechanism of clone selection, improves its affinity and finally leads to affinity mutation via reproducing itself and mutating. The affinity mutation itself, therefore, is an essentially Darwinian process of evolution and mutation. The mechanism of clone selection works by means of inheritance operator (e.g. cross, mutation) and corresponding population control. Fig 6.9 shows the *n* antibody (Ab_n) after cloning and hyper-mutation process.

6.6. Simulation Results

In order to verify the impact of the use of AIS on the optimization of the PI gain tuning, the optimum modulus criterion (OMC) and poles and placement (PP) method are considered in analytical simulation by using mfile/Matlab. Table 6.2 shows the PI controller parameters of current control loop obtained by three different methods. Figs. 6.10 and 6.11 show the d-axis and q axis current response of SSC when step change occurs in the d-axis current reference. Fig. 6.12 shows the d-axis current response when step change occurs in d-axis current reference of GSC. It is seen that the AIS method has better performance compared with other method.

Table 6.2.

PI Controller Parameters

PI Controller	Optimum Modulus Criterio (OMC)		Pole and Placment (PP)		Arificila Immune System (AIS)	
	Kp	*Ti*	*Kp*	*Ti*	*Kp*	*Ti*
PI 2	3.8197	0.7162	3.5250	0.7162	2.9251	0.7095
PI 4	3.8197	0.7162	3.5250	0.7162	2.3342	0.5571
PI 6	0.4163	0.0500	0.4940	0.050	0.2559	0.0528
PI 7	0.4163	0.0500	0.4940	0.050	0.2559	0.0528

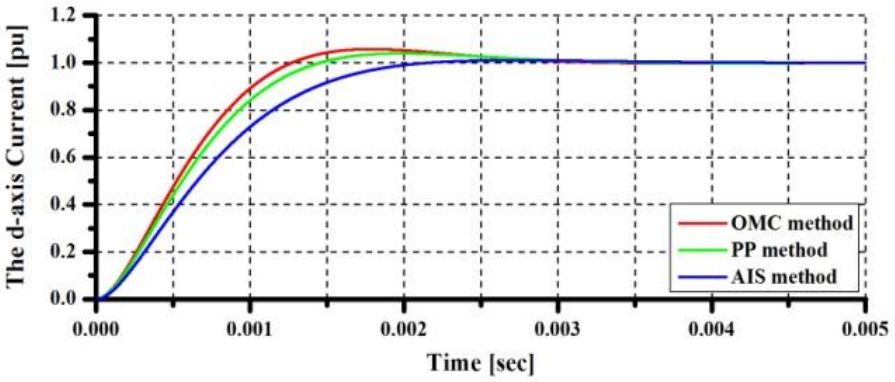

Fig. 6.10. The d-axis current response of SSC

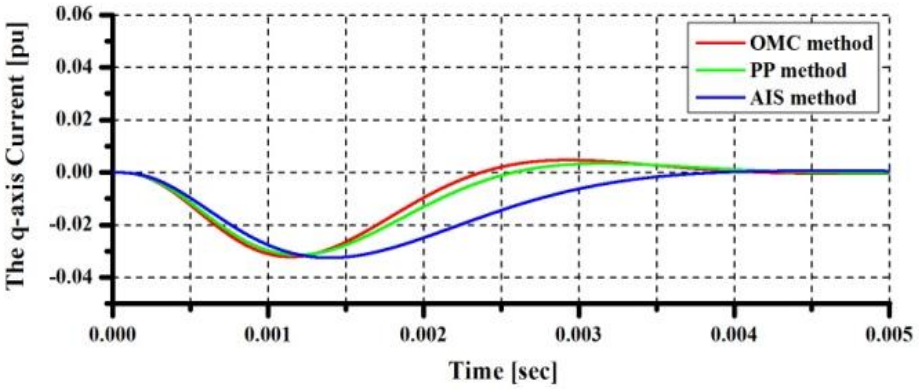

Fig. 6.11. The q axis current response of SSC

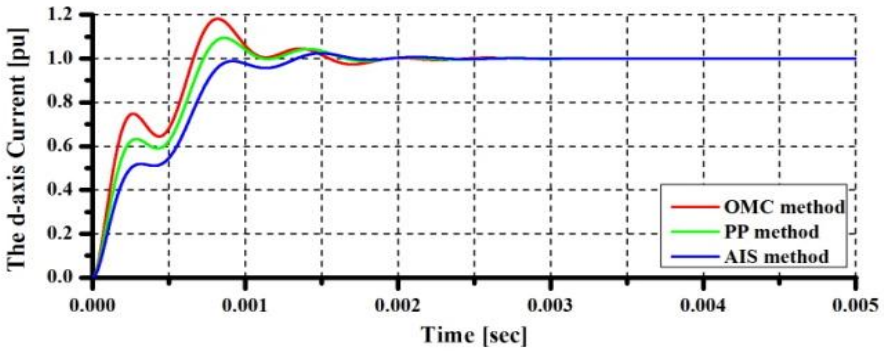

Fig. 6.12. The d-axis current response of GSC

Validity of the design and analysis method explained above has been evaluated using the model system shown in Fig. 6.2. To evaluate the dynamic performances of the proposed method, the wind speed data shown in Fig. 6.13 is used. Simulations were performed by using PSCAD/EMTDC. Fig. 6.14 depicts the rotor speed of the PMSG. The active power reference (P_{ref}), the active power output of PMSG (P_s), and the active power delivered to the grid (P_g) are shown in Fig. 6.15. It is seen that P_S and P_g follow P_{ref} very well. The reactive power outputs of the generator and the grid side converter are kept almost zero as shown in Fig. 6.16.

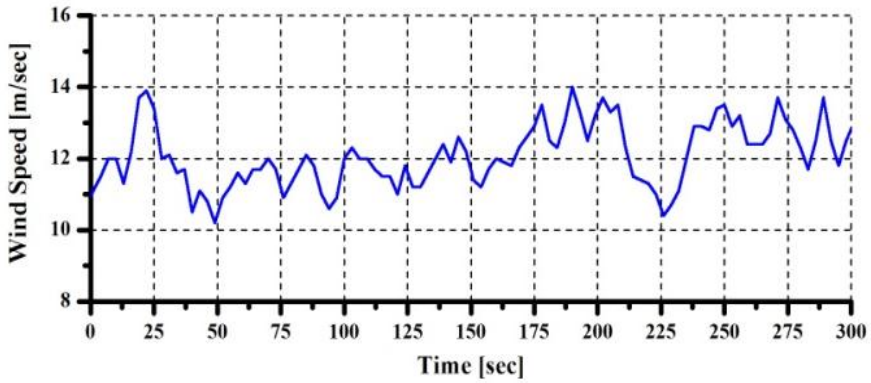

Fig. 6.13. Wind speed data

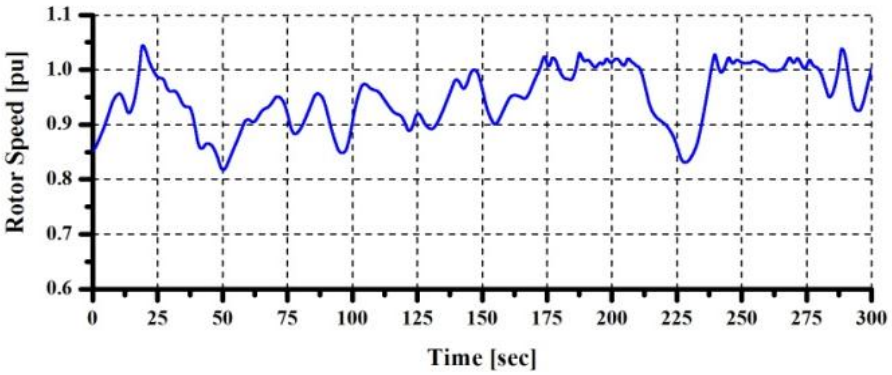

Fig. 6.14. Rotor speed of generator

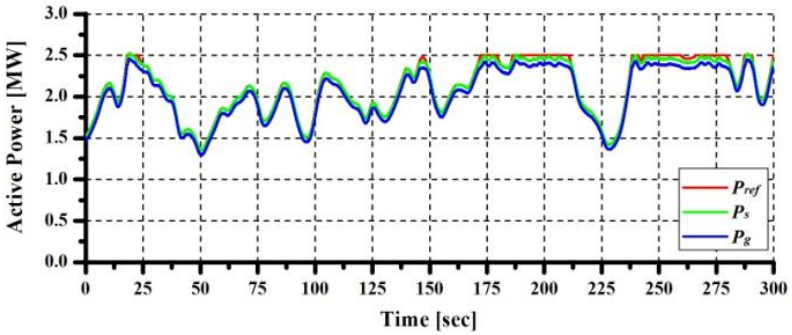

Fig. 6.15. Active power output

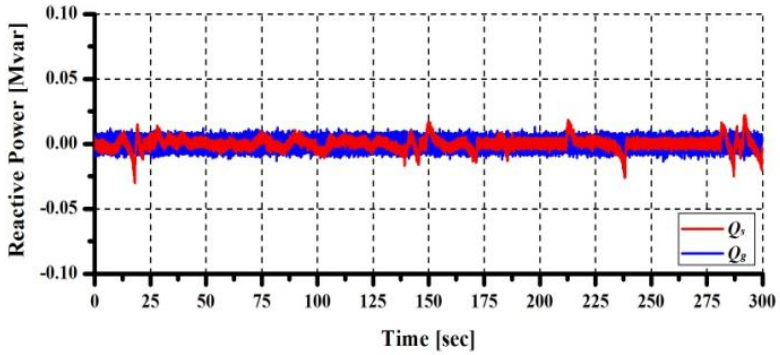

Fig. 6.16. Reactive power output

6.7. Chapter Summary

Novel design method of the current controlled voltage source back to back converter for 2.5 MW class of VSWT-PMSG has been presented. The artificial immune system mechanism is proposed to tune PI controller parameters in order to achieve optimum gain controller. According to the simulation results, it is concluded that the VSWT-PMSG controlled by the proposed method can effectively control active and reactive power delivered to the grid.

Chapter 7

Conclusion

Integration of large number of wind farms into grid power system have been increasing significantly since the last decade. The Fixed Speed Wind Turbines with Squirrel Cage Induction Generators (FSWT-SCIGs) are most widely used in wind farms due to their advantages of mechanical simplicity, robust construction, low specific mass and smaller outer diameter, and lower cost. However, the FSWT-SCIG directly connected to the grid does not have any low voltage ride-trough (LVRT) capability when a short circuit occurs in the grid system. Moreover, under steady state condition the reactive power consumption cannot be controlled and hence terminal voltage of the wind generator leads to large fluctuation which is a serious disadvantage of the SCIG wind turbine. Utilization of Flexible AC Transmission System (FACT) devices can be a better choice due to their abilities of flexible power flow control and good damping capability for power system dynamic oscillations, and can also be a very good system for wind power smoothing due to its response speed and high efficiency. However, the system cost becomes expensive when the FACTS devices are installed in wind farm.

Since last few years ago, Variable Speed Wind Turbine with Permanent Magnet Synchronous Generator (VSWT-PMSG) has become a promising and attractive type of wind turbine concept. The VSWT-PMSG system is equipped with power electronic converters which make it possible to control active and reactive power delivered to grid system, and hence it has strong low voltage ride through capability during fault condition on grid system. Compared with DFIG, PMSG is more efficient, and, it can support large reactive power. However, this type of wind generator has more complex construction and more expensive compared with other types. Therefore, combined installation of VSWT-PMSG and FSWT-SCIG in a wind farm can be efficient due to reduced system investment cost. VSWT-PMSG with power converters can be used to supply reactive power to recover network voltage in order to improve the LVRT of FSWT-SCIG when a fault occurs as well as to generate electric power in steady state operation.

Chapter 2 describes overview of detailed wind turbine generation system modeling. A brief introduction of basic principles of energy extraction from wind is presented. Then, drive train and pitch angel control models of wind turbine generator system considered in this study are explained. The topological overview and modeling are presented for both fixed speed and variable speed wind turbine generator systems. In addition, the two levels and three levels of back to back converters for PMSG are discussed.

In Chapter 3, a control strategy of VSWT-PMSG for stability augmentation of wind farm including fixed speed wind turbine with SCIG is investigated. A suitable control scheme for back-to-back converters of PMSG is developed to augment dynamic behaviour of the wind farms. The protection scheme using DC chopper is embedded on DC link circuit. Two power system models are analysed in simulation study to evaluate the effectiveness and capability of the proposed control strategy. In power system model 1, two wind farms composed of aggregated model of VSWT-PMSG and FSWT-SCIG are connected to an infinite bus. In power system model 2, two wind farms are connected to a multi machine power system. The simulation analyses for both transient and steady state characteristics are performed by using PSCAD/EMTDC. In power system model 1, the terminal voltage of wind farm can be recovered effectively during and after the asymmetrical (1LG and 2LG) faults and the symmetrical (3LG) fault condition and thus the transient stability of fixed speed wind generator can be enhanced. It is also demonstrated that the DC link voltage can be maintained almost constant by the proposed protection controller during the faults condition. Moreover, the steady state performance of the proposed system is analyzed using real wind speed data, and it is demonstrated that the voltage fluctuation of wind farm under randomly varying wind speed can be reduced, and the active power of wind farms can be delivered to the grid effectively. In power system model 2, the control strategy of variable speed permanent magnet wind generator for LVRT capability improvement of the wind farm including fixed speed induction generator has been investigated. From these results, it is clear that PMSG with the proposed controller can enhance the LVRT capability of wind farms during symmetrical three-line-to-ground fault condition. Moreover, the active and reactive power delivered to the grid system can be controlled effectively, and hence the overall system performances can be improved significantly.

In Chapter 4, a new control scheme for variable speed permanent magnet wind generator connected to grid through LCL filter is proposed in order to enhance stability of wind farms including fixed speed induction generators. Design and control approaches of back to back converters are developed in order for both active and reactive powers delivered to a power grid system to be controlled more effectively. The current controlled voltage source converter of PMSG system is developed based on the d-q rotating reference frame. The stability performances of the controller system such as characteristics of dynamic response and good margin are also investigated based on the Bode diagram. The control strategies of overall wind farm have been investigated in transient and steady state analyses to show the capability and effectiveness of the proposed method. The results show that the terminal voltage of wind farm can be recovered effectively during and after the unsymmetrical and the symmetrical faults, and thus the transient stability of fixed speed wind generator can be enhanced. In addition, the steady state performances show that the voltage fluctuation of wind

farm under varying wind speed can be controlled almost constants at rated value and the active power of wind farms delivered to the grid can be controlled effectively. Moreover, it is also shown that the proposed LCL filter can attenuate the harmonic distortions of current and voltage output very effectively.

In chapter 5, a new Fuzzy-PI controller for variable speed permanent magnet wind generator connected to a power grid through a LC filter is proposed and investigated in order to enhance its dynamic performances. The membership function of fuzzy logic control system is designed based on frequency response of the Bode diagram. The controller combines fuzzy logic to classical PI controller to adjust the PI gains online. Stabilizing effect of the proposed PMSG system on the fixed speed wind generators is also investigated. The results show that the proposed Fuzzy-PI controller is very effective in improving the transient stability of overall wind farm system during temporary and permanent fault conditions. The significant effect of proposed control system has been demonstrated especially in the permanent fault analysis. Moreover, the steady state performance of the proposed system is analyzed using variable wind speed data, and it is demonstrated that the terminal voltage of wind farm under randomly varying wind speed can be controlled constant. The results show that VSWT-PMSG with the proposed Fuzzy-PI controller can enhance the transient stability as well as the voltage stability of the wind farm when a fault occurs in the power system.

In Chapter 6, artificial immune system is proposed for control of voltage source converter of variable speed permanent magnet wind generator. Artificial immune system (AIS) is computational techniques based on immunological principles. In the AIS method, the objective function and constraints are represented as antigen. The method is followed to produce antibody as candidate solution on a feasible space through clonal selection operations. Through an affinity maturation and hyper-mutation, a specific antibody that most fits the antigen become a solution. The method is proposed to tune PI controller parameters of current controlled voltage source converter of the VSWT-PMSG. The analytical simulation studies have been performed using mfile/Matlab. In order to verify the effectiveness of the proposed method, the simulation studies using PSCAD/EMTDC have also been performed. Simulation results show that the proposed method is very effective in enhancing the dynamic stability of the wind generator system.

Therefore, this work can contribute to enhance the stability of grid connected wind farm in transient and steady state condition. The LVRT capability of the grid connected wind farm can be improved significantly by using VSWT-PMSG with the proposed control methods. In addition, combined installation of VSWT-PMSG and FSWT-SCIG in a wind farm analyzed in this study can reduce investment cost, because additional FACT device is not needed in the wind farm. Finally, it is hoped that this thesis will have great significance in wind power application, especially for stability augmentation of grid connected wind farm.

Acknowledgement

This thesis has been carried out at Department of Electrical and Electronic Engineering of Kitami Institute of Technology, Japan for the partial fulfillment of the requirement for the degree of Ph.D. This Thesis deals with the stability augmentation of grid connected wind farm by variable speed permanent magnet wind generator.

It is my great pleasure to acknowledge the generous contribution of many individuals, experts and institutions. At first, I express my deep sense of gratitude and indebtedness to my reverend supervising professor, Prof. Junji Tamura for his advice, constant encouragement, valuable guidance and never ending enthusiasm. I shall ever remain grateful to him for his hearty cooperation, financial support and amiable demeanor in accomplishing this work. Prof. Junji Tamura has kindly reviewed this manuscript, and provided me with many helpful suggestions, and also conducted the review panel.

I am deeply grateful to co-supervisors Associate Prof. Rion Takahashi of Electrical and Electronic Engineering Department, Kitami Institute of Technology, Japan and Assistance Prof. S. M. Muyeen of Electrical Engineering Department of Petroleum Institute, Abu Dhabi, UAE for their inspiration, support and kindness I have been provided with. I am indebted to Associate Prof. Rion Takahashi and Assistance Prof. S. M. Muyeen who inspired me and helps a lot in my research and during my stay in Kitami. I am also indebted to Assistant Professor of our laboratory, Dr. Atsushi Umemura for his kind support. I wish to thank Mr. Masatoshi Kotake for his help during my study.

I am also grateful to Prof. Kousaku Yoshida, Prof. Shinya Obara, Prof. Hiroshi Tanimoto, and Associate Prof. Rion Takahashi for their kind review of this thesis.

I wish to express my gratefulness to Kitami Institute of Technology, which has given me a unique opportunity to augment my engineering knowledge as well as has given me financial support during my study and attendance in various national and international conferences. I would like to thank Directorate General High Education of Ministry of National Education of Republic Indonesia for providing me with a scholarship. I am so grateful to Muhammadiyah University of Surabaya, Indonesia, which has supported me to study in Japan with necessary study leave and deputation. Special thank for Prof. Imam Robandi for his support and motivation, which has inspirited me to study in Japan.

Also, Hitachi Research Laboratory is highly appreciated for their support and collaboration during internship program in Ibaraki, Japan, which gave me the opportunity to learn new ideas in my research. I am also indebted to Prof. Minwon Park for gave me opportunity and support during visiting research student program in Center of Advance Power Technology Application Laboratory of Changwon National University, Republic of Korea.

Many thank to Prof. MRI Sheikh for his valuable suggestion and cooperation at the beginning in my study life in Kitami. I would also like to thanks to Dr. Okedu, Miss Liu and all members of our laboratory for their kindness and encouragement.

My ultimate gratitude goes to my parents, Muhammad Arsyad and Masjuwita (alm). It is because of their endless pray; finally I can accomplish this work. My most heartfelt acknowledgement must go to my wife, Ida Sriandiani for her endless patient, love and support. Also to my son Kenshi-kun and my daughter Yuki-chan thank you for your love, which makes this work so joyful. Finally, Ya Allah, thank you very much for everything.

Marwan Rosyadi

March, 2013, Kitami Japan

References

[1] British Electricity International, Modern Power Station Practice: Incorporating modern power system practice, 3rd Edition, 12 volume set, Pergamon. ISBN 0-08-040510-X. 1991.

[2] Babcock & Wilcox Co., Steam: Its Generation and Use, 41st edition, ISBN 0-9634570-0-4, 2005.

[3] Thomas C. Elliott, Kao Chen, Robert Swanekamp, Standard Handbook of Power plant Engineering, 2nd edition, McGraw-Hill Professional, ISBN 0-07-019435-1, 1997.

[4] REN21, Renewables 2011 Global Status Report, Version 1.1, July 2011. Online: http:// www.ren21.net

[5] The Global Wind Energy Council (GWEC), Global wind report 2010, April 2011. [Online].Available: http://www.gwec.net

[6] R. Doherty, E. Denny, M. O'Malley, "System operation with a significant wind power penetration", *IEEE Power Engineering. Summer Meeting*, Vol. 1, pp. 1002–1007, Jun. 2004.

[7] K.S. Salman, A.L.J. Teo, "Windmill modeling consideration and factors influencing the stability of a grid-connected wind power-based embedded generator", *IEEE Trans. Power System*, Vol. 18. No. 2, pp. 793–802, May 2003.

[8] Z. Litipu, K. Nagasaka, "Improve the reliability and environment of power system based on optimal allocation of WPG", *IEEE. Power Systems Conf. Expo.*, Vol. 1, pp. 524–532, Oct. 2004.

[9] N. Dizdarevic, M. Majstrovic, S. Zutobradic, "Power quality in a distribution network after wind power plant connection", *IEEE Power Syst. Conf. Expo.*, Vol. 2, pp. 913–918. Oct. 2004.

[10] Jauch C, Matevosyan J, Ackermann T, Bolik S., "International comparison of requirements for connection of wind turbines to power systems", *Wind Energy*, Vol. 8. No. 3, pp. 295–306, Jul. 2005.

[11] Y. Shankir, "Review of wind turbines' drive systems and why Gearless direct drive", *RCREEE Wind Energy Building Capacity Program – Stage 2 Rabat*, Tangier 29 March – 2 April, 2010.

[12] J. Tamura, T. Yamazaki, M. Ueno, Y. Matsumura, and S. Kimoto, "Transient stability simulation of power system including wind generator by PSCAD/EMTDC", *IEEE Porto Power Tech*, Vol. 4, Paper no. EMT-108, 2001.

[13] M. R. I. Sheikh, S.M. Muyeen, Rion Takahashi, Junji Tamura, "Transient Stability Enhancement of Power System Including Wind Farm by Using SMES", *International Workshop on Modern Science and Technology 2010 (IWMST 2010)*, No.4, pp.253-258, Sept. 2010.

[14] E. S. Abdin and W. Xu, Control design and dynamic performance analysis of a wind turbine-induction generator unit," *IEEE Transaction Energy Convers*., Vol. 15, No. 3, pp. 91–96, Mar. 2000.

[15] C.L. Souza et al, "Power system transient stability analysis including synchronous and induction generator", *IEEE Porto Power Tech*, Vol. 2, pp.6, 2001.

[16] Thomas Ackermann, *Wind power in power system*, UK: John Wiley & Sons, 2005.

[17] H.F. Wang, F. Li, and R.G. Cameron, "FACT control design based on power system non parametric model", I*EE Proc. -Gener. Trans. Distrib.*, Vol.146, No.5, pp.409-415, 1999.

[18] L. Gyugyi, "Unified power flow control concept for flexible ac transmission system", *Proc. Inst. Elect. Eng. C.* Vol.139. No.4, pp.323-331, 1992.
[19] L. Gyugyi: "Dynamic compensation of AC transmission line by solid state synchronous voltage source", *IEEE Trans, Power Delivery*, Vol.9, No.2, pp. 904-911, 1994.
[20] M.R.I.Sheikh, S.M. Muyeen, R.Takahashi, J.Tamura, "Smoothing Control of Wind Generator Output Fluctuations by PWM Voltage Source Converter and Chopper Controlled SMES," *European Trans. Electrical Power*, Vol. 21, Issue-1, pp. 680-697, Jan. 2011.
[21] L. Zhang, C. Shen, M. L. Crow, L. Dong, S. Pekarek, S. Atcitty, "Performance indices for the dynamic performance of FACTS and FACTS with energy storage," *Elect. Power Compon. Syst.*, Vol. 33, No. 3, pp. 299–314, Mar. 2005.
[22] S. M. Muyeen, M. H. Ali, R. Takahashi, T. Murata, and J. Tamura, "Wind generator output power smoothing and terminal voltage regulation by using STATCOM/BESS," *The IEEE Powertech 2007 Conference*, Lausanne, Switzerland, Ref No. 258, 2007.
[23] S. B. Papaefthimioun, S. A. Papathanassiou, "Simulation and control of variable speed wind turbine with synchronous generator", *The XVII International Conference Electrical Machines (ICEM) 2006*, Chania, Crete Island, Greece, Ref. No. 593, Sept 2-5, 2006.
[24] S. M. Muyeen, R. Takahashi, T. Murata, J. Tamura, M. H. Ali, "Transient stability analysis of permanent magnet variable speed synchronous wind generator," *International Conference on Electrical Machines and Systems (ICEMS) 2007*, Soul Korea, pp.288-293, Oct 2007.
[25] A. D. Hansen and G. Michalke: "Modeling and control of variable speed multi-pole permanent magnet synchronous generator wind turbine", *Wind Energy*, Vol.11, no.5, 10.1002/we.278, pp.537-554, 2008.
[26] T.sun, Z. Chen, and F. Blaabjerg: "Transient stability of DFIG wind turbines at an external short-circuit fault," *Wind Energy*, Vol.8, No.3, pp. 354-360, 2005.
[27] R. Takahashi, J. Tamura, M. Futami, M. Kimura, K Ide, "A new control method for wind energy conversion system using a double-fed synchronous generator", *IEEJ Power and Energy*, Vol.126, No.2, pp.225-235, Feb 2006
[28] K.E. Okedu, S. M. Muyeen, R. Takahashi, and J. Tamura, "Stabilization of wind farms by DFIG-based variable speed wind generators", *International Conference on Electrical Machines and Systems (ICEMS) 2010*, Incheon Korea, pp. 464-469, Oct 2010.
[29] K. E. Okedu, S.M. Muyeen, R. Takahashi, J. Tamura, "Wind Farm Stabilization by using DFIG with Current Controlled Voltage Source Converters Taking Grid Codes into Consideration", *IEEJ Transaction on Power and Energy*, Vol. 132, No. 3, pp. 251-259, Mar. 2012.
[30] H. Polinder, S.W.H. de Haan, M.R. Dubois, J. Slootweg, "Basic operation principles and electrical conversion systems of wind turbines", *2004 Nordic Workshop on Power and Industrial Electronics*, Paper 069, Trondheim, Norway. 2004.
[31] G. Michalke, A.D. Hansen, T. Hartkopf, "Control strategy of a variable speed wind turbine with multipole permanent magnet synchronous generator", *2007 European Wind Energy Conference and Exhibition*, Milan, Italy, May 2007.
[32] T. J. E. Miller, *Brushless permanent-magnet and reluctance motor drive*, New York: Oxford Univ. Press (1989)
[33] Shuhui Li, Timothi A. Haskew, Ling Xu, "Conventional and novel control design for direct driven PMSG wind turbines," *Journal of Electric Power System research*, Vol. 80, pp. 328-338, March. 2010.

[34] L. M. Fernandes, C. A. Garcia, F. Jurado, "Operating Capability as a PQ/PV node of a Direct-Drive Wind Turbine based on a permanent magnet synchronous generator", *Renewable Energy*, Vol. 35, pp. 1308-1318, 2010.
[35] S. M. Muyeen, R. Takahashi, T. Murata, J. Tamura, "Multi-Converter Operation of Variable Speed Wind Turbine Driving Permanent Magnet Synchronous Generator during Network Fault", *12th International Conference on Electrical Machines and Systems (ICEMS 2009)*, LS1C-4, Nov. 2009.
[36] S. M. Muyeen, A. Al-Durra, J. Tamura, "Variable speed wind turbine generator system with current controlled voltage source inverter", *Electric Power Systems Research*, Vol. 80, pp. 328–338, 2010.
[37] S. M. Muyeen, R. Takahashi, T. Murata, J. Tamura, "A Variable Speed Wind Turbine Control Strategy to Meet Wind Farm Grid Code Requirements", *IEEE Transaction on Power Systems*, Vol .25, No. 1, pp. 331-340, Feb. 2010.
[38] W. A. Hill and S. C. Kapoor, "Effect of two-level PWMsources on plant power system harmonics," *IEEE-IAS Annual Meeting*, pp. 1300–1306, 1998.
[39] M. Liserre, F. Blaabjerg, S. Hansen, "Design and Control of an LCL-filter based Three-phase Active Rectifier", *IEEE Transaction on Industry Applications*, Vol. 41 , No. 5, pp. 1281 – 1291, Sept/Oct. 2005.
[40] V. Blasko and V. Kaura, "A novel control to actively damp resonance in input lc filter of a three-phase voltage source converter", *IEEE Transaction on Industry Application*, Vol. 33, No. 2, pp. 542–550, Mar./Apr. 1997.
[41] B. Ferdi, C; Benachaiba; S. Dib, R. Dehini, "Adaptive PI control of dynamic voltage restorer using fuzzy logic", *Journal of Electrical Engineering: Theory and Application*, Vol. 1, pp. 165-173, 2010.
[42] J. W. Dixon, J. M. Contardo, and L. A. Moran, "A Fuzzy controlled active front-end rectifier with current harmonic filtering characteristics and minimum sensing variable," *IEEE Transaction on Power Electronics*, Vol. 14, No. 4, pp. 363-377, 1999.
[43] R. M. Martins, A. D. Oliver, S. F. Silva, "Fuzzy logic to correct power factor considering power quality," *Proceedings of EPE*, Switzerland. 1999.
[44] P. Mattaveli. L Rossetto, G. Spiazzi, and P. Tenti, "General-purpose fuzzy controller for DC-DC converters," *IEEE Transaction on Power Electronics*, Vol. 12, No. 1, pp. 79-85, 1997.
[45] M. Rukonuzzaman, M. Nakaoka, "Fuzzy logic current controller for three-phase voltage source PWM-inverters", *Industry Application Conference*, Vol. 2, pp. 1163 – 1169, 2000.
[46] B. Friedland, *Advanced Control System Design*, Prentice Hall, 1996.
[47] G. H. Cohen and G. A. Coon, "Theoretical Consideration of Related Control," *Trans. ASME*, Vol. 75, pp. 827-834, 1953.
[48] S. Tavakoli, M. Tavakoli, "Optimal tuning of pid controllers for first order plus time delay models using dimensional analysis," *The Fourth International Conference on Control and Automation (ICCA'03*), Montreal, Canada, 10-12 June 2003.
[49] L. N. De Castro, F. J. Von Zuben, "*Artificial Immune Systems: Part I – Basic Theory And Applications*", Technical Report, Dec 1999.
[50] L. N. De Castro, F. J. Von Zuben, "Learning and Optimization Using the Clonal Selection Principle', *IEEE Transaction on Evolutionary Computation*, Vol.6, No. 3, pp. 239-251, 2002.
[51] Wind Power, Rowan University Clean Energy Program, [Available Online]: www.rowan.edu/colleges/engineering/clinics/cleanenergy/cleanenergy_homepage.htm, (Accessed on 2 November 2012).

[52] Wind Energy Basics theory. [Online]: http://windeis.anl.gov/guide/basics/index.cfm, (Accessed on 2 November 2012).

[53] Wind Energy, [online]: http://leedintl.net/wind_energy. (Accessed on 2 November 2012).

[54] Fthenakis, V., Kim, H. C. "Land use and electricity generation: A life-cycle analysis", *Renewable and Sustainable Energy Reviews*, Vol. 13. Issues 6–7, pp. 1465–1474, Aug./Sept. 2009.

[55] R. Y. Redlinger, P. D. Andersen, P. E. Morthorst, *Wind Energy in The 21st Century*, 1st Edition, Palgrave, New York, 2002.

[56] Betz, A., *Introduction to the Theory of Flow Machines*, D. G. Randall, Trans. Oxford: Pergamon Pres., 1966.

[57] S. Heier, *Grid integration of wind energy conversion systems*, John Wiley & Sons Ltd, 1998.

[58] MATLAB documentation center [online] on http://www.mathworks.co.jp/jp/help/. (Accessed on 3 November 2012).

[59] S. M. Muyeen, J. Tamura, and T. Murata, *Stability Augmentation of a Grid Connected Wind Farm, Green Energy and Technology*, Springer-Verlag, 2009.

[60] Alejandro Rolan et all, "Modeling of a Variable Speed Wind Turbine with a Permanent Magnet Synchronous Generator", *IEEE International Symposium on Industrial Electronics (ISlE 2009)* , Seoul, Korea, July 5-8 2009.

[61] M. Yin, G.Li, M. Zhou, C. Zhao, "Modeling of the wind turbine with permanent magnet synchronous generator for integration", I*EEE Power Engineering Society General Meeting*, Tampa, Florida, pp. 1-6, 2007.

[62] I. Boldea, *Synchronous Generators, United States of America*, Taylor and Francis, 2006.

[63] S.E. Lyshevski, *Electromechanical Systems, Electric Machines, and Applied Mechatronics*, CRC, 1999.

[64] P. Kundur, *Power system stability and control*, New York: McGraw-Hill, 1994.

[65] P. K. Chaturvedi, S. Jain, P. Agrawal, R. K. Nema, K. K. Sao, "Switching losses and harmonic investigation in multilevel inverters," *IETE Journal of research*, Vol. 54, Issue 4, pp. 297-307, Jul./Aug. 2008.

[66] J. Rodr´ıguez, J. S. Lai, Fang Zheng Peng, "Multilevel inverters: A survey of topologies, controls, and applications," *IEEE Trans. Ind. Electron.*, Vol. 49, No. 4, pp. 724-738, Aug. 2002.

[67] PSCAD/EMTDC User's Manual, Manitoba HVDC Research Center, Canada (1994)

[68] A. Gole, V. K. Sood, and L. Mootoosamy: "Validation and analysis of a grid control system using d–q–z transformation for static compensator systems", C*onf. Elect. Computer Engineering*, Montreal, QC, Canada, pp. 745–748.1989

[69] IEEE Recommended Practice for Excitation System Models for Power System Stability Studies, IEEE Std. 421.5-1992.

[70] Computer Models for Representation of Digital-Based Excitation Systems, IEEE Transactions, 1996.

[71] Hydraulic Turbine and Turbine Control Models for System Dynamic Studies, Working Group on Prime Mover and Energy Supply Models for System Dynamic Performance Studies, Transactions on Power Systems, Vol. 7, No. 1, February 1992.

[72] Dynamic Models for Fossil Fuelled Steam Units on Power System Studies, Working Group on Prime Mover and Energy Supply Models for System Dynamic Performance Studies, Transactions on Power Systems, Vol. 6, No. 2, May 1991.

[73] Federal Energy Regulatory Commission (FERC), United States of America, Docket no. RM05-4-000; Order no. 661-A, Interconnection for Wind Energy, Dec 12, 2005.

[74] IEEE Std. 519-1992 - IEEE Recommended Practices and Requirement for Harmonic Control in Electrical Power Systems ″U IEEE Industry Applications Society/ Power Engineering Society., 1992.

[75] F. L. M. Antunes S. V. Araujo. "Lcl filter design for grid-connected npc inverters in offshore wind turbines", *The 7th International Conference in Power Electronics*, Daegu, Korea ,1:1133–1138, 22-26 October, 2007.

[76] L. Wang, J.-Y. Liou, "Simulations of a commercial wind power generation system with four wind-turbine induction generators," I*EEE Power Engineering Society General Meeting 2007*, Tampa, FL, pp. 1–7, 2007.

[77] B. Farid O. Amar, "A Study of New Techniques of Controlled PWM Inverters", *European Journal of Scientific Research*, Vol.32, No.1. pp. 77-87, 2009

[78] A. Draou,Y. Sato, T. Kataoka, "Anewstate feedback based transient control of PWM AC to DC voltage type converters," I*EEE Trans. Power Electron.*, Vol. 10, No. 6, pp. 716–724, Nov. 1995.

[79] M. Lindgren and J. Svensson, "Control of a voltage-source converter connected to the grid through an LCL-filter-application to active filtering," *IEEE PESC'98*, Vol. 1, pp. 229–235, 1998.

[80] J. R. Espinoza, G. Joos, E. Araya, L. A. Moran, and D. Sbarbaro, "Decoupled control of PWM active-front rectifiers using only dc bus sensing," *IEEE-IAS Annu. Meeting*, Vol. 4, pp. 2169–2176, 2000.

[81] E. J. Bueno, F. Espinosa, F. J. Rodríguez, J. U. S. Cobreces, "Current control of voltage source converters connected to the grid through an LCL-filter," *IEEE PESC'04*, Vol. 1, pp. 68–73, 2004.

[82] T. CY Wang, Z. H. Ye, G. Sinha, X. M. Yuan. "Output Filter Design for a Grid-interconnected Three-Phase Inverter," *PESC'03*, Acapulco, Mexico, Vol. 2, pp. 779-784, Jun. 2003.

[83] E. Twining and D. G. Holmes, "Grid current regulation of a three-phase voltage source inverter with an LCL input filter," *IEEE PESC'02*, Vol. 3, pp. 1189–1194, Jun. 2002.

[84] M. Godoy Simões and M. Friedhofer, "An implementation methodology of a fuzzy based decision support algorithm," *International Journal of Knowledge-Based Intelligent Engineering Systems*, Vol.1, No. 4, pp. 267-275. Oct. 1997.

[85] L.A. Zadeh, "Fuzzy Sets," *Inform. Contr*., vol. 8, pp. 338-353, 1965

[86] http://en.wikipedia.org/wiki/Fuzzy_control_system

[87] Ian S. Shaw, *Fuzzy Control of Industrial Systems: Theory and Applications*, Kluwer Academic Publishers; ISBN: 0792382498, 1998.

[88] B. Friedland, *Advanced Control System Design*, Prentice Hall, 1996.

[89] J. E.Hunt, D. E.Cooke, "Learning Using an Artificial Immune System", *Journal of Network and Computer Applications*, Vol. 19, pp. 189-212, 1996.

[90] Dasgupta, D., "Artificial Neural Networks and Artificial Immune Systems: Similarities and Differences", Proc. of the IEEE SMC, 1, 1997, pp. 873-878.

[91] D. F. McCoy, V. Devaralan, "Artificial Immune Systems and Aerial Image Segmentation", *Proceedings of the SMC'97*, pp. 867-872. 1997.

[92] D. Dasgupta, *Artificial Immune Systems and Their Applications*, Springer-Verlag. 1999

[93] S. A. Hofmeyr, S. Forrest, "Immunity by Design: An Artificial Immune System", *Proc. of GECCO'99*, pp. 1289-1296, 1999.

[94] S. A.Hofmeyr, *An Interpretative Introduction to the Immune System in Design Principles for the Immune System and Other Distributed Autonomous Systems*, Eds. I. Cohen & L. A. Segel, Oxford University Press. 2000.

[95] A. S Perelson, M. Mirmirani, G. F. Oster, "Optimal Strategies in Immunology I. B-Cell Differentiation and Proliferation", *J. Math. Biol.*, Vol. 3, pp. 325-367. 1976.

[96] A. S Perelson, M. Mirmirani, G. F. Oster, "Optimal Strategies in Immunology II. B Memory Cell Production", *J. Math. Biol.*, Vol. 5, pp. 213-256. 1978.

List of Publications

Transaction/Journal Papers:

[1] **Marwan Rosyadi**, S. M. Muyeen, Rion Takahashi, Junji Tamura, "Stability Augmentation of Wind Farm using Variable Speed Permanent Magnet Synchronous Generator," IEEJ Transaction on Industry Applications, Vol. 131-D, No. 11, pp.1276-1283, Nov. 2011.

[2] **Marwan Rosyadi,** S. M. Muyeen, Rion Takahashi, Junji Tamura, "A New Control Approach to Variable Speed PM Wind Generator for Enhancing Dynamic Stability of Wind Farm," The International Review of Automatic Control – Theory and Applications (IREACO), Vol. 5. No. 5, pp. 606-616, Sept. 2012.

[3] **Marwan Rosyadi**, S. M. Muyeen, Rion Takahashi, Junji Tamura, "A Design Fuzzy Logic Controller for a Permanent Magnet Wind Generator to Enhance the Dynamic Stability of Wind Farms," *Applied Sciences.* Vol. 2, No. 4, pp. 780-800, Nov. 2012.

[4] **Marwan Rosyadi**, S. M. Muyeen, Rion Takahashi, Junji Tamura, "Stabilization of Fixed Speed Wind Generator by using Variable Speed PM Wind Generator in Multi-Machine Power System," Journal of International Conference on Electrical Machines and Systems, Vol.2, No.1, pp.111-119, March 2013.

International Conference Papers:

[5] **Marwan Rosyadi**, S.M. Muyeen, Rion Takahashi, Junji Tamura, "Transient Stability Enhancement of Variable Speed Permanent Magnet Wind Generator using Adaptive PI-Fuzzy Controller", Proc. of 2011 IEEE PES PowerTech, Paper ID No.87, Trondheim, Norway, June 19-23, 2011.

[6] **Marwan Rosyadi**, S.M. Muyeen, Rion Takahashi, Junji Tamura, "Low Voltage Ride-Through Capability Improvement of Wind Farms using Variable Speed Permanent Magnet Wind Generator", Proc. of International Conference on Electrical Machines and Systems (ICEMS) 2011, Paper ID No. 127, Beijing, China., August 20 – 23, 2011.

[7] **Marwan Rosyadi,** S. M. Muyeen, Rion Takahashi, Junji Tamura, "New Controller Design for PMSG Based Wind Generator with LCL-Filter Considered", Proc. of the 2012 XXth International Conference on Electrical Machines (ICEM2012), pp.2110-2116, 2012.

[8] **Marwan Rosyadi**, S. M. Muyeen, Rion Takahashi, Junji Tamura, "Voltage Stability Control of Wind Farm using PMSG based Variable Speed Wind Turbine", Proc. of the

2012 XXth International Conference on Electrical Machines (ICEM2012), pp.2190-2195, 2012.

[9] **Marwan Rosyadi**, S. M. Muyeen, Rion Takahashi, and Junji Tamura, "Fuzzy Logic Controlled Voltage Source Converter in Grid Connected Application via LCL Filter", 2012 International Conference on Electrical Machines and Systems (ICEMS2012), #DS1G4-8(6 pages), 2012.

[10] **Marwan Rosyadi**, S. M. Muyeen, Rion Takahashi, and Junji Tamura, "Stabilization of Fixed Speed Wind Generator by Using Variable Speed PM Wind Generator in Multi-Machine Power System", 2012 International Conference on Electrical Machines and Systems (ICEMS2012), #DS2G5-4(6 pages), 2012.

[11] **Marwan Rosyadi**, S. M. Muyeen, Rion Takahashi, and Junji Tamura, "Artificial Immune System Based Design of Current Controlled Voltage Source Converter for PM Wind Generator", 2012 International Conference on Electrical Machines and Systems (ICEMS2012), #LS2C-2(6 pages), 2012.

[12] **Marwan Rosyadi**, S. M. Muyeen, Rion Takahashi, and Junji Tamura, "Novel Control Design of Variable Speed PM Wind Generator Considering Grid Code Requirement", 2012 International Conference on Electrical Machines and Systems (ICEMS2012), #LS5C-1(6 pages), 2012.

[13] **Marwan Rosyadi**, S.M. Muyeen, Rion Takahashi, Junji Tamura, "Fuzzy-PI Controller Design for PM Wind Generator to Improve Fault Ride Through of Wind Farm," Proc. of the *International Conference on Renewable Energy Research and Applications (ICRERA), Paper ID. 25, Nagazaki, Japan, November 11-14, 2012.*

[14] **Marwan Rosyadi**, S.M. Muyeen, Rion Takahashi, Junji Tamura, "Dynamic Stability Improvement of Grid Connected Converter using Fuzzy Compensator Controller" Proc. of the *International Conference on Renewable Energy Research and Applications (ICRERA), Paper ID. 35, Nagazaki, Japan, November 11-14, 2012.*

Branch Conference and Technical meeting Papers:

[15] **Marwan Rosyadi**, M.R.I. Sheikh, S.M. Muyeen, Rion Takahashi, Junji Tamura, " Stability Enhancement of Fixed Speed Wind Generator using Permanent Magnet Wind Generator," Proc of: 2010 Joint Conventional Record, The Hokkaido chapters of Institute of Electrical and Information Engineer, Japan, No.33, Sapporo, 23-24 Oct 2010.

[16] **Marwan Rosyadi**, M.R.I. Sheikh, S.M. Muyeen, Rion Takahashi, Junji Tamura, "A Control Strategy of Direct-Drive Permanent Magnet Wind Generator for Wind Farm Stabilization", The papers of Technical Meeting on Rotating Machinery, IEE Japan, RM-10-117, Oct 20-21, 2010.

[17] **Marwan Rosyadi**, S.M. Muyeen, Rion Takahashi, Junji Tamura, ”Stabilization of Wind Farms by PMSG based Variable Speed Wind Generator with Adaptive PI-Fuzzy Controller”, The papers of Joint Technical Meeting on Motor Drive and Rotating Machinery, IEE Japan, RM-11-34, May 18, 2011.

[18] **Marwan Rosyadi**, S.M. Muyeen, Atsushi Umemura, Rion Takahashi, Junji Tamura, “Voltage Stability Improvement of Wind Farm by PM Wind Generator with Fuzzy Logic Current Controlled VSC,” Proc. of 2012 Joint Conventional Record, The Hokkaido chapters of IEEJ, No.42, Sapporo, Oct 2012.

[19] **Marwan Rosyadi**, S.M. Muyeen, Atsushi Umemura, Rion Takahashi, Junji Tamura,” Fuzzy Logic Controller Design of Grid Connected LCL Filter based Voltage Source Inverter,” Proc. of 2012 Joint Conventional Record, The Hokkaido chapters of IEEJ, No.31, Sapporo, Oct 2012.